Nucleosynthesis of exotic nuclei and hypernuclei in expanding nuclear matter after relativistic collisions

Alexander Botvina

(collaboration with M.Bleicher, N.Buyukcizmeci, Yu.Lebed, R.Ogul, J.Pochodzalla, W.Trautmann, J.Steinheimer, T.Reichert, I.Mishustin, K.Gudima, S.Avdeyev, V.Karnaukhov)

14 MPD meeting, Dubna, Russia

16 October, 2024

Low energy reactions : Nucleation processes via binary particle collisions. It takes place at very low density

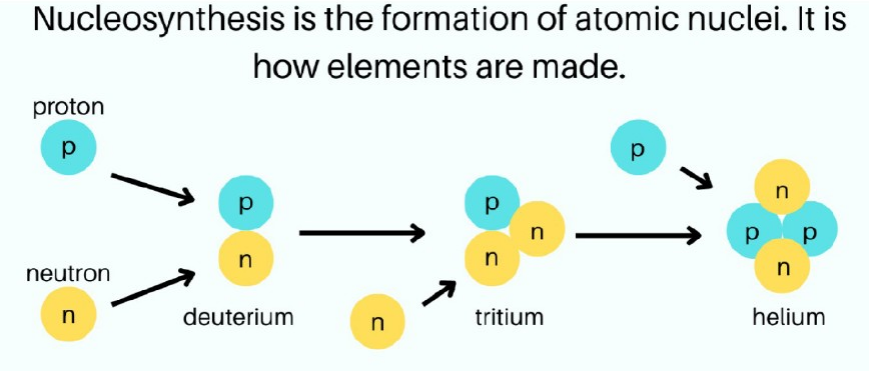

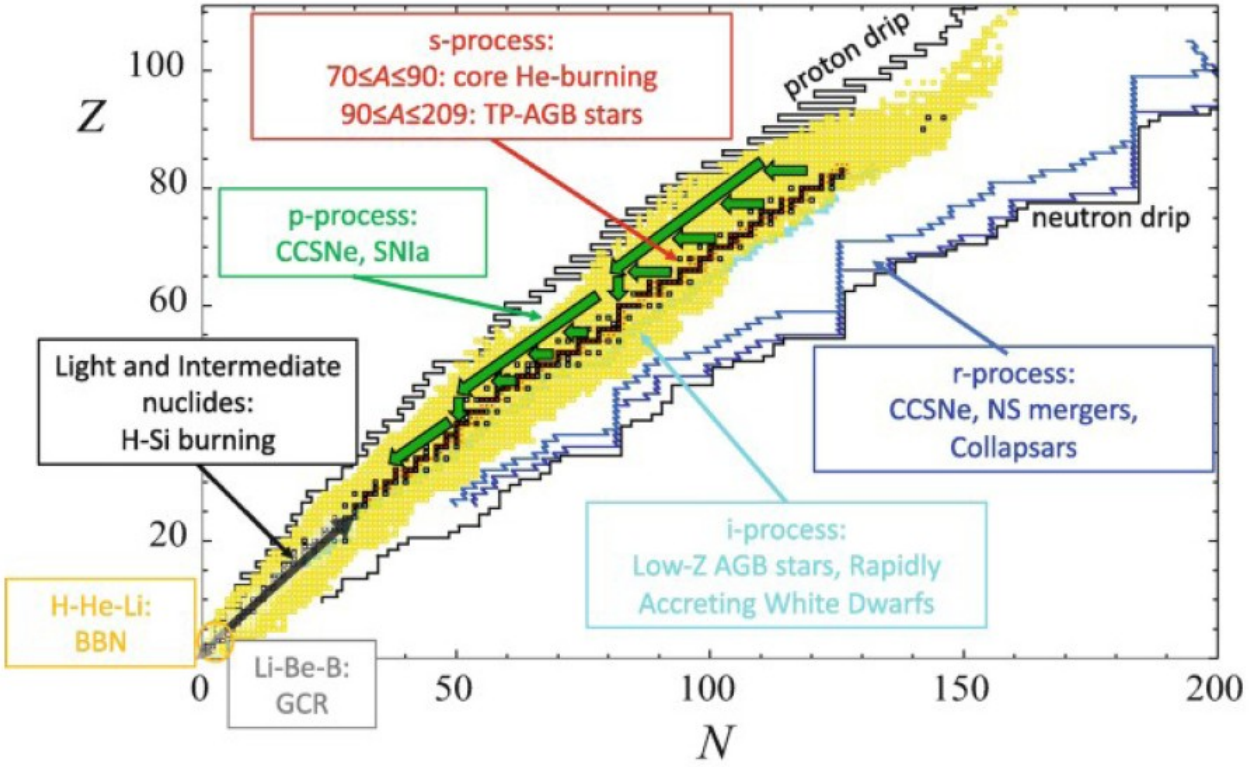

Nucleosynthesis in Universe: Low-energy reactions involve collective processes via the compound nucleus formation.

Low/intermediate energies: hadron/lepton collisions with nuclei (+ peripheral ion collisions), the compound mechanism.

Dinamical stage with particle emission and production of excited nuclear residues

Preequlibrium emission + equilibration

Collective many-body process of nucleosynthesis

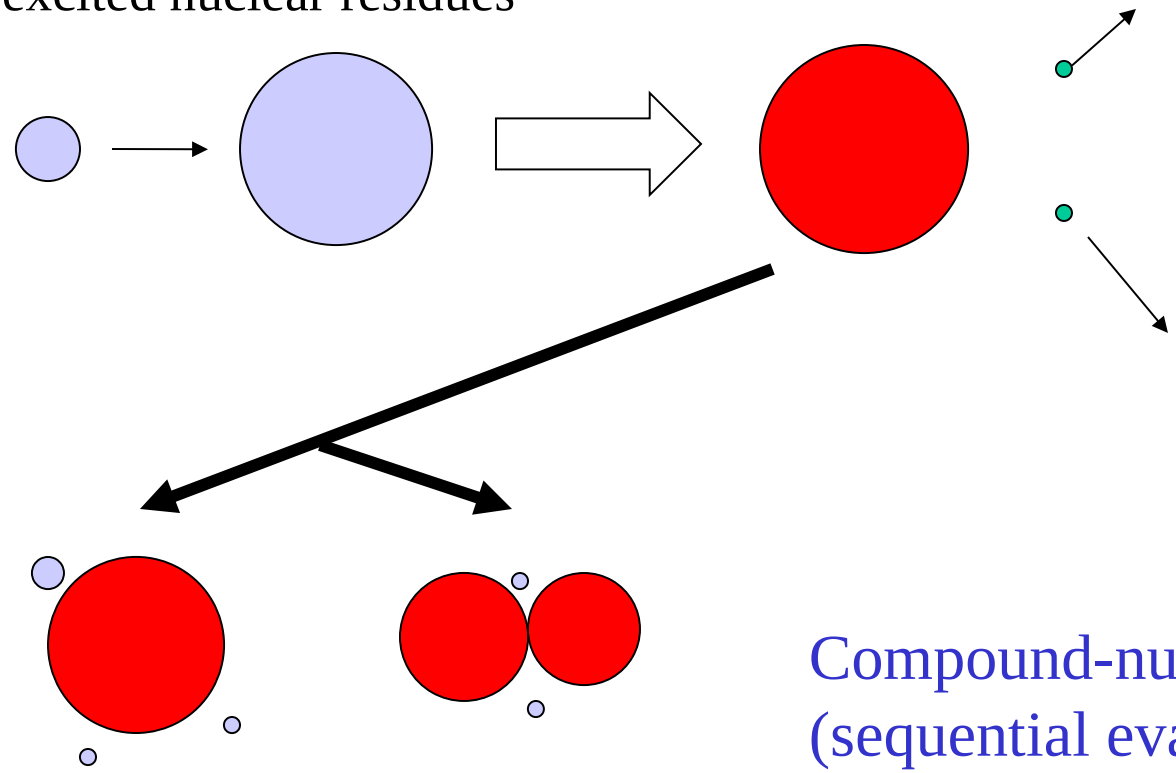

Statistical approach

N.Bohr (1936)

N.Bohr, J.Wheeler (1939)
V.Weisskopf (1937) …

evaporation fission

Compound-nucleus decay channels (sequential evaporation or fission) dominate at low excitation energy of thermal sources E^{*}<2-3 MeV/nucl

Qualitative picture of dynamical stage of the reaction leading to fragment production (e.g., UrQMD calculations)

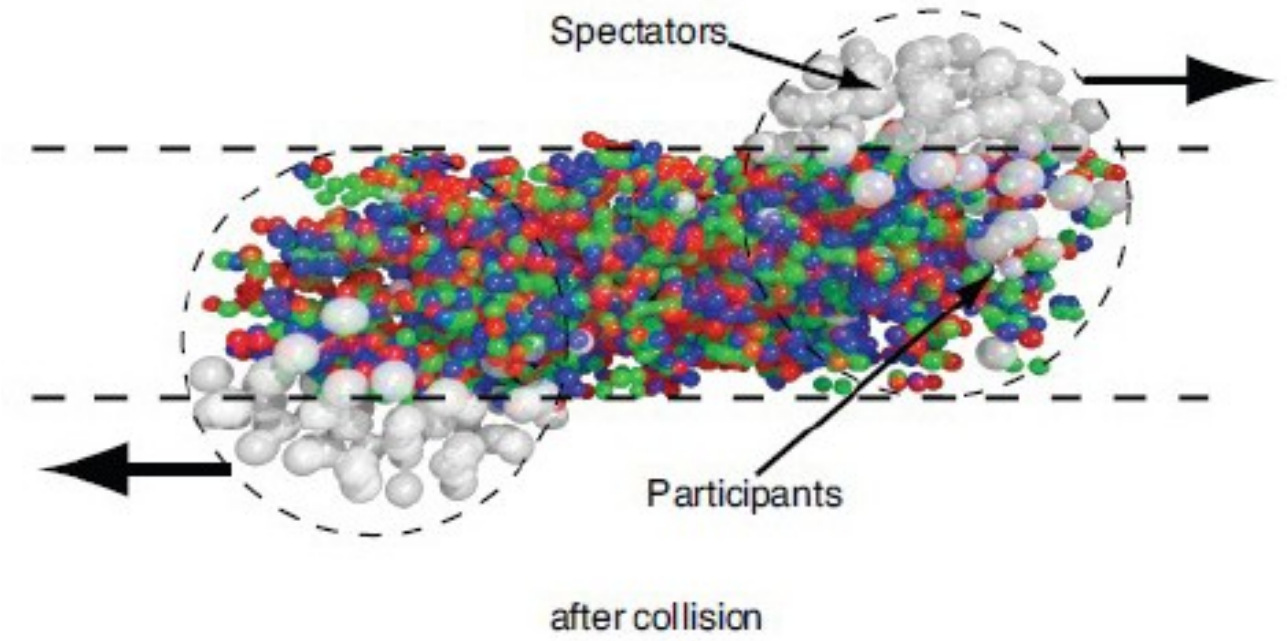

Very high energy is deposited into the nuclear system.
Compound nucleus conception may not work.

Fragment formation is possible from both participant nucleons and spectators

High excitation energy: New collective process – expansion of matter + nucleation/multifragmentation in the freeze-out state

Dinamical stage with particle emission and production of excited nuclear residues

Preequlibrium emission + equilibration

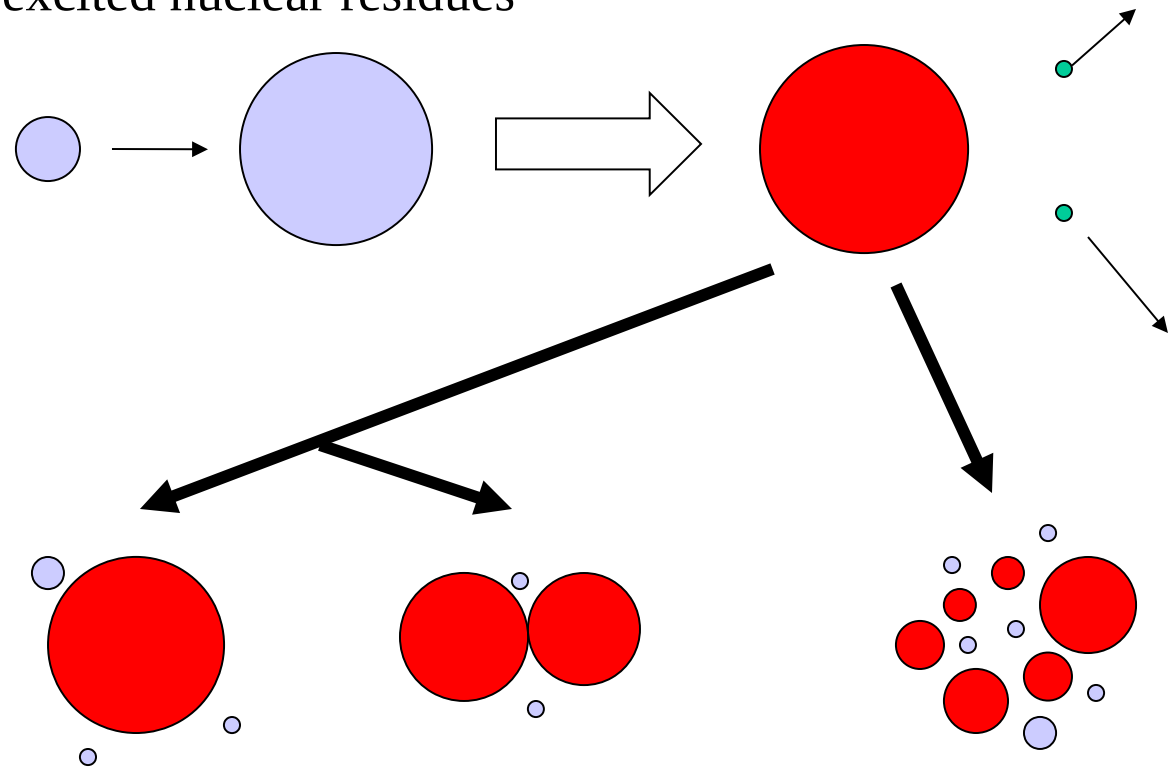

evaporation

fission

multifragmentation

Statistical approach

since 1980-th, conception: statistical freeze-out volume

At high excitation energy E^*>3-4 MeV/nucl there is a simultaneous break-up into many fragments (e.g. microcanonical SMM: Phys.Rep.**257**(1995)133)

Production of large excited nuclear residues in reactions as a result of the peripheral collisions of nuclei, and/or the fusion (central collisions) at low- and intermediate-(Fermi) energies:

Formation of a single excited source after pre-equilibrium emission of light particles. It expands and evolves to the coexistence region of nuclear liquid- and gas-phases, where nuclear fragments are formed.

The mechanism was confirmed by many experimental studies of multifragmentation

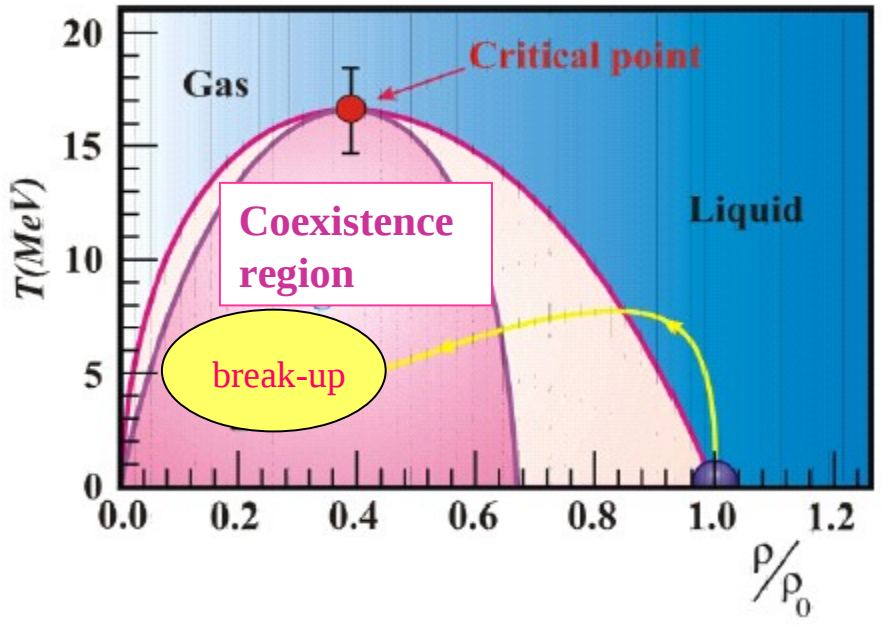

Statistical Multifragmentation Model (SMM)

J.P.Bondorf, A.S.Botvina, A.S.Iljinov, I.N.Mishustin, K.Sneppen, Phys. Rep. **257** (1995) 133

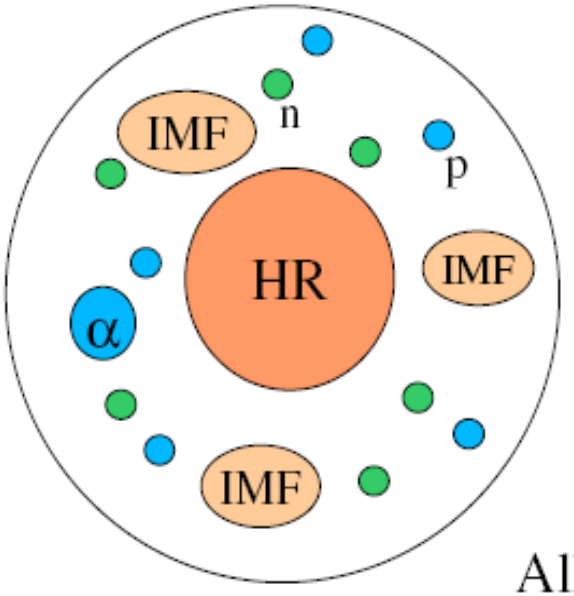

Ensemble of nucleons and fragments
in thermal equilibrium characterized by

neutron number N_0

proton number Z_0, $N_0+Z_0=A_0$

excitation energy $E^*=E_0-E_{CN}$

break-up volume $V=(1+\kappa)V_0$ freeze-out

All break-up channels are enumerated by the sets of fragment multiplicities or partitions, $f=\{N_{AZ}\}$

Statistical distribution of probabilities: $W_f \sim \exp\{S_f(A_0, Z_0, E^*, V)\}$
under conditions of baryon number (A), electric charge (Z) and energy (E*) conservation, including compound nucleus.

The formation of nuclear fragments in collisions of nuclei is a many-body process, there is no a dominating channel. The theoretical explanation requires both dynamical and statistical approaches.

It can be subdivided into two main stages:

1) Dynamical stage leading to the production of new baryons (+ in some cases, lightest nuclei) and to excited equilibrated nuclear systems, e.g., dense nuclear residues and baryonic clusters at the diluted density.

2) Statistical disassembly of the systems consisting of produced baryons (including the nuclear residues/clusters), which leads to the production of final nuclei.

UrQMD PHSD DCM GiBUU

Production mechanisms of nuclear cluster species including anti-matter, hyper-matter in relativistic HI and hadron collisions:

- Production of all kind of particles (anti- , strange, charmed ones) in individual binary hadron collisions. Effects of nuclear medium can be included.
- Secondary interactions and rescattering of new-born particles are taken into account. (Looks as partial ‘thermalization’.)
- Stochastic separation (coalescent-like) of produced baryons into composite (normal. exotic, anti- , hyper-) nuclear species.
- Capture of produced baryons by big excited nuclear residues.

Statistical decay of excited nuclear species into final nuclei

- Multifragmentation into small nuclei (high excitations),
- Evaporation and fission of large nuclei (low excitations),
- (Fermi-) Break-up of small nuclei into lightest ones.

At sub-nuclear density: subdivision of matter into multiple clusters consisting of dynamically produced/spectator baryons, when baryons are close in the phase space (because of the remaining interaction). The clusters are excited, and are in chemical equilibrium leading to the nucleation inside clusters. This case can be realized in Heavy- Ion collisions of medium/high energies.

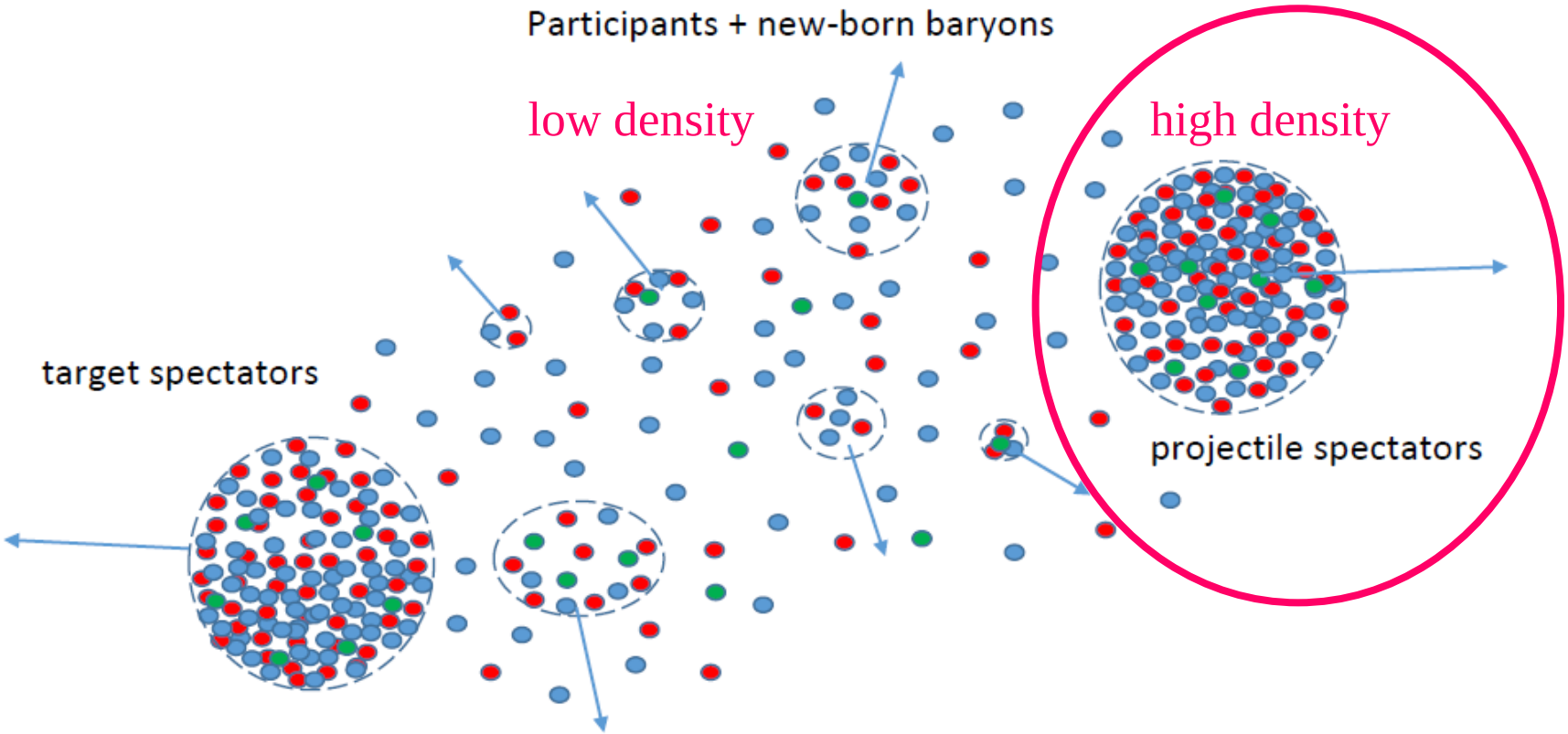

Production of large nuclear fragments in reaction initiated by high energy light particles and in peripheral nucleus-nucleus collisions:

Formation of excited nuclear residues (projectile/target) after the dynamical stage.

Multifragmentation in intermediate and high energy nuclear reactions

Experimentally established:

1) few stages of reactions leading to multifragmentation,
2) short time ~100fm/c for primary fragment production,
3) freeze-out density is around $0.1\rho_0$,
4) high degree of equilibration at the freeze-out,
5) primary fragments are hot.

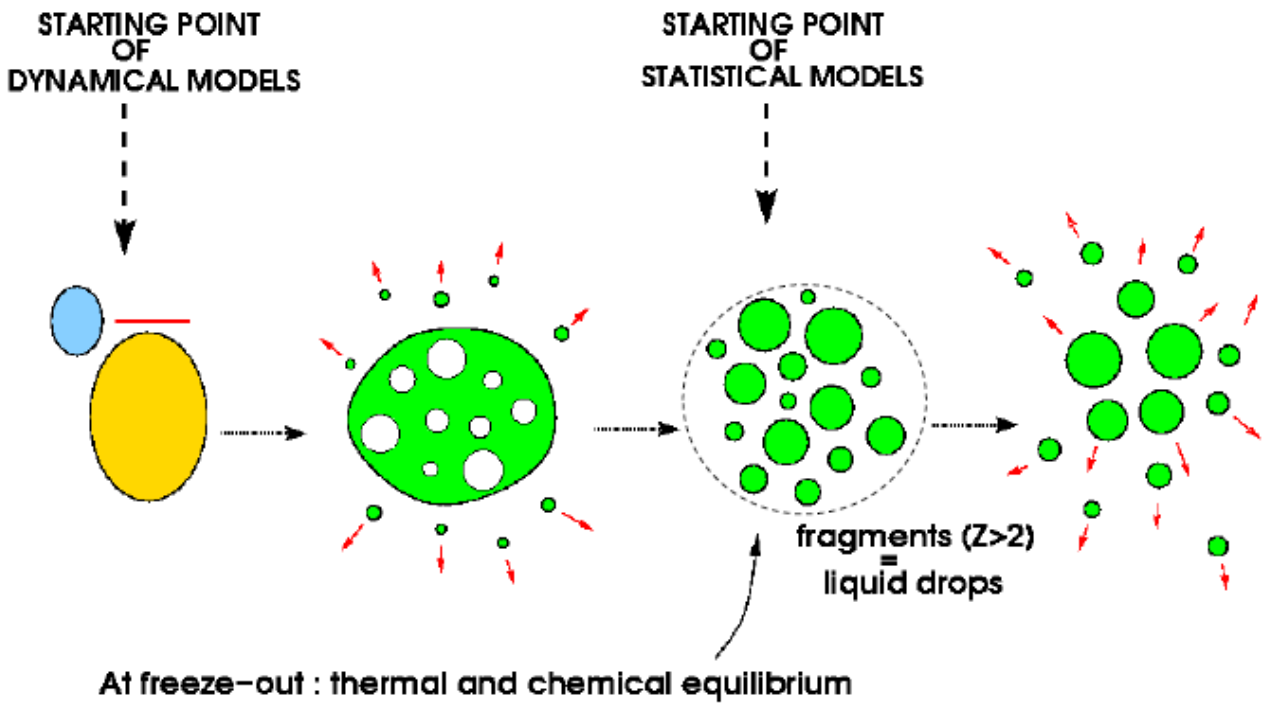

Two-stage multifragmentation of 1*A* GeV Kr, La, and Au

EOS collaboration: fragmentation of relativistic projectiles

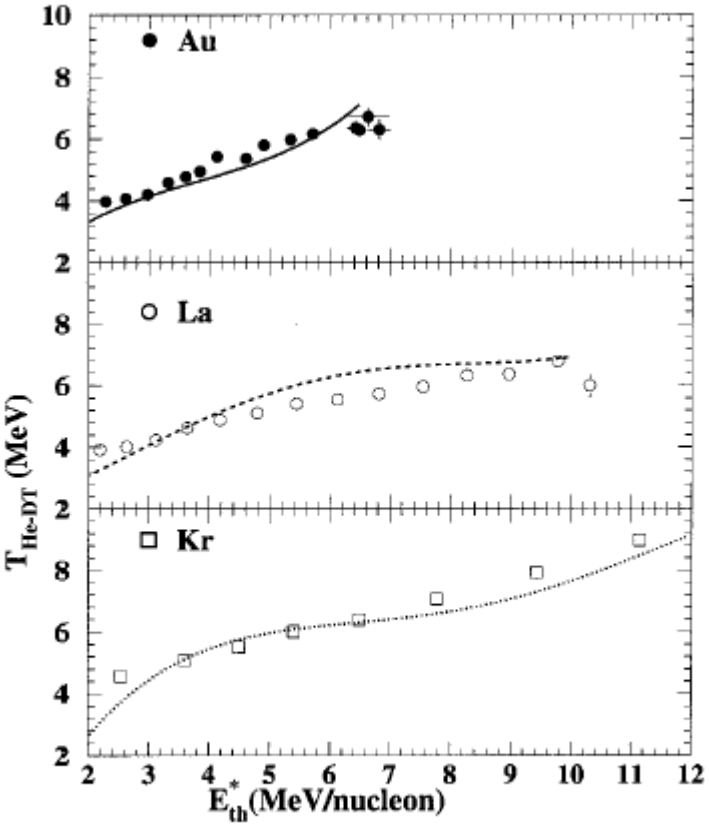

FIG. 19. Caloric curves (T_f vs E^*_{th}/A) for Kr, La, and Au. Points are experimental and curves are from SMM.

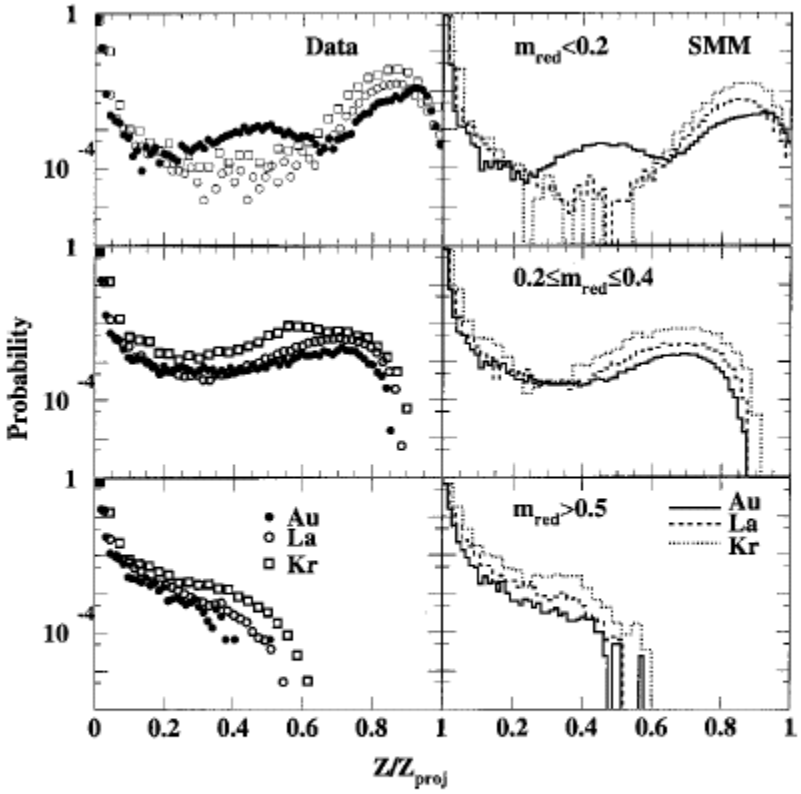

FIG. 24. Second stage fragment charge distribution as a function of $Z/Z_{\text{projectile}}$. Results are shown for three reduced multiplicity intervals for both data and SMM.

R.Ogul et al. PRC **83,** 024608 (2011) **ALADIN@GSI**

Isospin-dependent multifragmentation of relativistic projectiles

124,107-**Sn**, 124-**La** (600 A MeV) + **Sn** → projectile (multi-)fragmentation

Very good description is obtained within Statistical Multifragmentation Model, including fragment charge yields, isotope yileds, various fragment correlations.

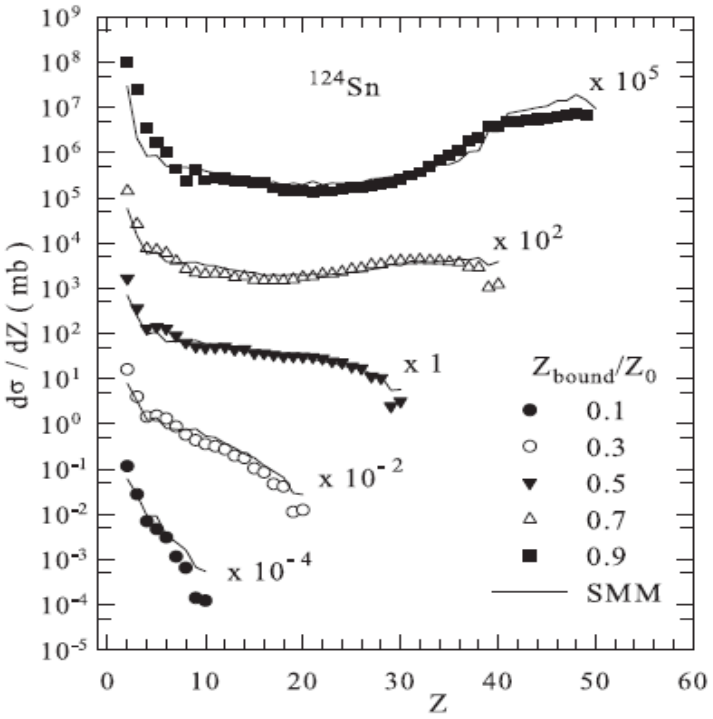

Statistical (chemical) equilibrium is established at break-up of hot projectile residues ! In the case of strangeness admixture we expect it too !

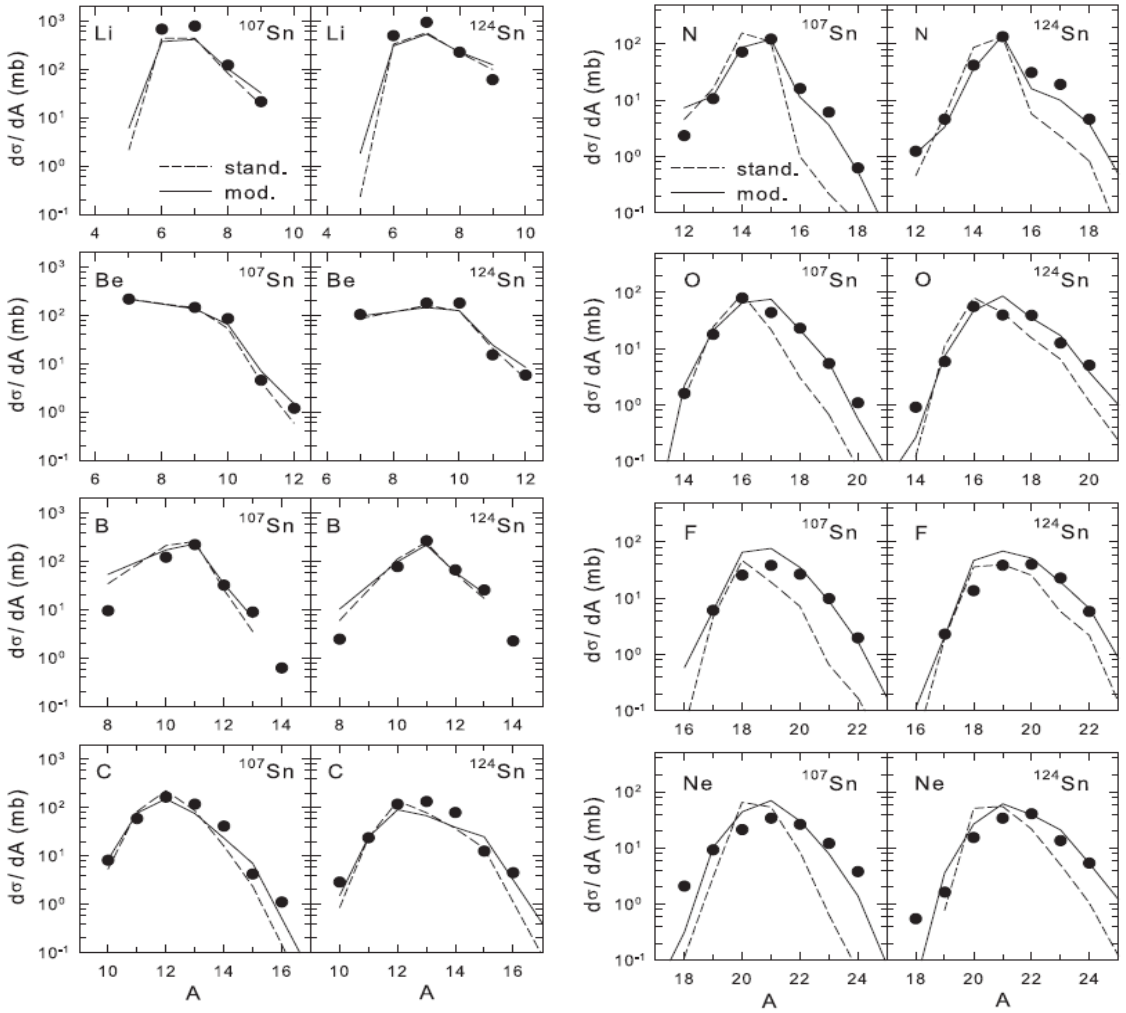

ALADIN data

GSI

multifragmentation of relativistic projectiles

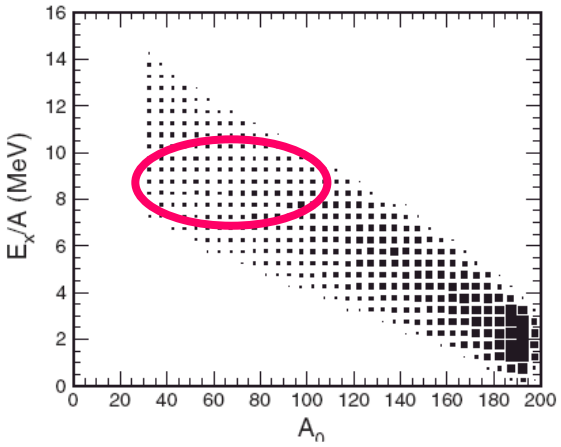

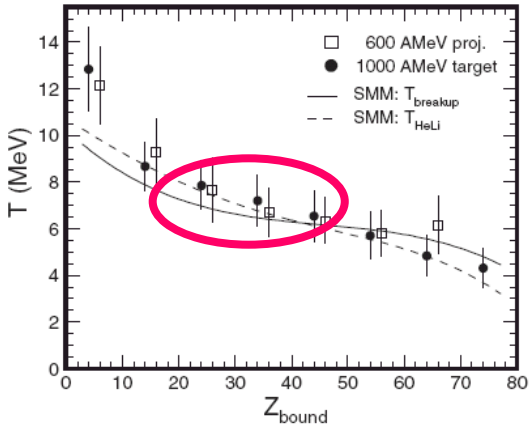

Au(600MeV/n)+C,Al,Cu

A.S.Botvina et al.,
Nucl.Phys. A584(1995)737

H.Xi et al.,
Z.Phys. A359(1997)397

comparison with SMM (statistical multifragmentation model)

Statistical equilibrium has been reached in these reactions

Au(600MeV/n)+Cu

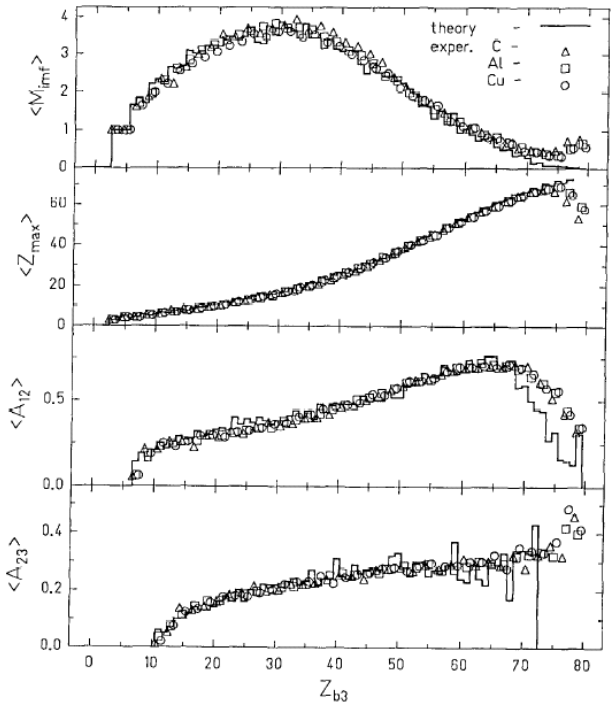

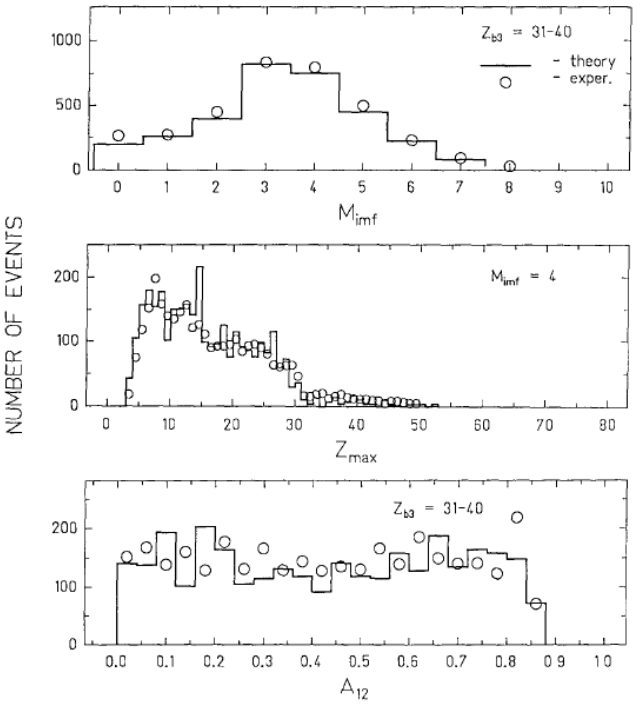

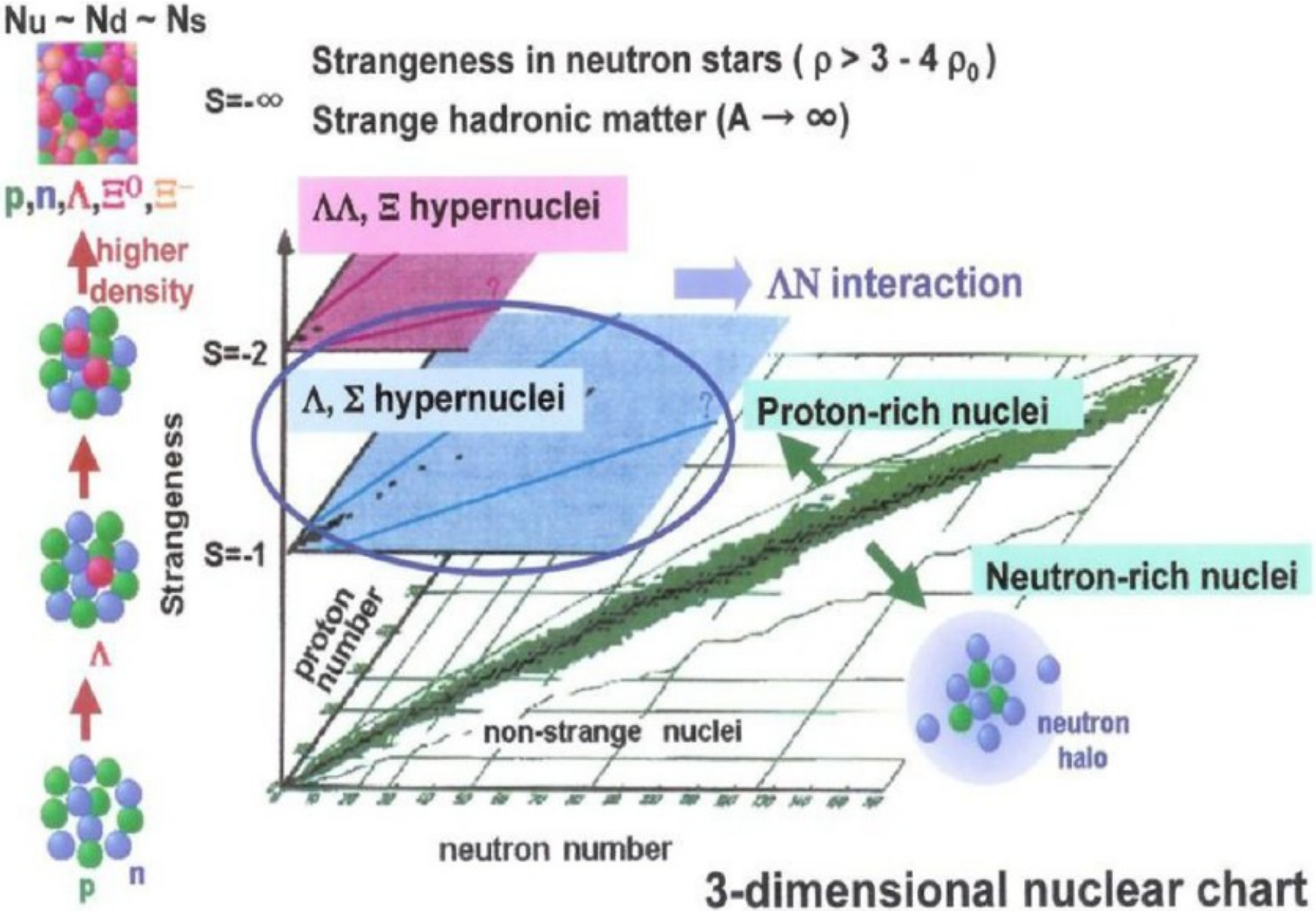
Nu ~ Nd ~ Ns
Strangeness in neutron stars (ρ > 3 - 4 ρ0)
S=-∞
Strange hadronic matter (A → ∞)
p,n,Λ,Ξ0,Ξ−
higher density
ΛΛ, Ξ hypernuclei
ΛN interaction
S=-2
Λ, Σ hypernuclei
Proton-rich nuclei
S=-1
Neutron-rich nuclei
Strangeness
proton number
non-strange nuclei
neutron halo
neutron number
Λ
p
n
3-dimensional nuclear chart

All transport modes predict similar picture: baryons can be produced at all rapidities, in participant and spectator kinematic regions.

Wide rapidity distribution of produced Λ!

Calculation: DCM
PRC**84**(2011)064904

S.Albergo et al.,
E896:
PRL88(2002)062301

Au(11AGeV/c)+Au

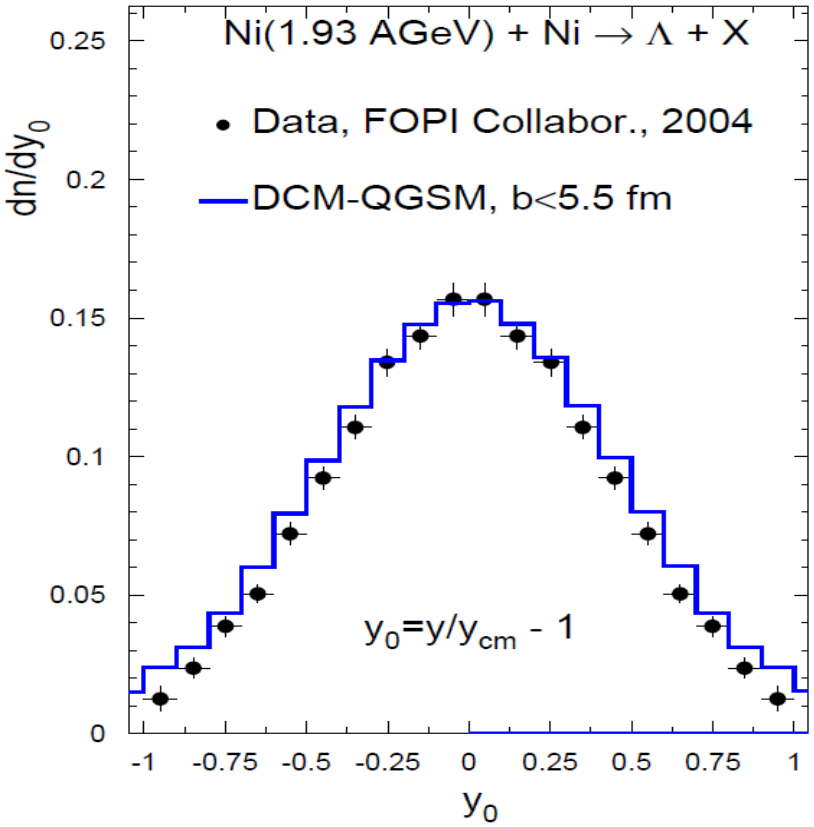

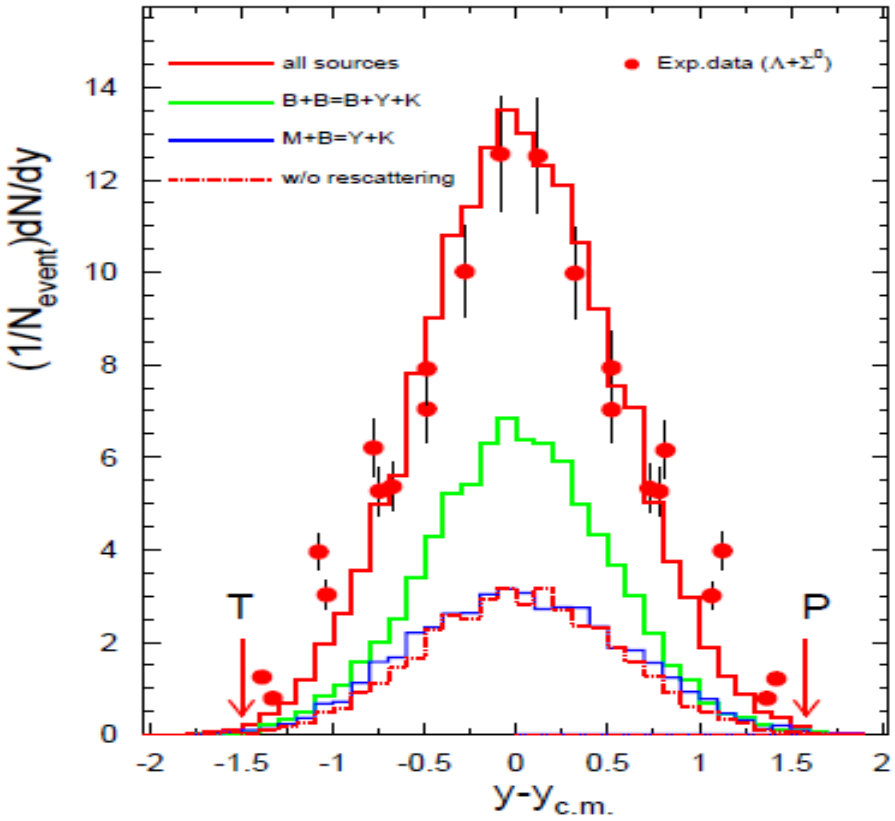

A.S.Botvina and J.Pochodzalla, Phys. Rev.C76 (2007) 024909

Generalization: statistical de-excitation model for nuclei with Lambda hyperons

In these reactions we expect analogy with

multifragmentation in intermediate and high energy nuclear reactions

+ nuclear matter with strangeness

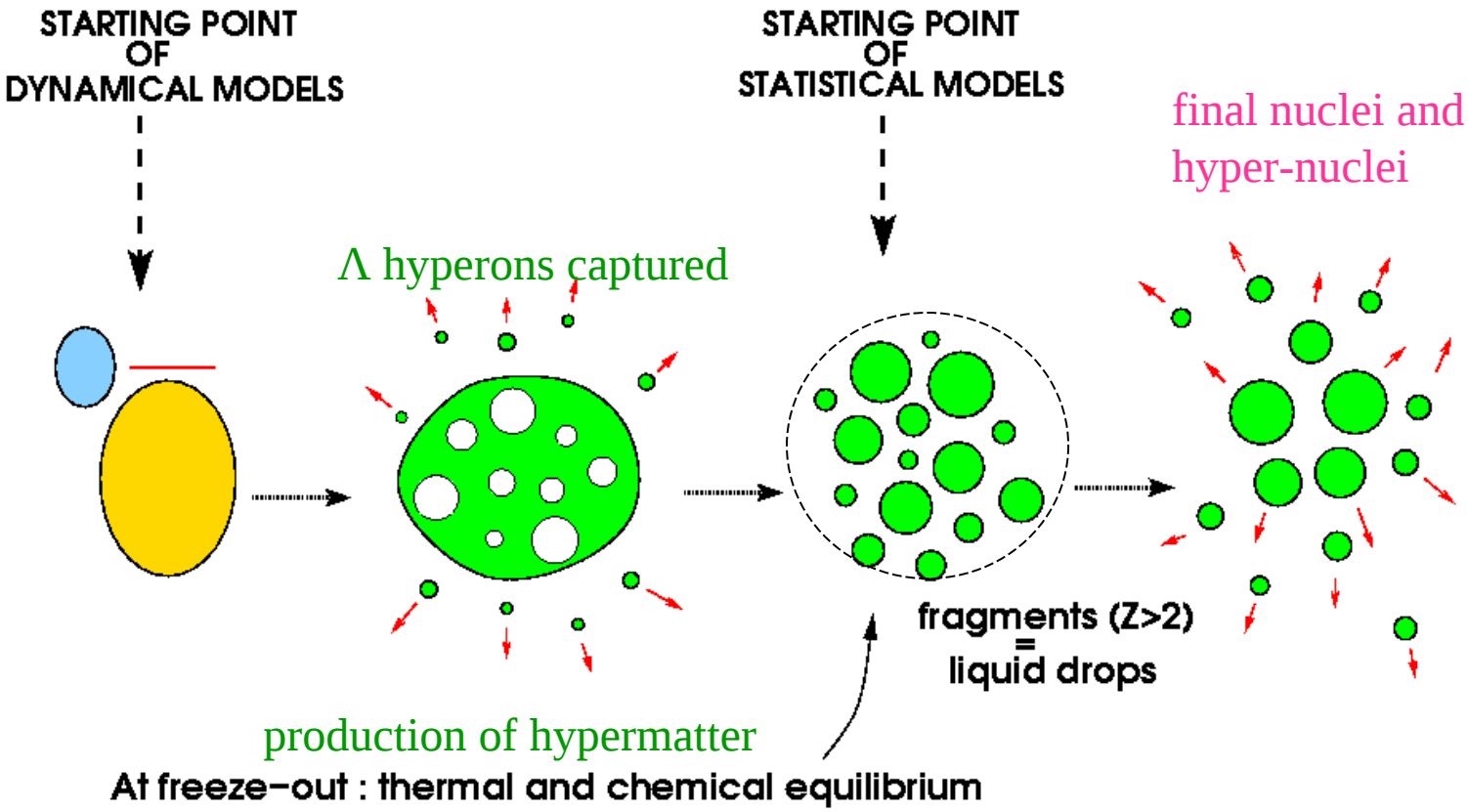

Production of excited hyper-residues in peripheral collisions, decaying into hypernuclei (target/projectile rapidity region).

DCM and UrQMD + CB predictions: Phys. Rev. C95, 014902 (2017)

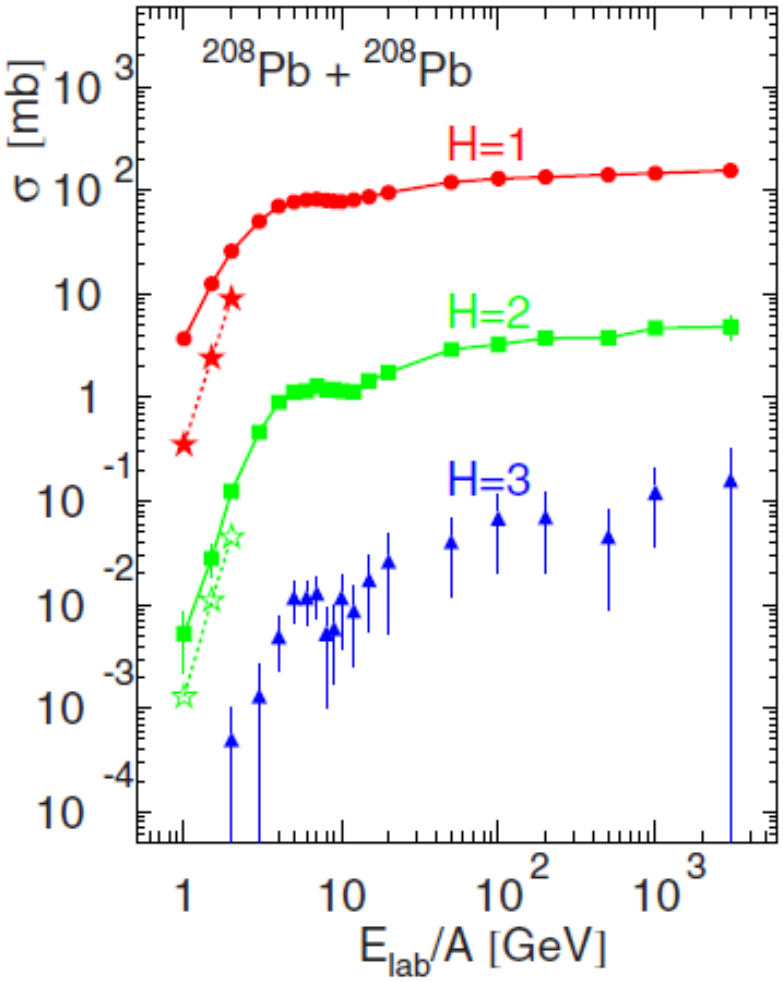

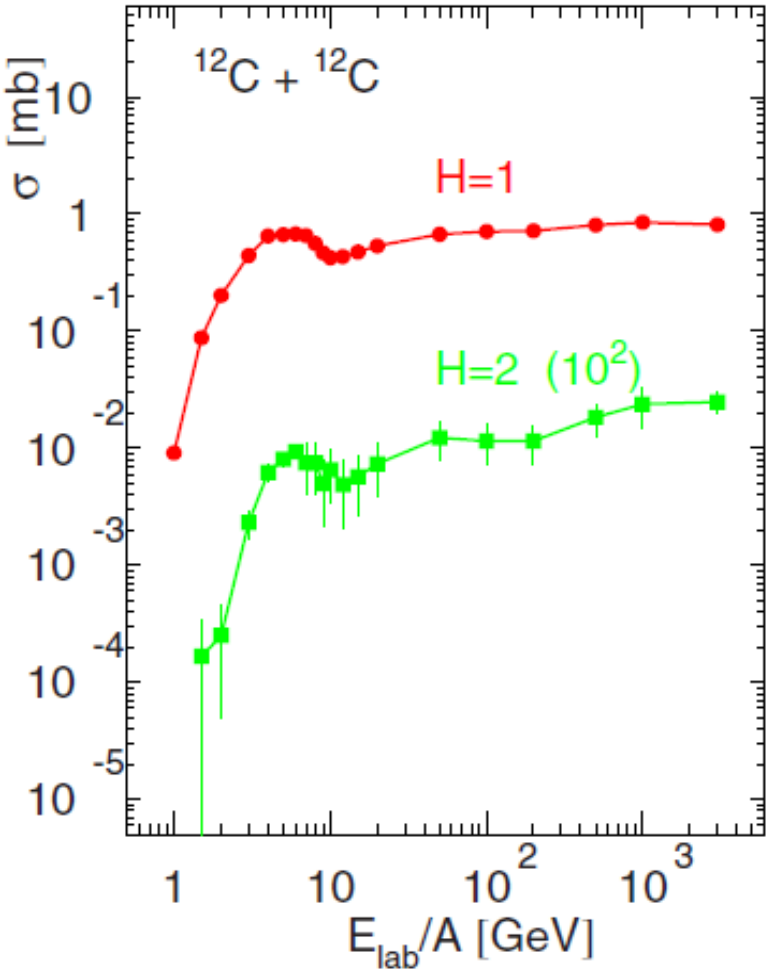

Production of light hypernuclei in relativistic ion collisions

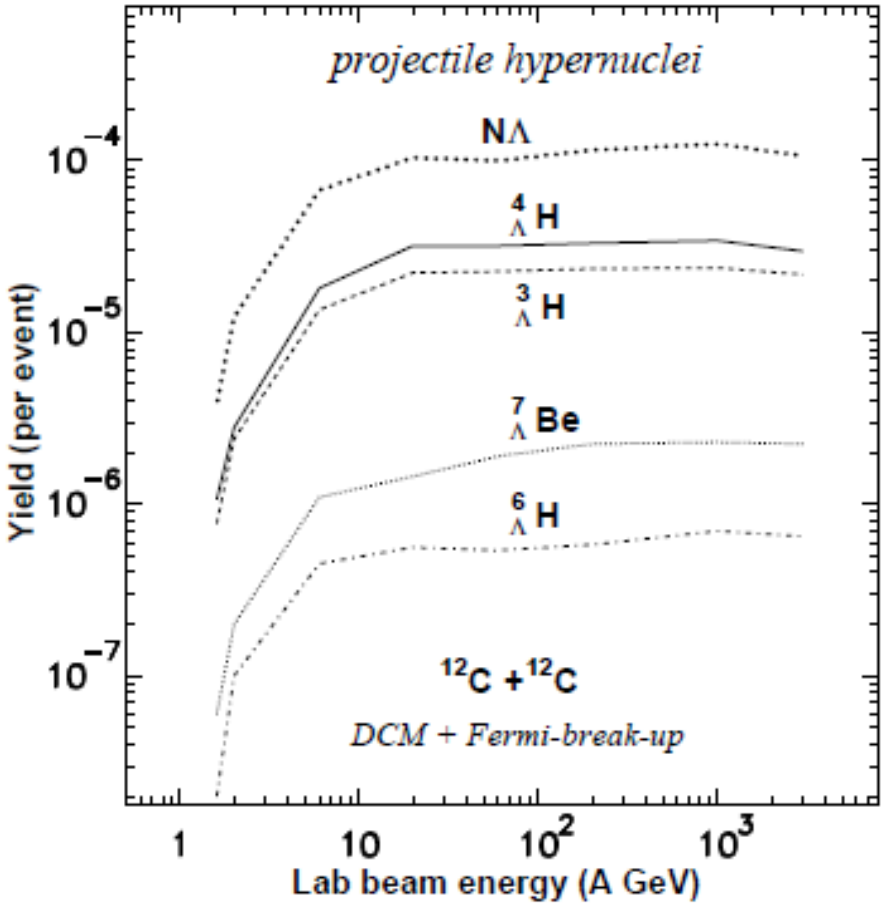

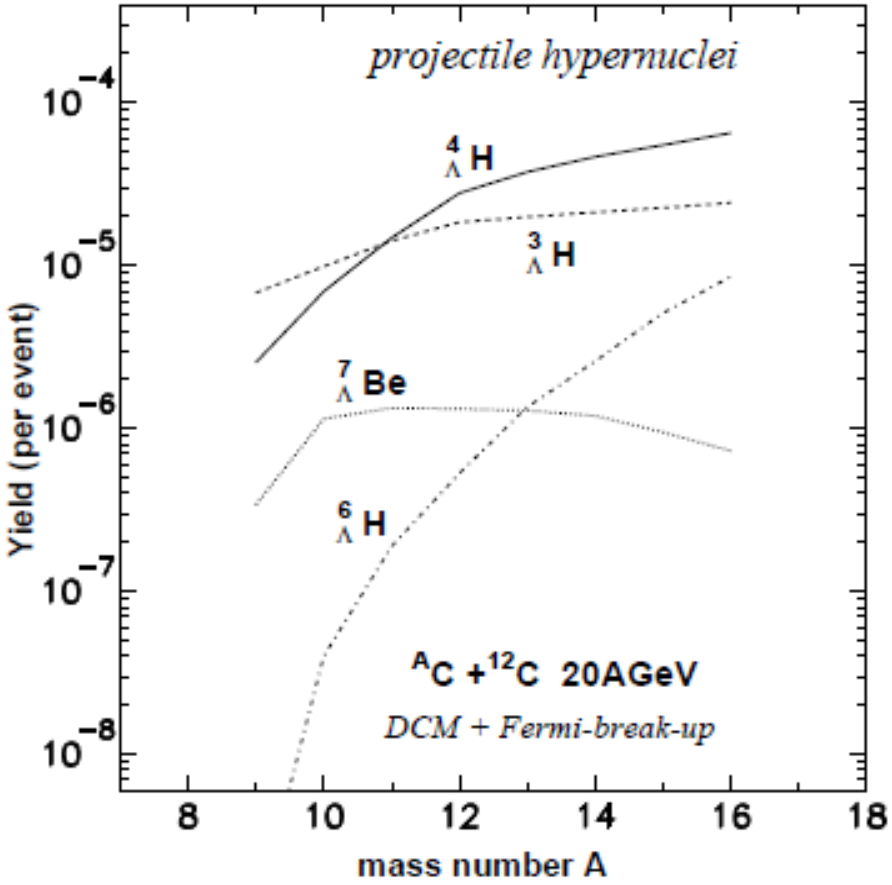

One can use exotic neutron-rich and neutron-poor projectiles, which are not possible to use as targets in traditional hyper-nuclear experiments, because of their short lifetime. Comparing yields of hypernuclei from various sources we can get info about their binding energies and properties of hyper-matter.

A.S.Botvina, K.K.Gudima, J.Pochodzalla, PRC 88, 054605, 2013

At sub-nuclear density: subdivision of matter into multiple clusters consisting of dynamically produced/spectator baryons, when baryons are close in the phase space (because of the remaining interaction). The clusters are excited, and are in chemical equilibrium leading to the nucleation inside clusters. This case can be realized in Heavy- Ion collisions of medium/high energies.

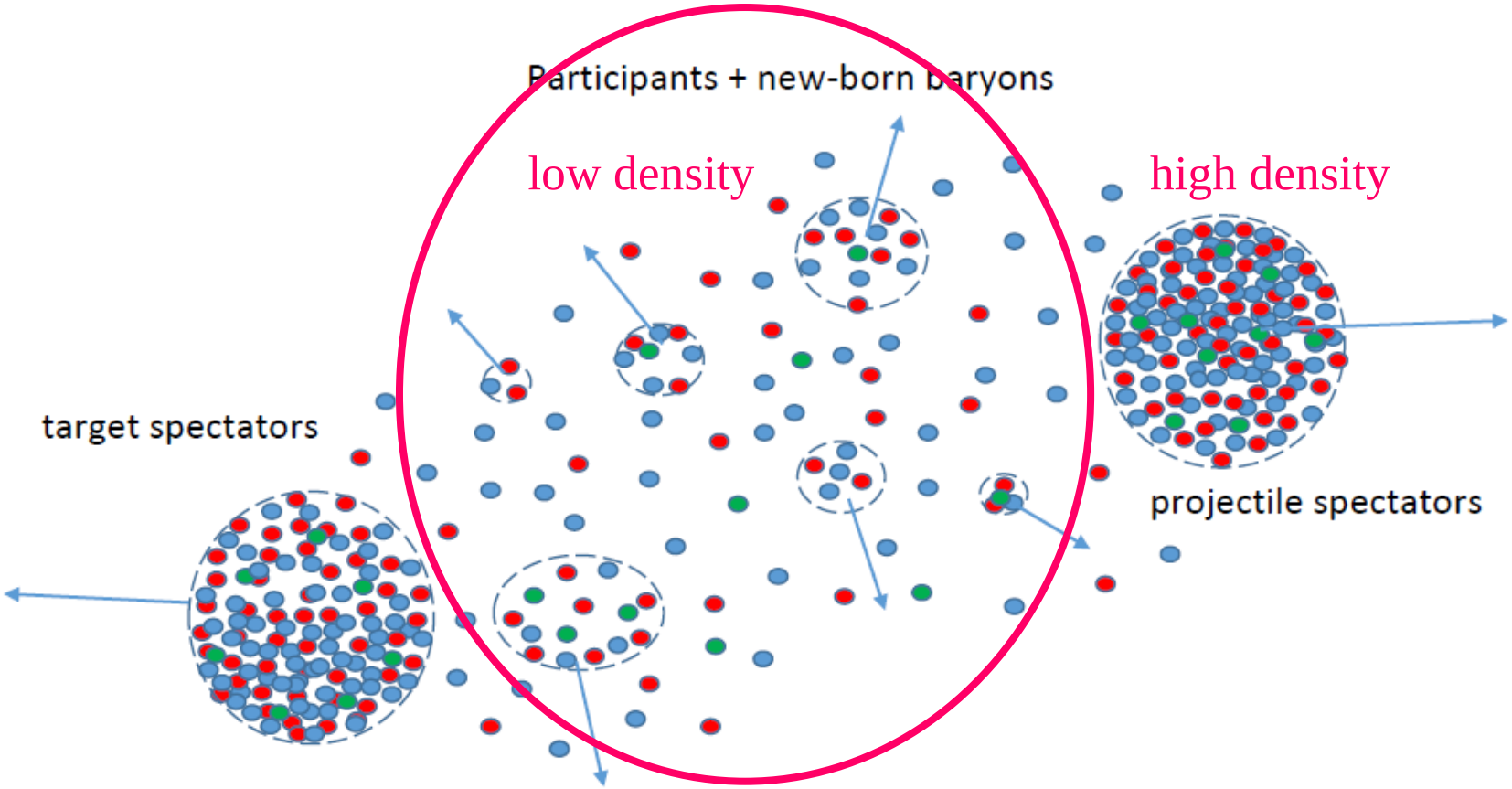

CENTRAL COLLISIONS: formation of excited isotropic nuclear matter

Nuclear system expands to low densities and passes the density around 0.1 of normal nuclear density, which corresponds to the freeze-out adopted in the statistical models. Baryons can still interact and form nuclei at this density. We divide the nuclear matter into clusters in local chemical equilibrium and apply SMM to describe the nucleation process in these clusters.

dynamical expansion after collision/compress.

Baryonic clusters in local equilibrium (freeze-out)

nuclei formation inside the clusters - SMM

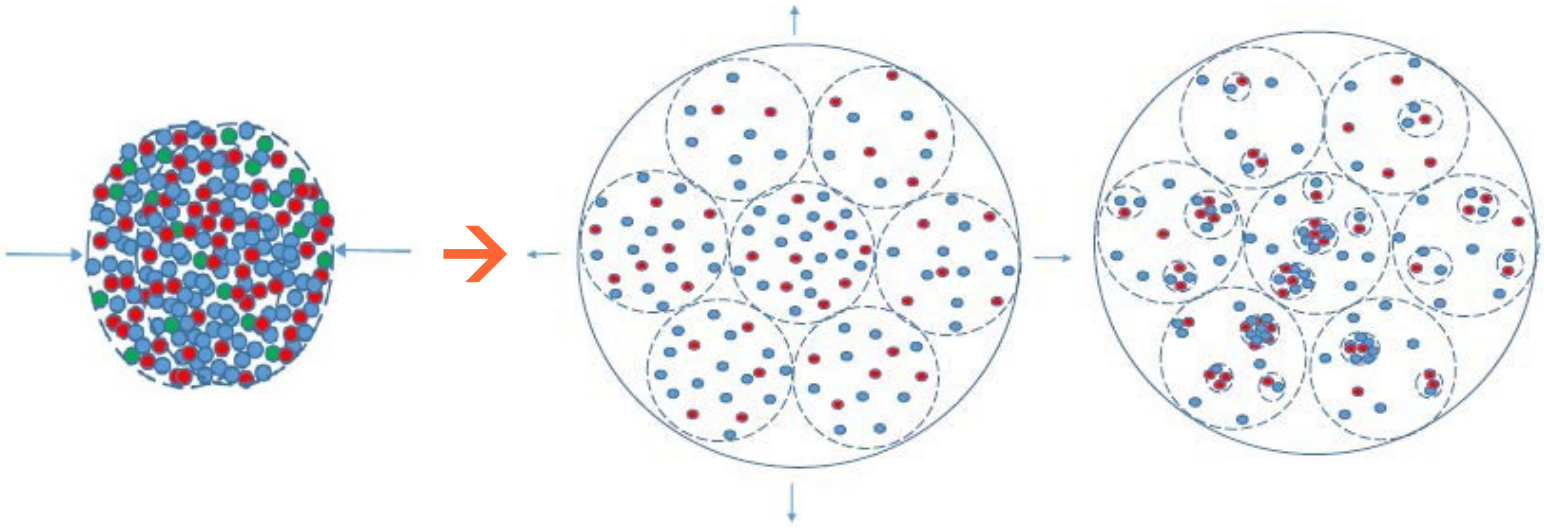

CENTRAL COLLISIONS: one can apply the special selection of events of nucleus-nucleus collisions (e.g., ERAT criterion in FOPI experiment). This selection can also require the special model application.

To describe the nuclei formation with controlled models:

Phys.Rev.C103 (2021) 064602 + Phys.Rev.C106 (2022) 014607

Besides UrQMD the dynamical stage is simulated with the phase space generation (PSG) . They provide very different momenta distributions of baryons which cover the most important limits expected after this stage.

Selection of primary clusters (at low freeze-out density) by using the clusterization of baryon (CB) model (Phys. Lett. B742, 7 (2015)): according to their velocities $|Vi - V0| \le Vc$ and coordinates $|Xi - X0| \le Xc$.

Statistical formation of nuclei inside these clusters with SMM: de-excitation of the excited clusters. The excitation energy (or local temperature) of such clusters is important characteristics for the nuclear matter corresponding to coexistence region of NLGPhT.

Baryon distributions (UrQMD and PSG) and baryonic clusters (CB) calculated for central collisions Au + Au at 3A GeV

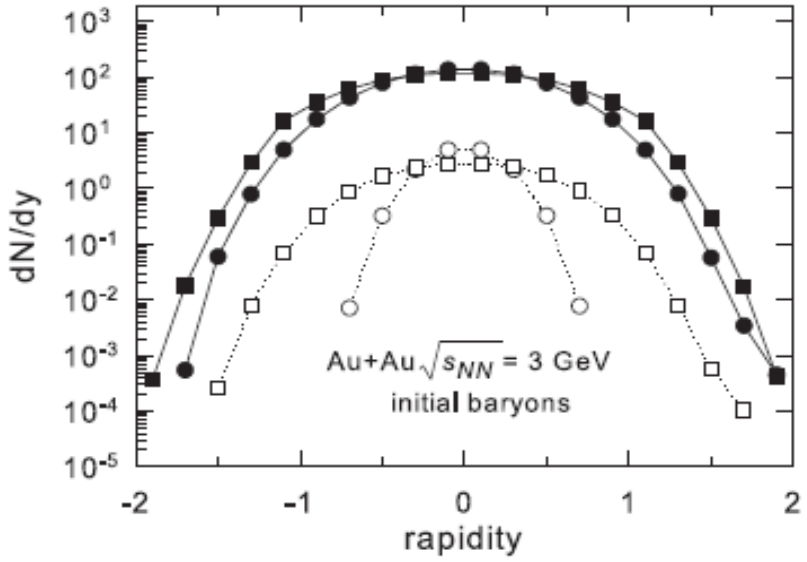

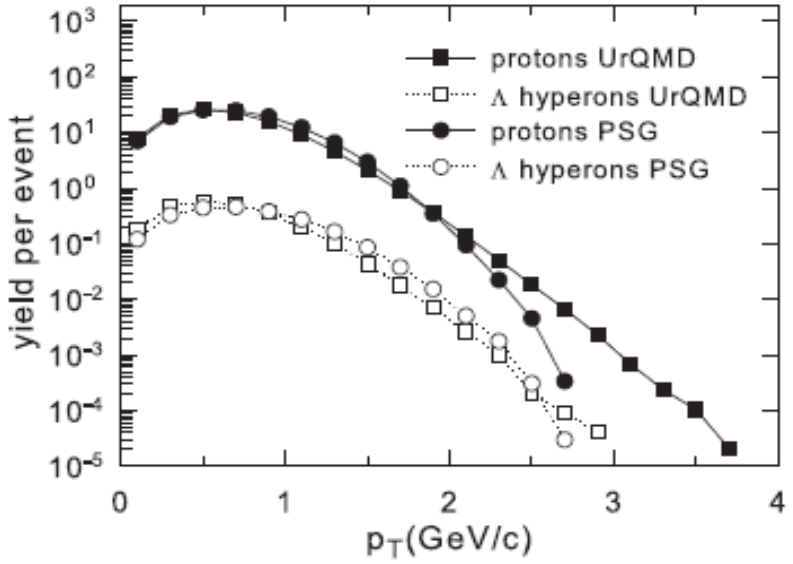

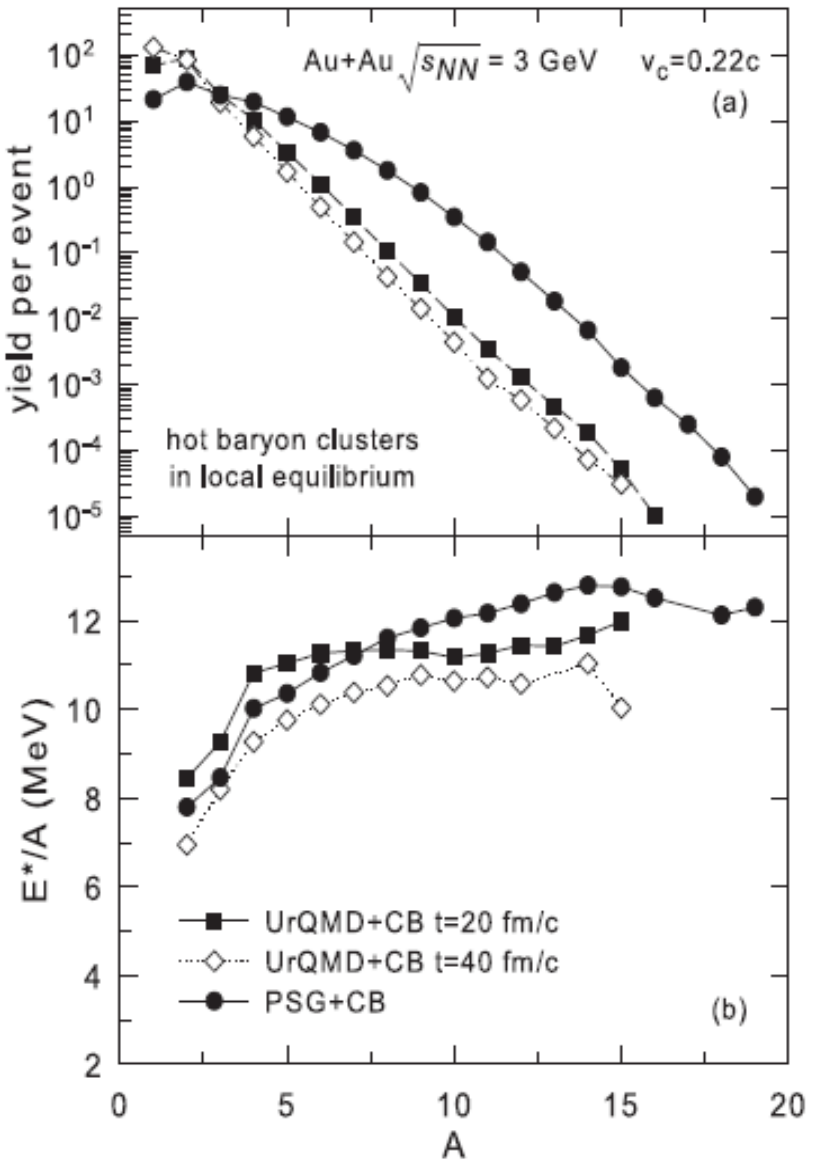

For the first, the consistent comparison with FOPI@GSI experimental data - Nucl. Phys. A848(2010)366 - on fragment production in central HI collisions is performed: Both charge yields and flow energies.
Phys.Rev.C103(2021)064602 and Phys.Rev.C106(2022)1014607

yields of nuclei in different reactions:

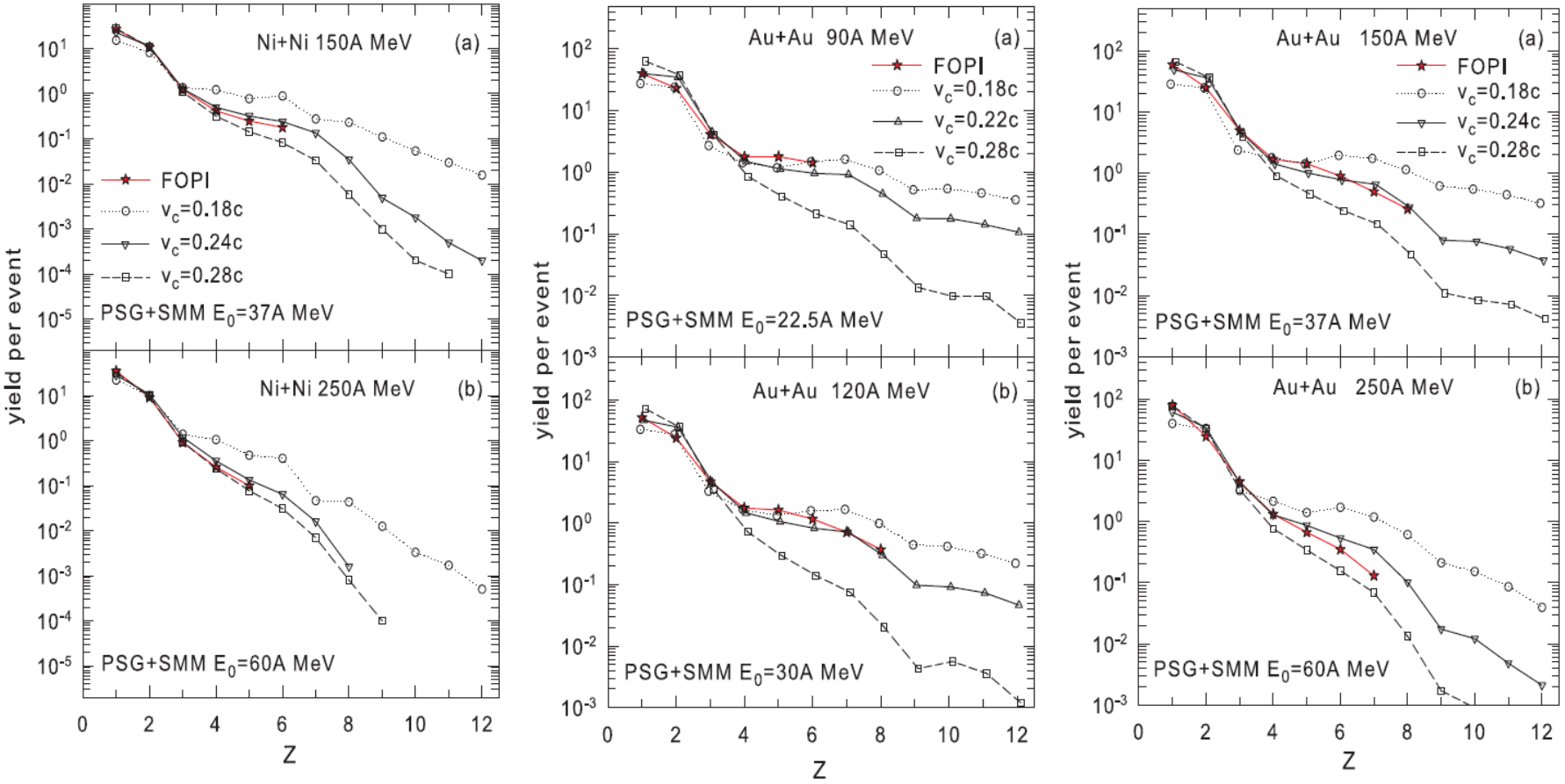

(until now the production of nuclei (Z>2) in central collisions was not possible to describe consistently under assumption of global chemical equilinrium)

kinetic energies of nuclei in different reactions:

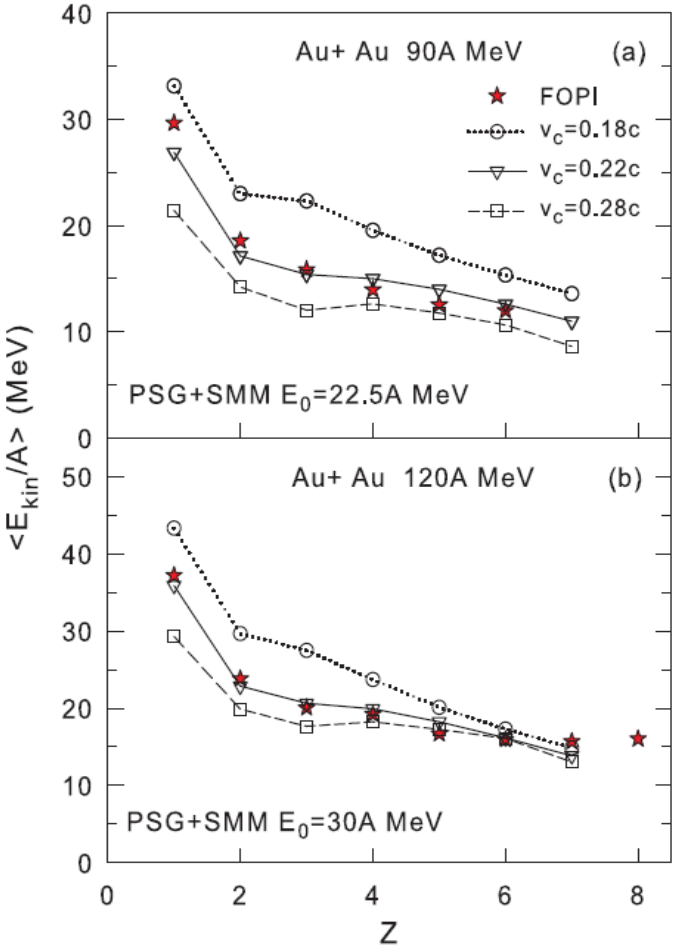

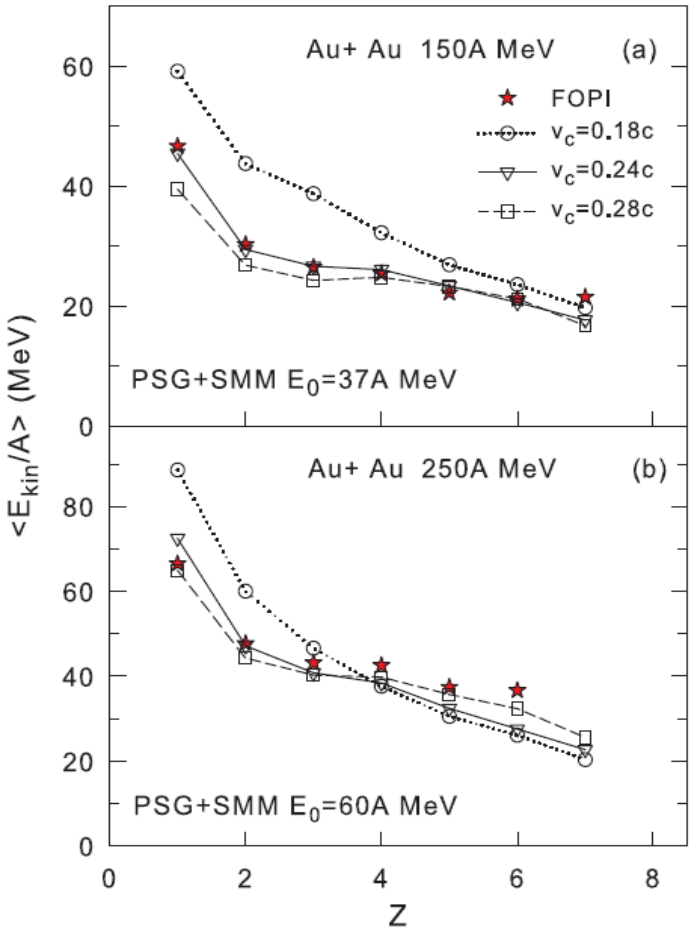

Important beam energy dependence of the light nuclei yields in Au+Au relativistic central collisions can be explained within our approach too.

Note: in simplistic coalescence picture yields of 3He are larger than 4He yields at all energies. FOPI experimental data (red symbols) show intersection with increasing energy.

Relative behavior of yields of 3He and 4He with energy is important confirmation of the nucleation via decay of local statistical sources

Phys.Rev.C103 (2021) 064602

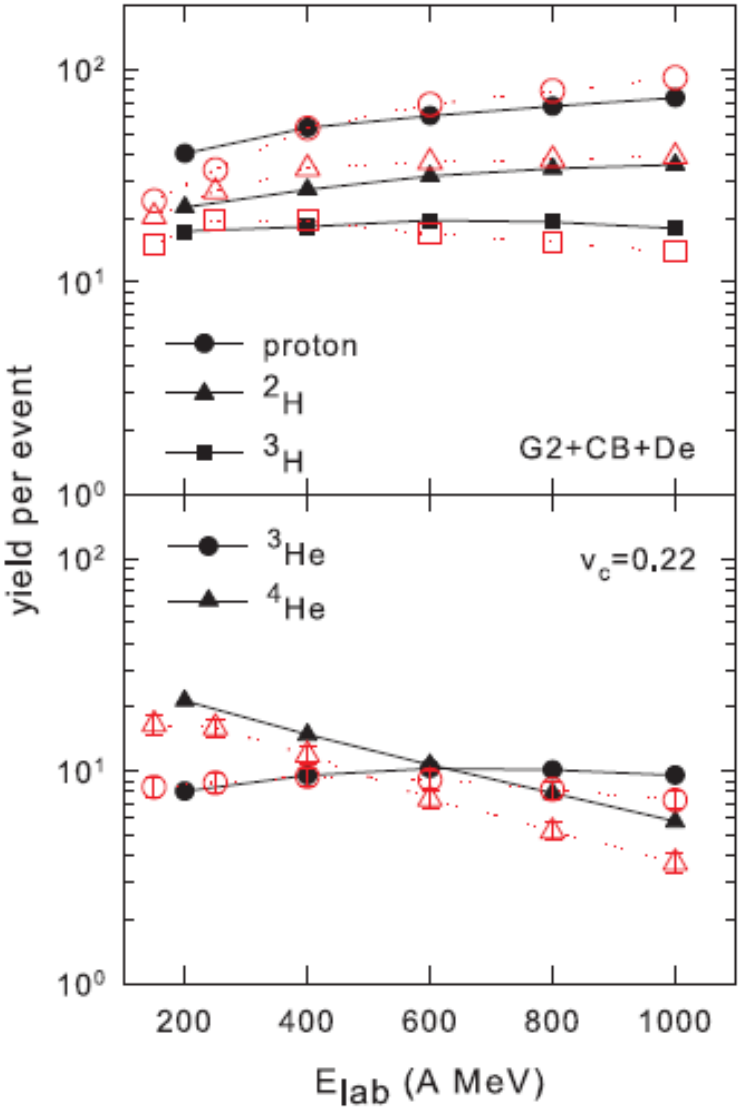

However, the description is possible if there is a limit for the excitation energy of the clusters: 6–10 MeV/nucleon, close to their binding energies. Temperature T=6--8 MeV (according to the statistical model) which corresponds to the coexistence region of the liquid-gas type phase transition in nuclear matter.

We may speak about an universal mechanism for nuclei formation both in peripheral and central heavy-ion collisions , independently on the way how the low density matter is produced: by thermal-like expansion of the excited residues (peripheral col.) or by dynamical-like expansion (central col.)

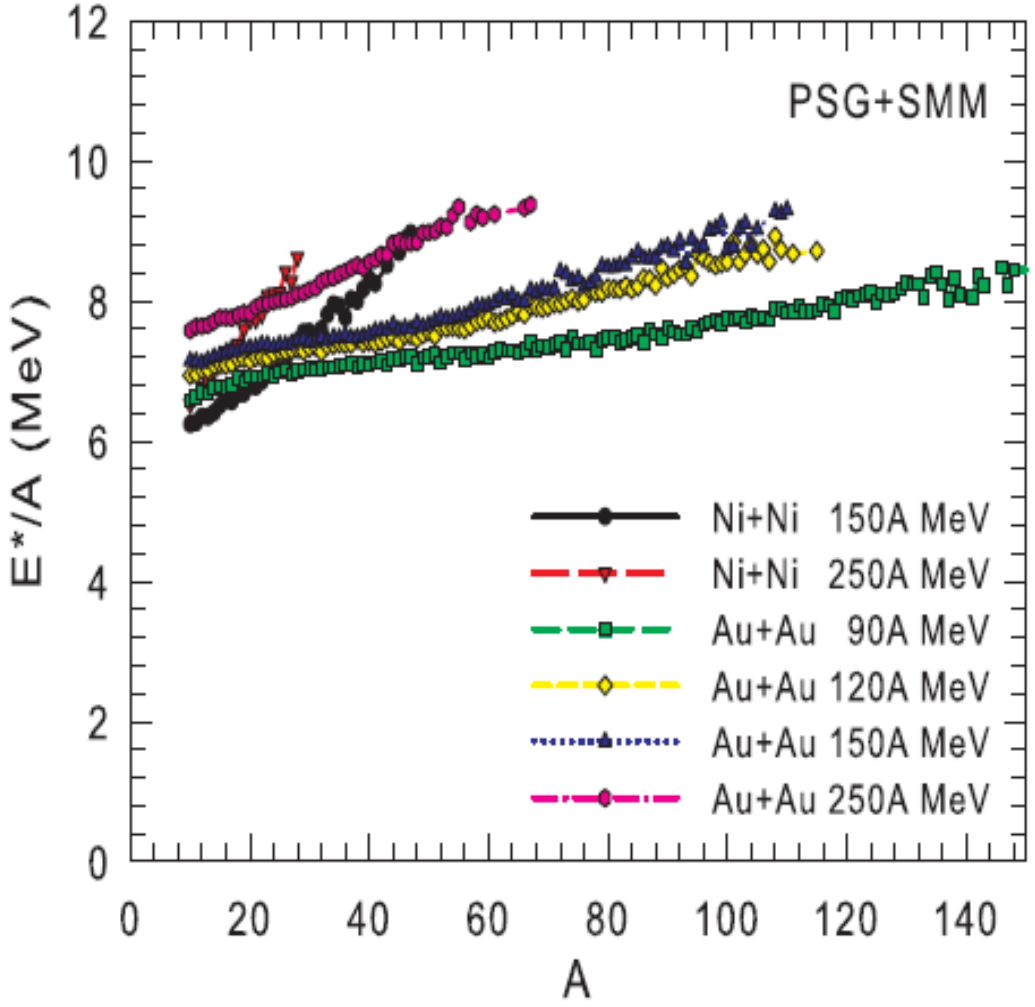

Conclusion on the nuclei production (disintegration of excited nuclei, or nucleation of individual baryons) described with the statistical approach:

Evolution of the statistical mechanism toward highly excited finite nuclear systems -

Compound nucleus conception – excitation energies from 0 to 2-3 MeV/nucleon

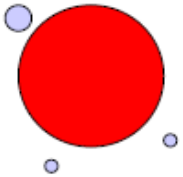

Freeze-out volume conception – excitation energies from 2-3 to around 8-10 MeV/nucleon

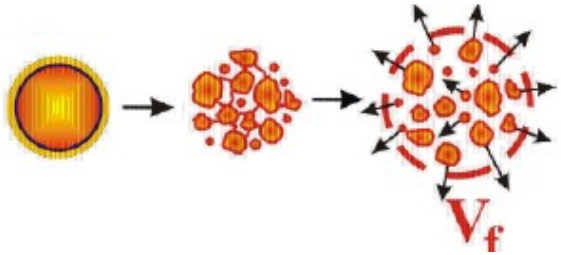

At energies more than 8-10 MeV/nucleon – fragmentation of the expanding nuclear matter at low density into locally equilibrated clusters with moderate energies (around 8-10 MeV/nucleon) and nucleation (nucleosynthesis) in such clusters

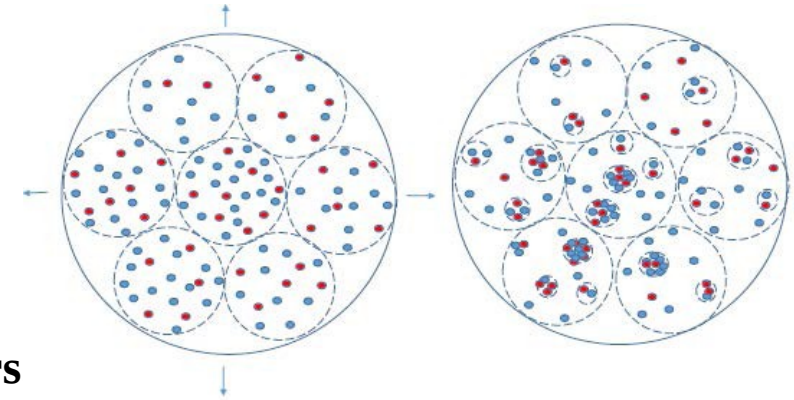

Hypernuclei yields in central collisions (Au+Au, 3AGeV) - comparison with **STAR** experiment (PRL,**128**(2022)202301): PRC, 108, 054904 (2023)

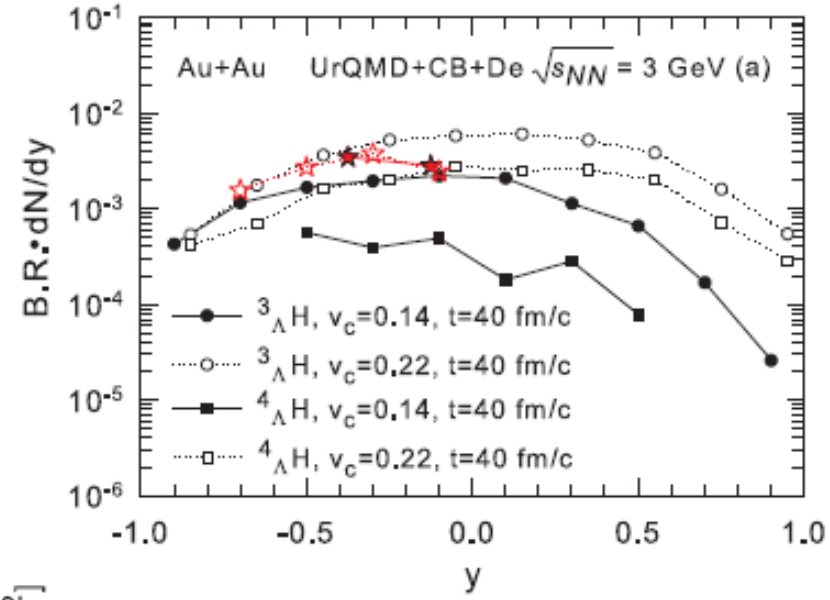

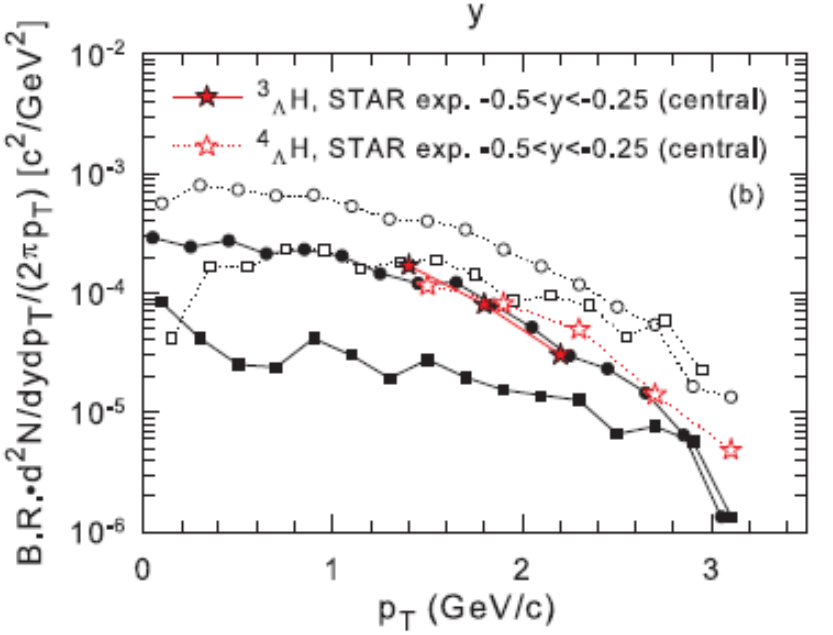

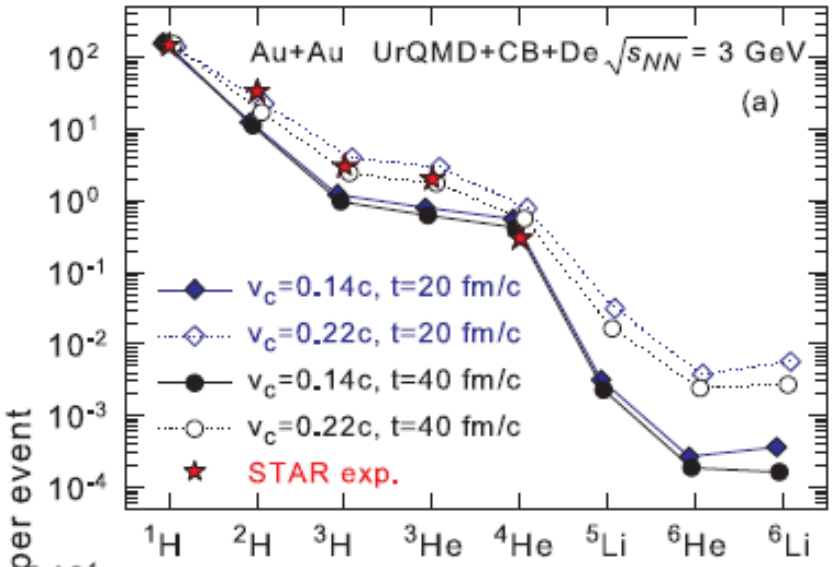

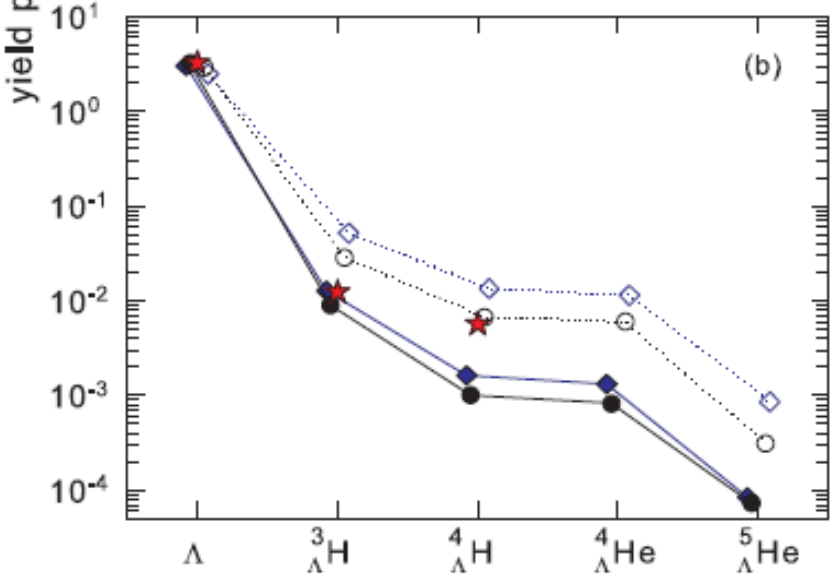

Advantage of relativistic HI collisions:
Abundant yield of exotics and double strange hypernuclei: NNΛ , ΛΛ (H-dibaryons) and others, which are difficult to produce in conventional hypernuclear experiments,

HI collisions produce hypermatter and allow for the investigation of the hyperon and nucleon interaction: There is a hyper-nucleosynthesis at low (subnuclear) density.

Correlations between particle are necessary to measure, to reveal the nucleation mechanism.

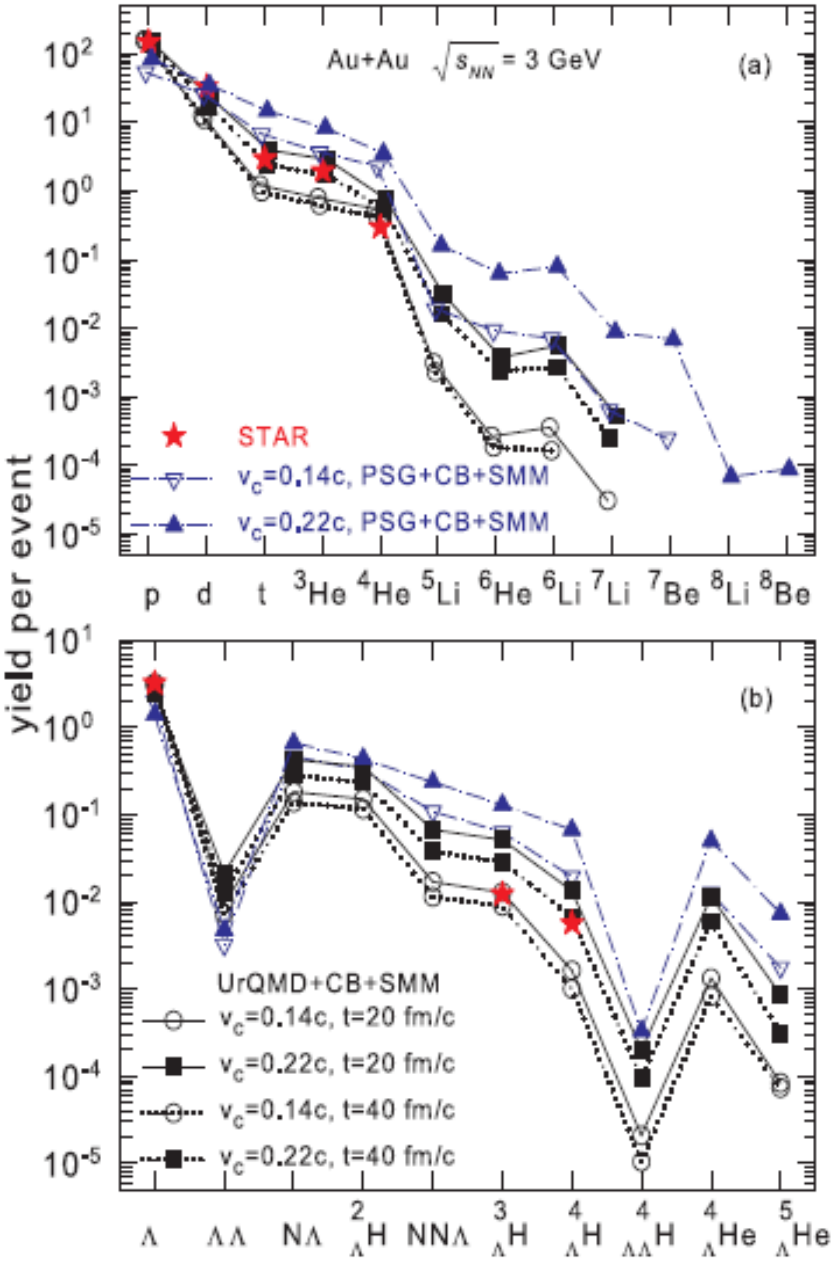

Production of hypernuclei in HI central collisions (GSI energy)

Basing on this general mechanism we can predict the hypernuclei yields in relativistic central collisions too. Many different light hypernuclei can be produced. The correlations between nuclear species exist and it can be used for their identification.

Phys.Rev.C103 (2021) 064602

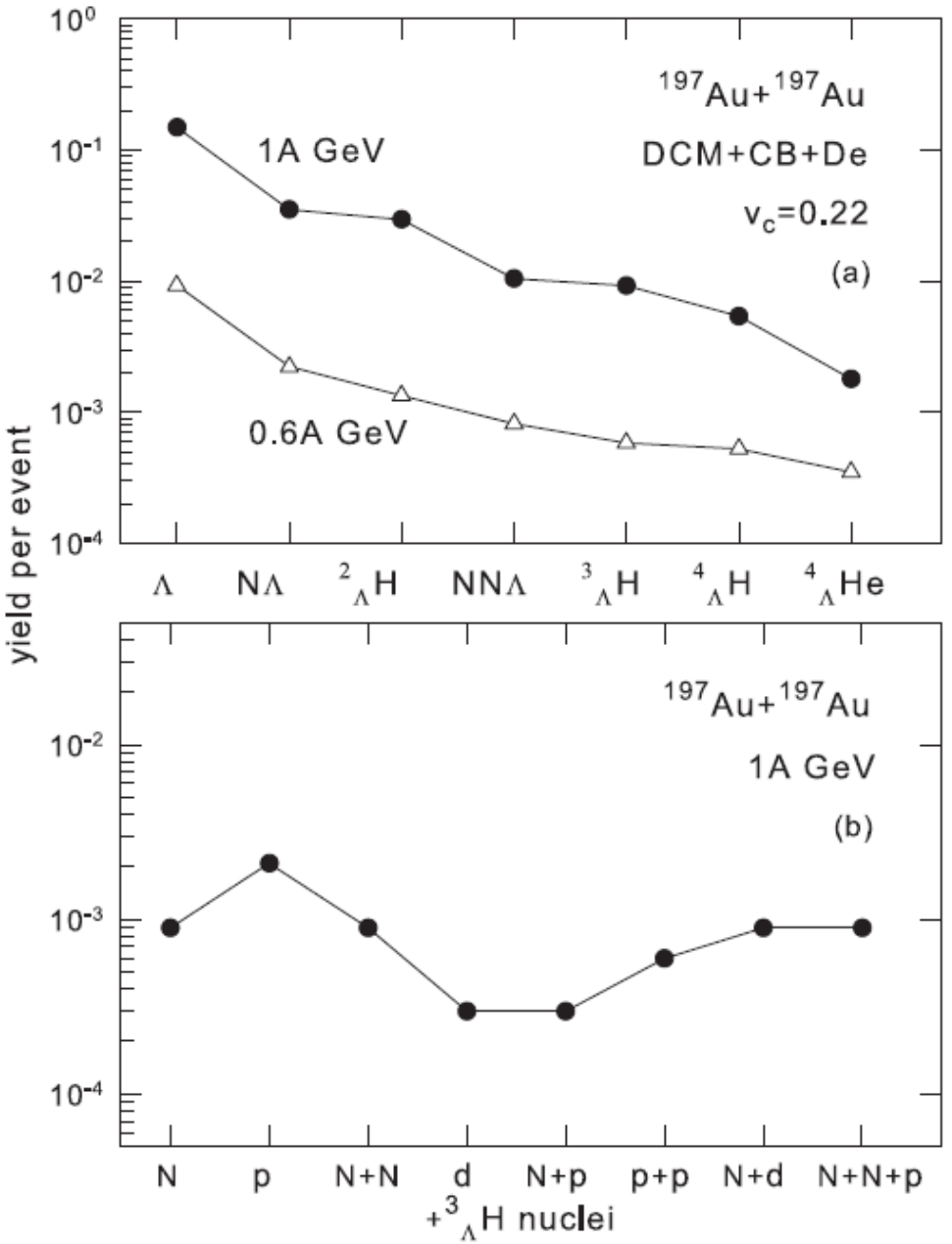

Conclusions

Collisions of relativistic ions are promising reactions leading to the nucleosynthesis of nuclei, exotic clusters with very different isospin, including hypernuclei. One can describe the process via the dynamical production of baryons and statistical nucleosynthesis.

Mechanisms of formation of hypernuclei in reactions: Strange baryons (Λ, Σ, Ξ, …) produced in particle collisions can be transported to the spectator residues and captured in nuclear matter. Another mechanism is the nucleation of baryons at subnuclear density. It leads to light clusters and is effective at all rapidities. Novel mechanism: The matter is subdivided into excited baryon clusters in local equilibrium and after the cluster decay the nuclei and hypernuclei of all sizes (and isospin), including short-lived weakly-bound states, multi-strange nuclei can be produced.

Advantages over other reactions: there is no limit on sizes and isotope content of produced exotic nuclei; probability of their formation may be high; a large strangeness can be deposited in nuclei.

Properties of hypernuclei (hyperon binding) can be addressed in novel way!

Correlations (unbound states) and lifetimes can be naturally studied.

EOS of hypermatter at subnuclear density and hyperon interactions in exotic nuclear matter can be investigated.

Additional slides for discussion:

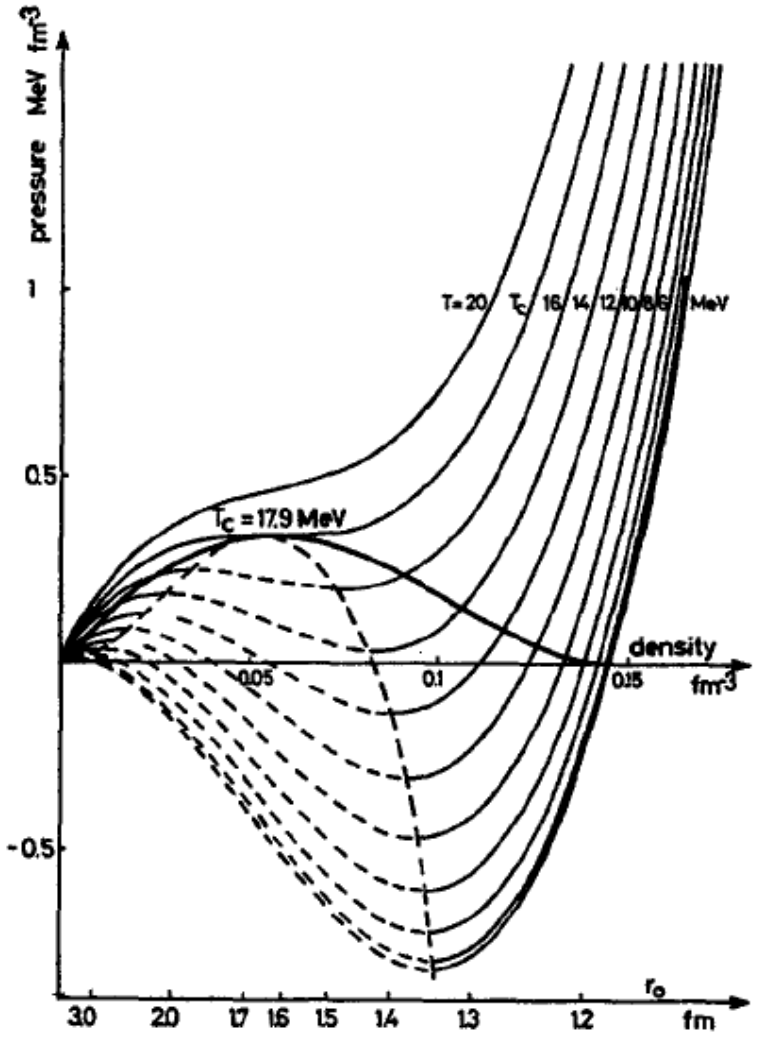

G. SAUER *et al.* *Nuclear Physics* **A264** (1976) 221--243

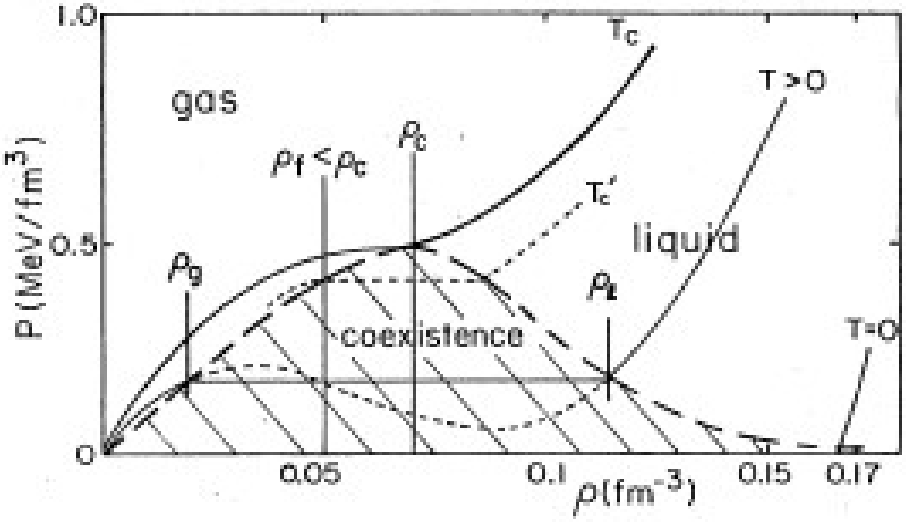

A. D. PANAGIOTOU, M. W. CURTIN, AND D. K. SCOTT

PHYSICAL REVIEW C **1985**

Physics Letters B 371 (1996) 175–180

Statistical multifragmentation in central Au + Au collisions at 35 MeV/u

MINIBALL + MULTICS

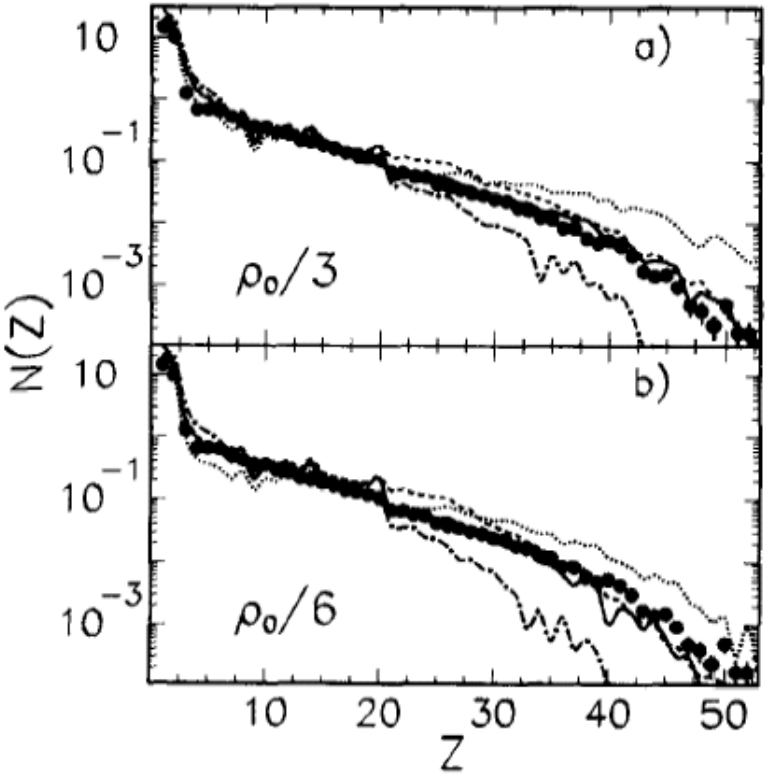

Fig. 1. Charge distribution $N(Z)$. Points show experimental data and lines show results of SMM predictions for sources with parameters $A_s = 343$, $Z_s = 138$, $E_s^*/A = 6.0$ MeV, $\rho_s = \rho_0/3$ (part a)) and $A_s = 315$, $Z_s = 126$, $E_s^*/A = 4.8$ MeV, $E_{flow}/A = 0.8$ MeV, $\rho_s = \rho_0/6$ (part b)). Dashed curves are the unfiltered calculations and solid curves are the filtered ones. The dot-dashed and dotted curves represent filtered calculations for thermal excitations $E_s^*/A + 1$ MeV/u and $E_s^*/A - 1$ MeV/u, respectively.

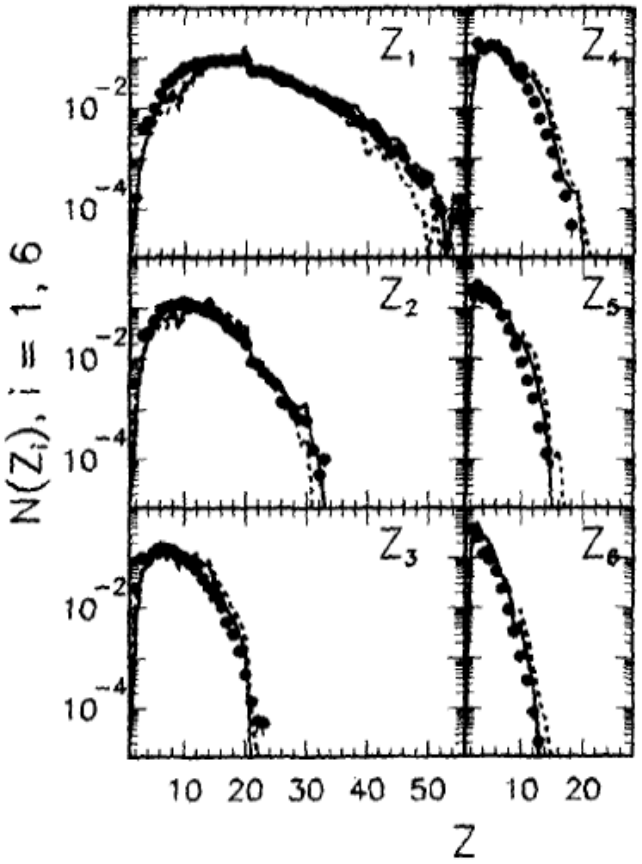

Fig. 2. Charge distribution of the six heaviest fragments, ordered such as $Z_i \geq Z_k$ if $i < k$. Experimental data are shown by points, the solid and dashed curves show the results of SMM calculations for $\rho_s = \rho_0/3$, and $\rho_s = \rho_0/6$, respectively (other source parameters as in Fig. 1).

MINIBALL + MULTICS

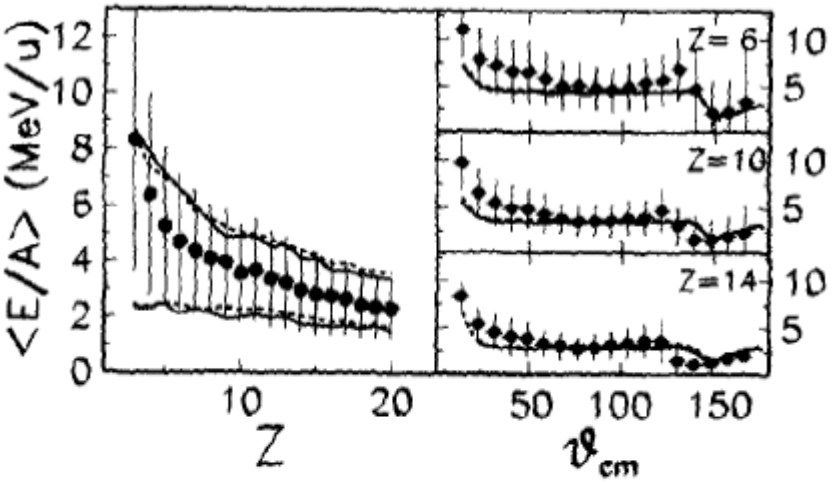

Fig. 3. Mean centre-of-mass kinetic energy per nucleon, $\langle E/A \rangle$, as a function of the charge Z, for fragments emitted at $\theta_{cm} = 90° \pm 10°$ (left panel) and (for $Z = 6, 10, 14$) as a function of θ_{cm} (right panels). Points give the experimental values of $\langle E/A \rangle$ and vertical bars give the standard deviations $\Delta E/A$ of the distributions. The solid and dashed lines are SMM predictions of $\langle E/A \rangle$ (in the left panel show the two values $\langle E/A \rangle \pm \Delta E/A$) for $\rho_s = \rho_0/3$, and $\rho_s = \rho_0/6$, respectively (other source parameters as in Fig. 1). The energy range is the same in the left and in each right panel.

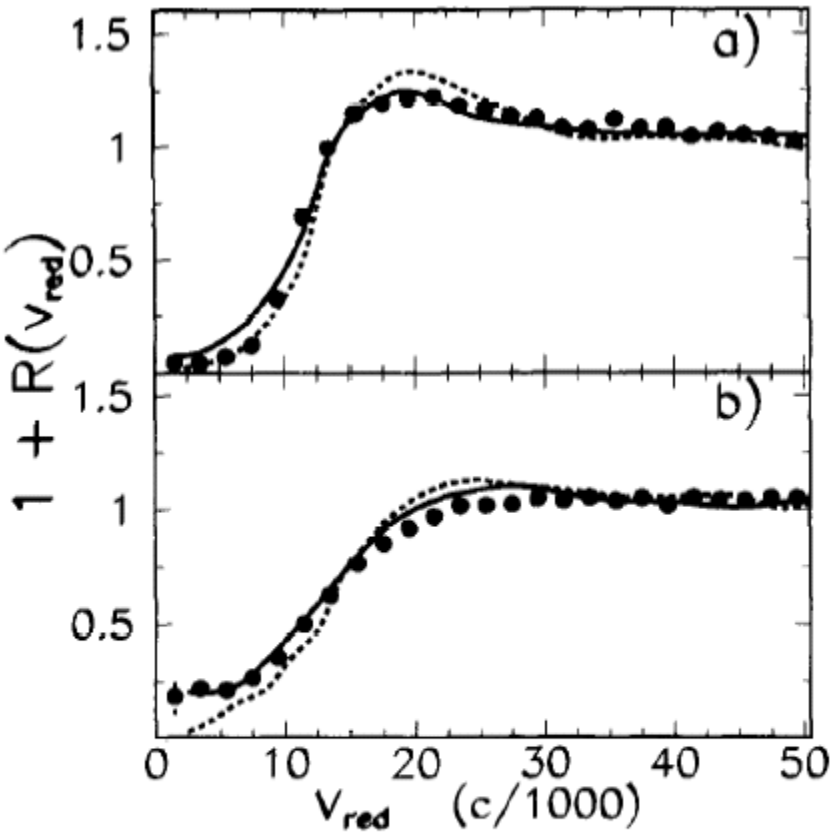

Fig. 4. Two-fragment correlation functions $1 + R(v_{red})$ for $3 \leq Z \leq 30$ and $8° \leq \theta_{lab} < 23°$ (part a)) and for $3 \leq Z \leq 10$ and $23° \leq \theta_{lab} \leq 40°$ (part b)). Full points show experimental data. The solid and dashed lines are SMM predictions for $\rho_s = \rho_0/3$, and $\rho_s = \rho_0/6$ (other source parameters as in Fig. 1).

INDRA

Ni+Au 52A MeV

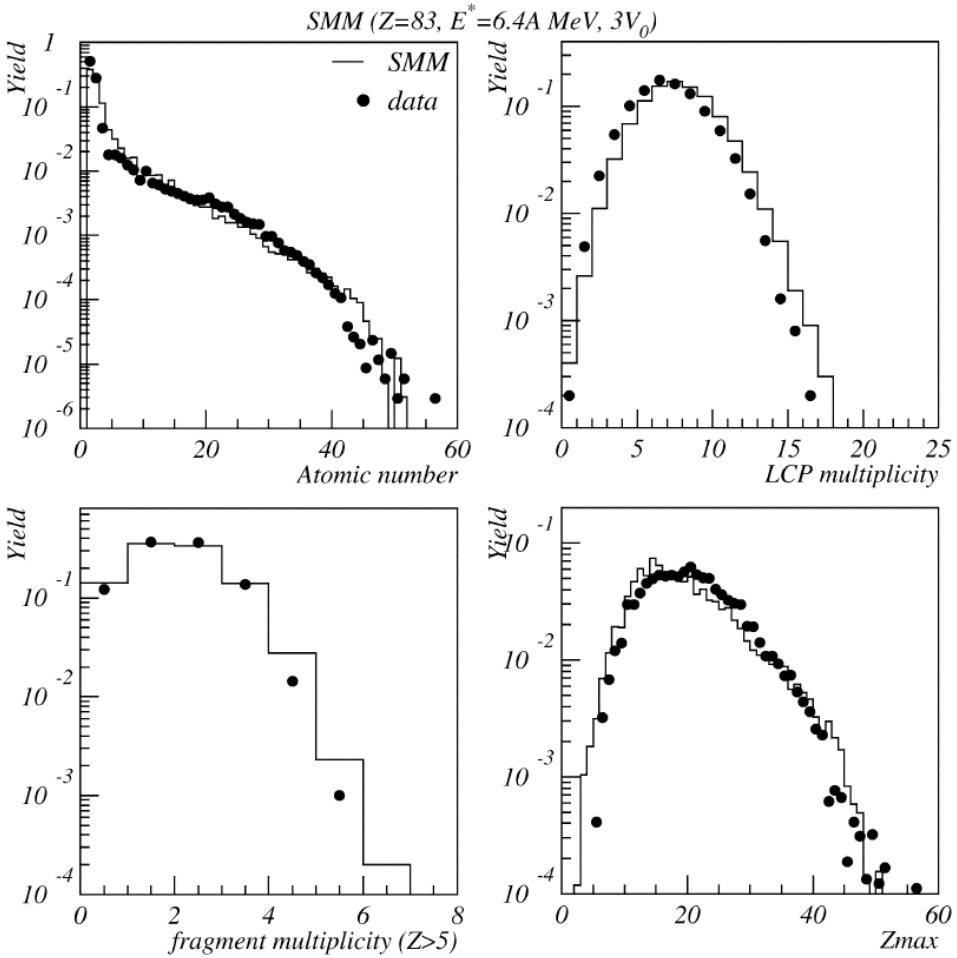

Fig. 10. Atomic number (a) for the 52*A* MeV Ni + Au data (symbols) and SMM (histogram), LCP multiplicity ($Z \leqslant 2$) (b), Fragment multiplicity ($Z \geqslant 6$) (c) and atomic number distributions of the heaviest fragment (d). These comparisons are made in a restricted angular domain in the center of mass (60°–120°). All spectra are normalized to the number of events.

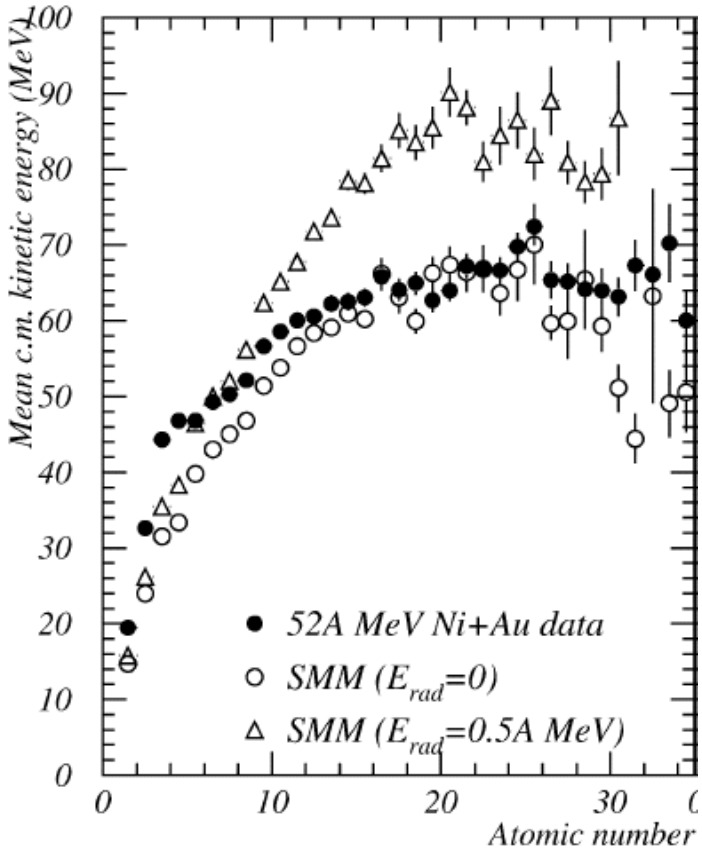

Nuclear Physics A 709 (2002) 367–391

Eur. Phys. J. A 3, 75–83 (1998)

Thermal multifragmentation in p + Au interactions at 2.16, 3.6 and 8.1 GeV incident energies

FASA

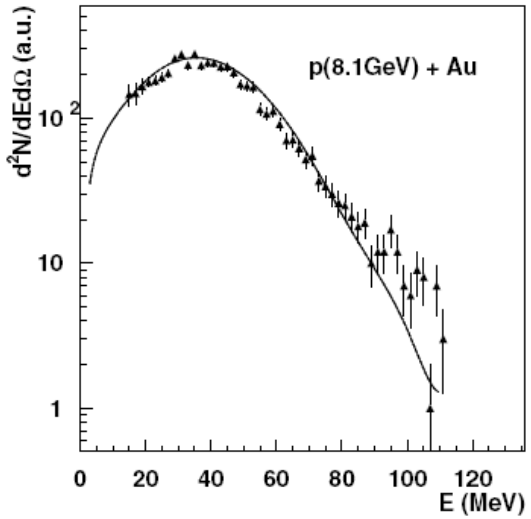

Fig. 8. Energy distribution of carbon isotopes obtained at 8.1 GeV incident energy compared to the one from the INC+Expansion+SMM calculation

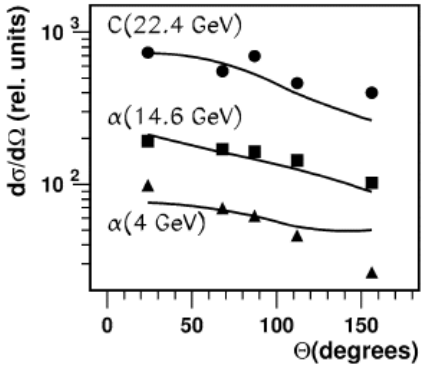

Fig. 9. Angular distributions of carbon (in laboratory system) for ^{4}He + Au and ^{12}C + Au collisions. The lines are calculated with RC + α + SMM.

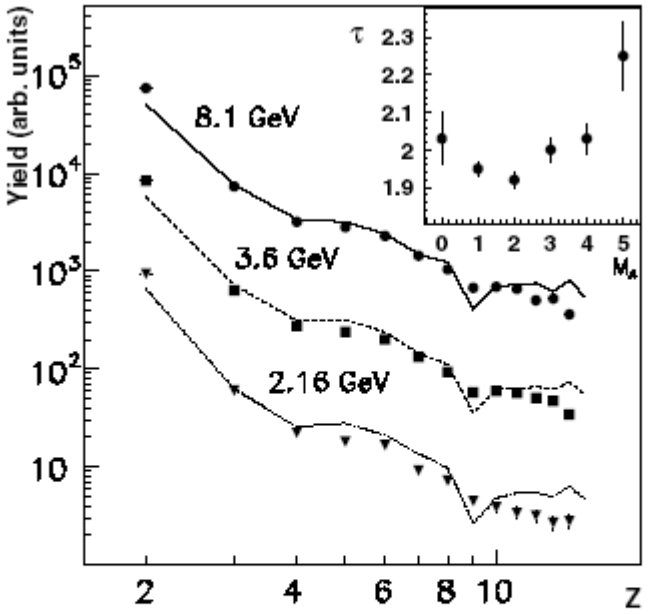

Fig. 10. Fragment charge distributions at the beam energies 8.1 GeV (top), 3.6 GeV (scaled by 1/4) and 2.16 GeV (scaled by 1/16). The lines are calculated by INC+Expansion+SMM (normalized at Z=3). The insert gives the τ-parameter deduced from the IMF-charge spectra for the beam energy of 8.1 GeV as a function of the measured IMF multiplicity

Multifragmentation versus sequential evaporation

ISIS π^-(8GeV/c)+Au

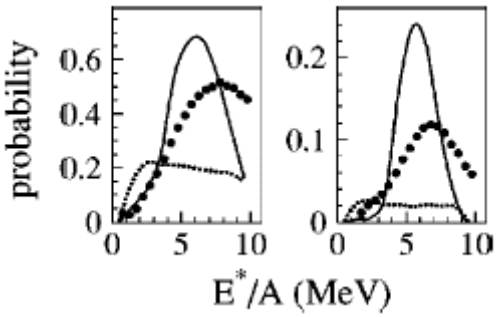

FIG. 3. Left panel: dots present the raw measured probability to detect an event with at least one heavy-fragment, $Z \geqslant 8$, and solid (dotted) line presents the SMM (GEMINI) model prediction filtered with the experimental detection efficiency. An initial angular momentum of $L = 20\hbar$ for the hot nucleus was assumed for GEMINI model calculations. Right panel: as in left panel, but for the probability of detecting events with at least two heavy-fragments, $Z \geqslant 8$.

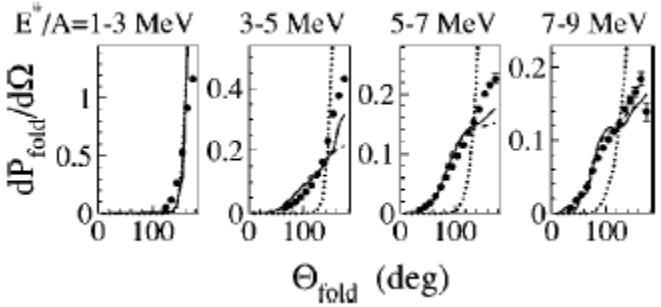

FIG. 2. The measured folding-angle (the angle between two $Z \geqslant 8$ fragments) probability for the indicated excitation-energy bins. Solid, dashed, and dotted lines show the SMM-hot, SMM-cold, and GEMINI model predictions, respectively, filtered with the experimental detection efficiency.

ALADIN Au (600 MeV/n) +X.

Nuclear Physics A556 (1993) 672–696

P. Kreutz et al. / Charge correlations

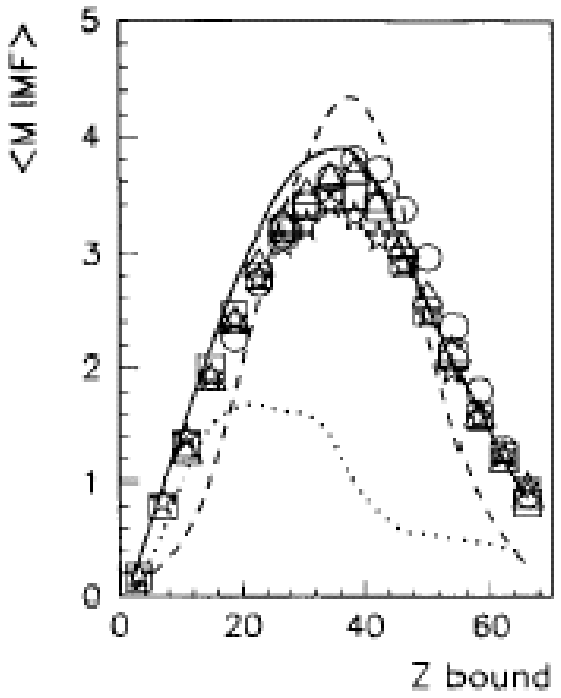

Fig. 15. The average multiplicity of IMFs as a function of Z_{bound} for Au 600 MeV/nucleon collisions on C (circles), Al (triangles), Cu (squares) and Pb (stars). The error bars are in most cases smaller than the size of the symbols. The lines are COPENHAGEN (dashed), GEMINI (dotted) and percolation (full) predictions.

Time scale of the thermal multifragmentation

ISIS collaboration

velocity correlations of fragments

π^-(8GeV/c)+Au

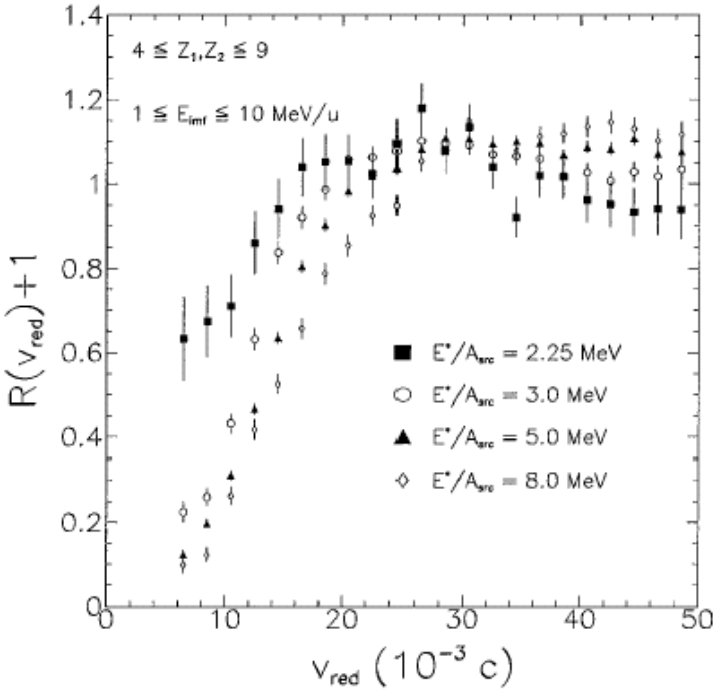

FIG. 1. Reduced velocity correlation functions generated for four different excitation energy per nucleon bins. IMF kinetic energy acceptance is in source frame is $E_{\mathrm{IMF}}/A = 1-10$ MeV.

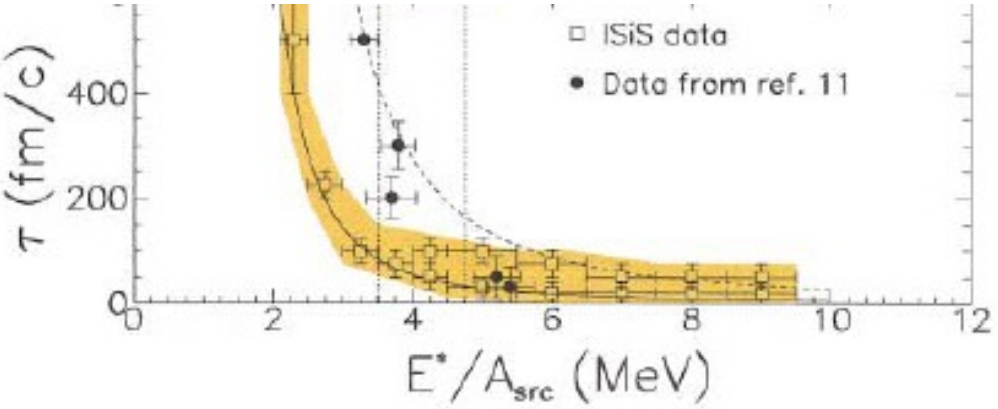

L.Beaulieu et al., Phys. Rev. Lett. **84**, 5971 (2000)

Time scale of the thermal multifragmentation

angle correlations of fragments

p(8.1 GeV) + Au

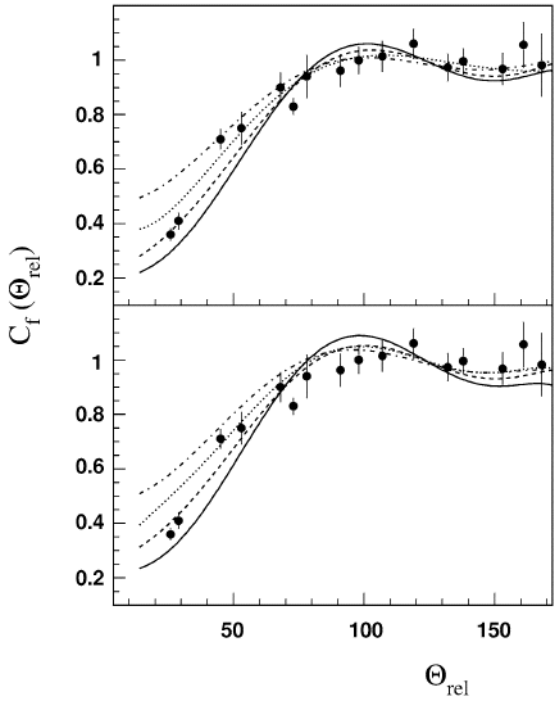

Fig. 5. Comparison of the measured correlation functions (full circles) with the calculated ones for different mean decay times of the fragmenting system: solid, dashed, dotted and dash-dotted lines for $\tau = 0$, 50, 100 and 200 fm/c. The upper panel is for the RC + α + SMM model with the parameters $(4, 8, \eta)$ (see notation in Fig. 4), the lower panel is for the same model, but with the parameters $(4, 4, \eta)$ allowing the fragments to overlap (see text).

FASA

collaboration

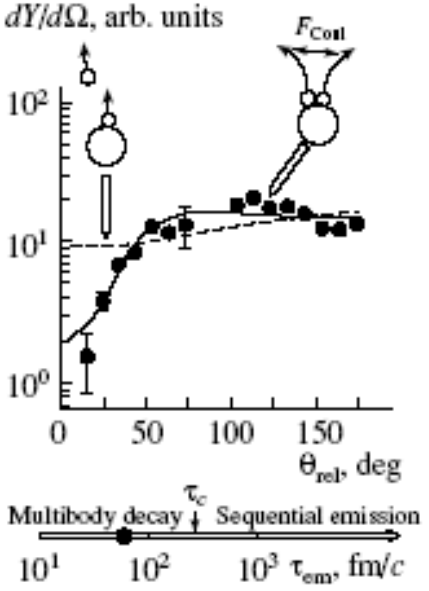

Fig. 5. Distribution of relative angles between coincident IMFs for ^{4}He(14.6 GeV) + Au collisions. The solid curve is calculated for the simultaneous emission of fragments; the dashed curve corresponds to the sequential, independent evaporation.

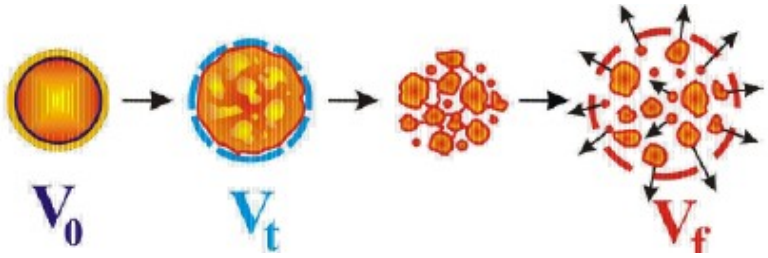

We consider the isotropic phase space generation of nucleons in microcanonical approach (PSG) with the total available energy which can correspond to the c.m. energy of colliding nuclei.

(A.Botvina, N.Buyukcizmeci, M.Bleicher, PRC 103 (2021) 064602; PRC 106 (2022) 014607)

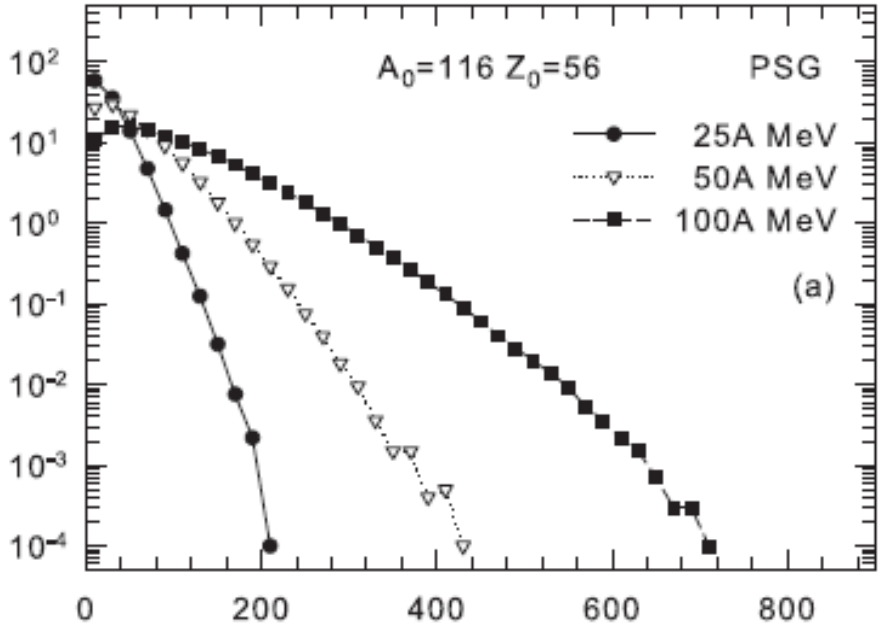

Energy and transverse-momentum distributions of nucleons after PSG

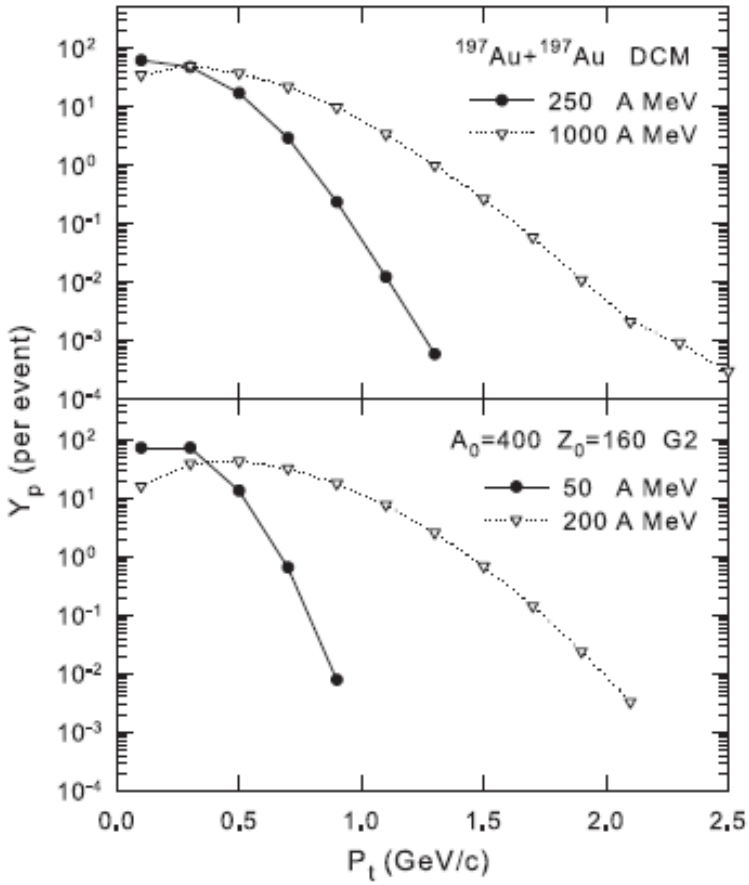

Nuclear system consists of primary clusters in local equilibrium:

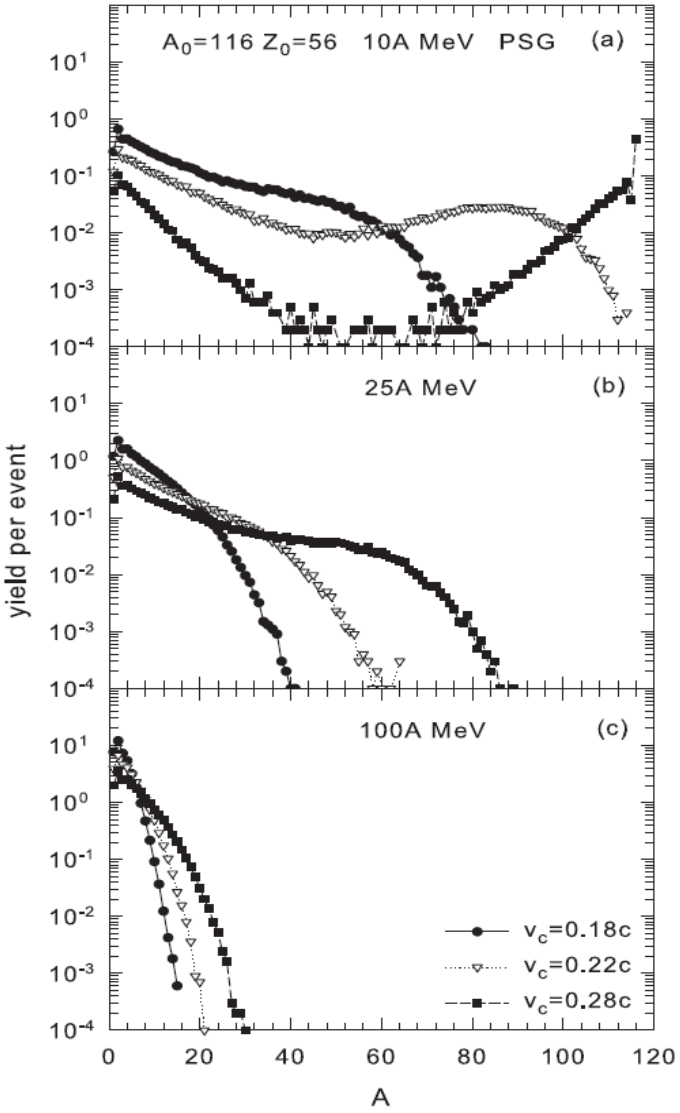

final nuclei after the statistical nucleation (disintegration of the excited clusters via SMM):

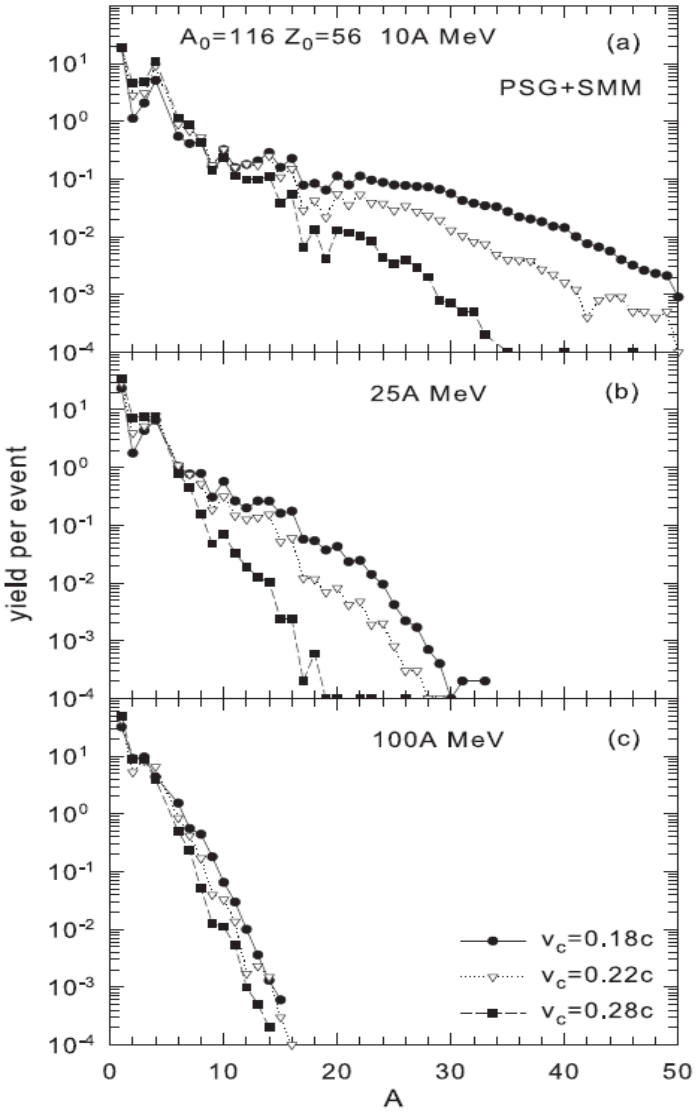

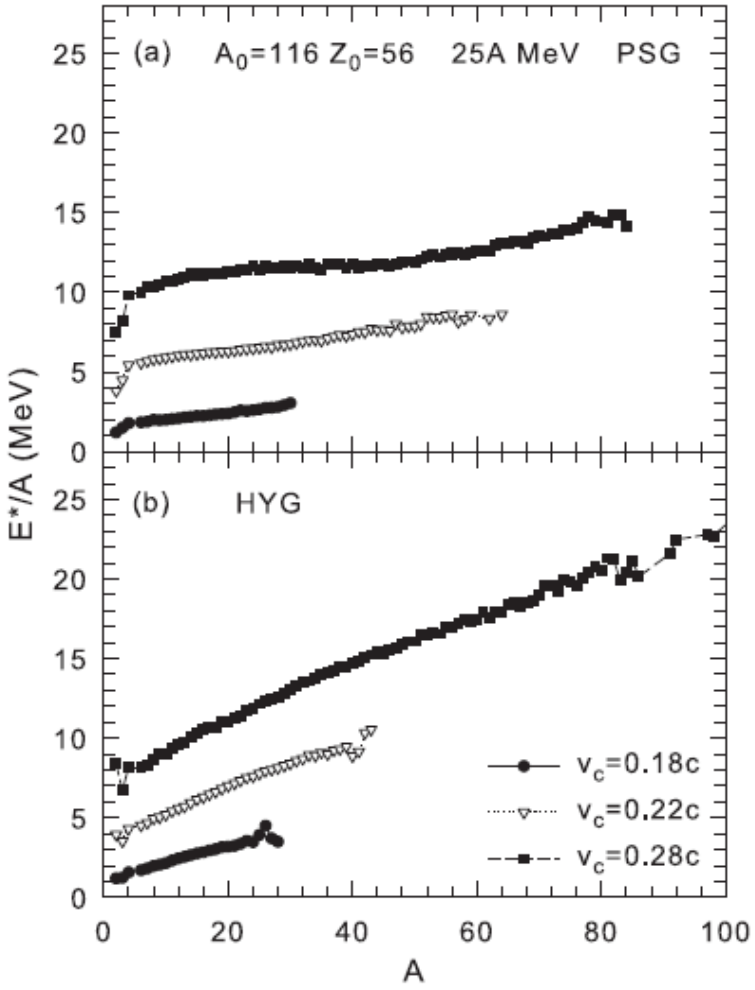

FIG. 3. Average internal energy of coalescent clusters versus their mass number A produced as a result of the coalescence (CB) in the sources with $A_0 = 116$ and $Z_0 = 56$ after PSG (a) and HYG (b). The source energy and coalescence parameters are shown in the panels.

Discovery of a Strange nucleus: Hypernucleus

M. Danysz and J. Pniewski, Philos. Mag. 44 (1953) 348

First-hypernucleus was observed in a stack of photographic emulsions exposed to cosmic rays at about 26 km above the ground.

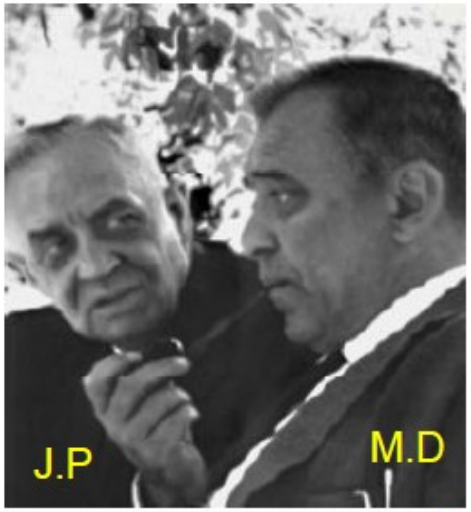

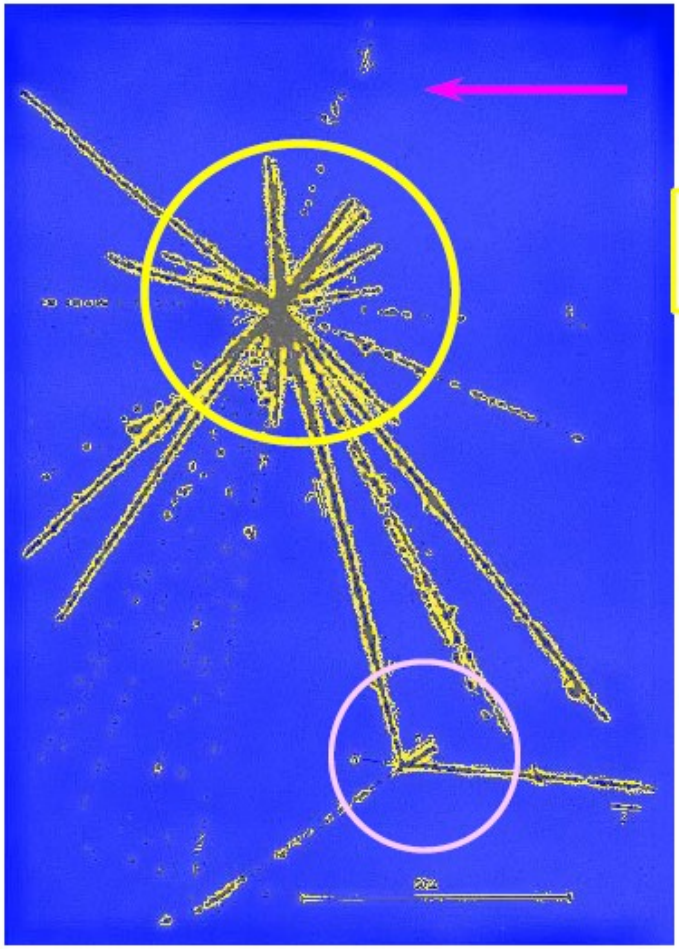

Incoming high energy proton from cosmic ray

colliding with a nucleus of the emulsion, breaks it in several fragments forming a star. **Multifragmentation !**

All nuclear fragments stop in the emulsion after a short path

From the first star, 21 Tracks => $9\alpha + 11H + 1\ {}_{\Lambda}X$

The fragment ${}_{\Lambda}X$ disintegrates later , makes the bottom star. Time taken ~ 10^{-12} sec (typical for weak decay)

This particular nuclear fragment, and the others obtained afterwards in similar conditions, were called **hyperfragments or hypernuclei.**

T.Saito, (for HypHI),
NUFRA2011 conference, and
Nucl. Phys. A881 (2012) 218;
Nucl. Phys. A913 (2013) 170.

C. Rappold et al.,
Phys. Rev. C88 (2013) 041001:
Λnn bound state ?

Production of hypernuclei in peripheral HI collisions: The HypHI project at GSI

T.R. Saito[a,b,c], D. Nakajima[a,d], C. Rappold[a,c,e], S. Bianchin[a], O. Borodina[a,b], V. Bozkurt[a,f], B. Göküzüm[a,f], M. Kavatsyuk[g], E. Kim[a,h], Y. Ma[a,b], F. Maas[a,b,c], S. Minami[a], B. Özel-Tashenov[a], P. Achenbach[b], S. Ajimura[i], T. Aumann[a], C. Ayerbe Gayoso[b], H.C. Bhang[f], C. Caesar[a], S. Erturk[f], T. Fukuda[j], E. Guliev[h], Y. Hayashi[k], T. Hiraiwa[k], J. Hoffmann[a], G. Ickert[a], Z.S. Ketenci[f], D. Khaneft[a,b], M. Kim[h], S. Kim[h], K. Koch[a], N. Kurz[a], A. Le Fevre[a,l], Y. Mizoi[j], M. Moritsu[k], T. Nagae[k], L. Nungesser[b], A. Okamura[k], W. Ott[a], J. Pochodzalla[b], A. Sakaguchi[m], M. Sako[k], C.J. Schmidt[a], M. Sekimoto[n], H. Simon[a], H. Sugimura[k], T. Takahashi[n], G.J. Tambave[g], H. Tamura[o], W. Trautmann[a], S. Voltz[a], N. Yokota[k], C.J. Yoon[h], K. Yoshida[m],

Projectile fragmentation: ^{6}Li beam at 2 A GeV on ^{12}C target

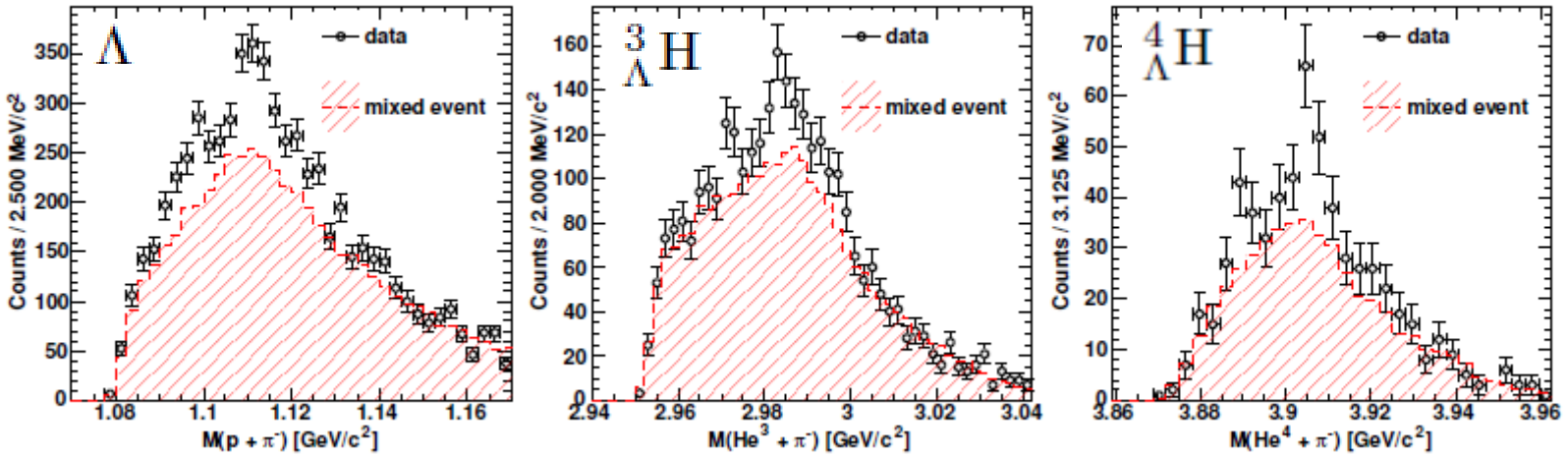

They have also observed a large correlation of $^{2}\mathrm{H} + \pi^{-}$
i.e., may be considerable production of Λn states

Λ-hyperon lifetime in very heavy hypernuclei produced in the p+U interaction

The recoil shadow method for the detection of fission fragments has been used to investigate delayed fission of very heavy Λ hypernuclei produced in the p-U interaction at the projectile energy of 1.5 GeV. From the measured distribution of delayed fission events in the shadow region and the calculated momenta of hypernuclei leaving the target the lifetime of the Λ hyperon in very heavy hypernuclei was determined to be $\tau = 2.40 \pm 60$ ps. The comparison of the number of delayed fission events with that of the prompt events leads to an estimation of the cross section for the production of Λ hypernuclei in p+U collisions at 1.5 GeV of $\sigma_{Hv} = 150^{+150}_{-80}$ μb. [S0556-2813(97)04506-8]

H. Ohm et al., PRC 55 (1997) 3062

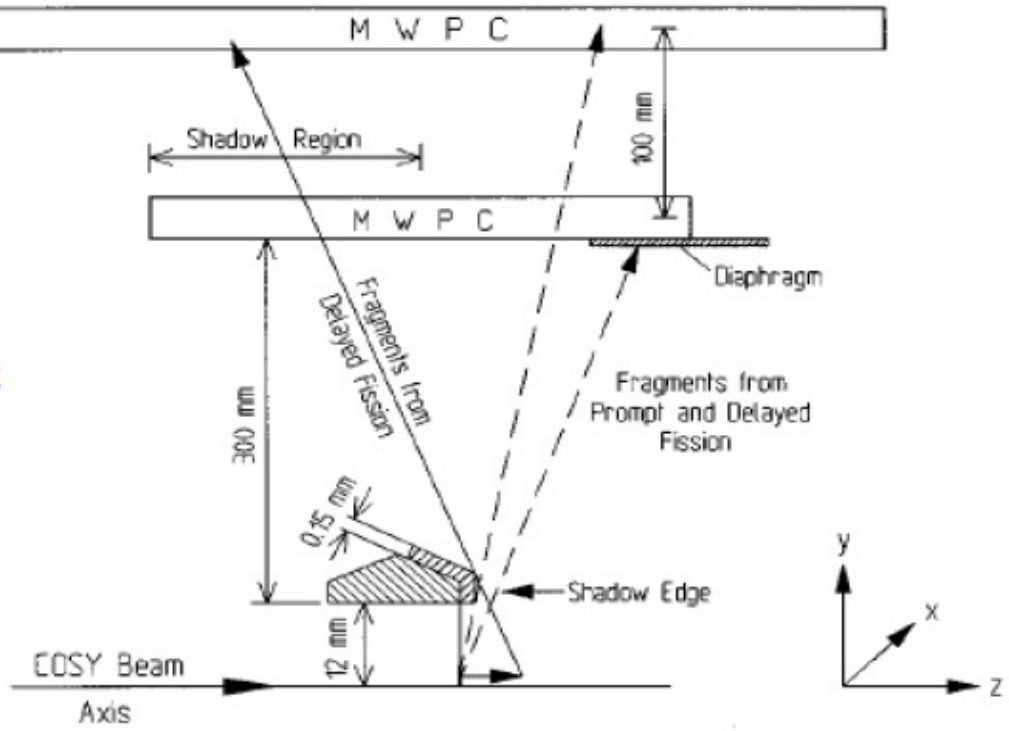

FIG. 1. Schematic presentation of the experimental setup. The thickness of the target holder is enhanced in the drawing to show the details. The real distances are given.

Statistical approach for fragmentation of hyper-matter

$$Y_{AZH} = g_{AZH} V_f \frac{A^{3/2}}{\lambda_T^3} \exp\left[-\frac{1}{T}\left(F_{AZH} - \mu_{AZH}\right)\right]$$

$$\mu_{AZH} = A\mu + Z\nu + H\xi$$

mean yield of fragments with mass number A, charge Z, and Λ-hyperon number H

$$F_{AZH}(T,V) = F_A^B + F_A^S + F_{AZH}^{sym} + F_{AZ}^C + F_{AH}^{hyp}$$

liquid-drop description of fragments: bulk, surface, symmetry, Coulomb (as in Wigner-Seitz approximation), and hyper energy contributions
J.Bondorf et al., Phys. Rep. **257** (1995) 133

$$F_A^B(T) = \left(-w_0 - \frac{T^2}{\varepsilon_0}\right) A \quad ,$$

$$F_A^S(T) = \beta_0 \left(\frac{T_c^2 - T^2}{T_c^2 + T^2}\right)^{5/4} A^{2/3} \quad ,$$

parameters ≈ Bethe-Weizsäcker formula:

$w_0 = 16$ MeV, $\beta_0 = 18$ MeV, $T_c = 18$ MeV

$$F_{AZH}^{sym} = \gamma \frac{(A - H - 2Z)^2}{A - H} \quad ,$$

$\gamma = 25$ MeV $\varepsilon_0 \approx 16$ MeV

$$\sum_{AZH} A Y_{AZH} = A_0, \sum_{AZH} Z Y_{AZH} = Z_0, \sum_{AZH} H Y_{AZH} = H_0.$$

chemical potentials are from mass, charge and *H*yperon number conservations

$$F_{AH}^{hyp} = E_{sam}^{hyp} = H \cdot (-10.68 + 48.7/(A^{2/3})).$$

-- C.Samanta et al. J. Phys. G: 32 (2006) 363
(motivated: single Λ in potential well)

$$F_{AH}^{hyp} = (H/A) \cdot (-10.68A + 21.27A^{2/3}).$$

-- liquid-drop description of hyper-matter

A.S.Botvina and J.Pochodzalla, Phys. Rev.C76 (2007) 024909

Abundant hyper-isotope production in multifragmentation (SMM)

Important features of these reactions: wide fragment/isotope distributions

Statistical regularities of fragment production can be employed to learn about fragments!

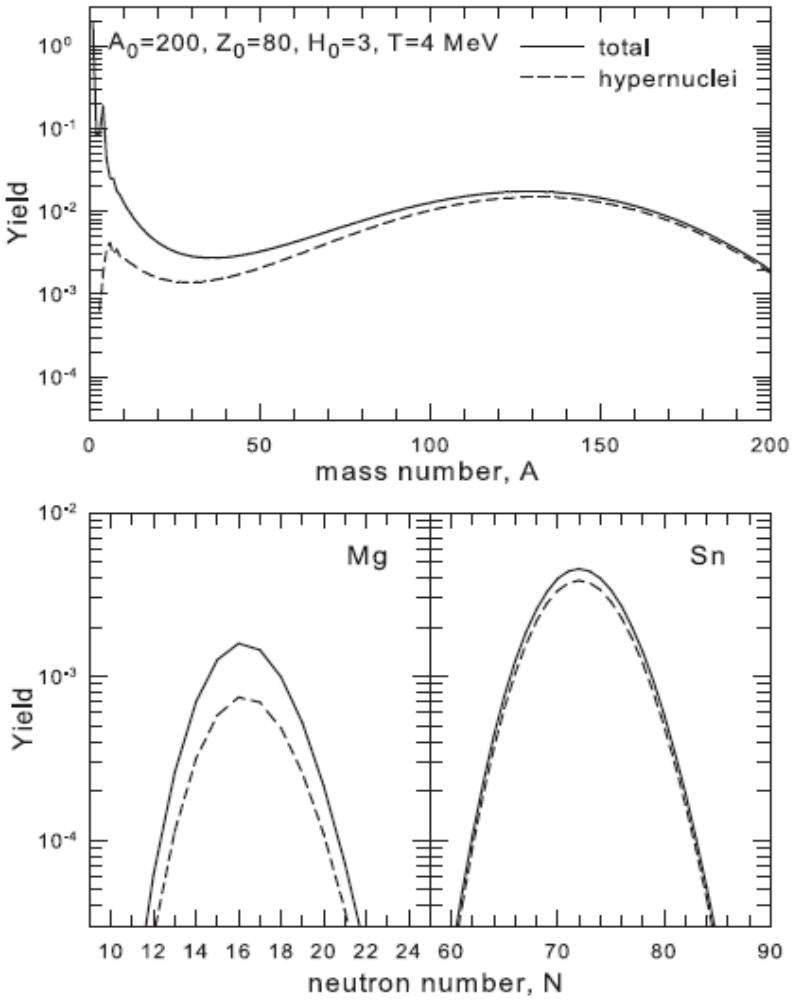

Yields of fragments: $$Y_{A,Z,H} = g_{A,Z,H} \cdot V_f \frac{A^{3/2}}{\lambda_T^3} \exp\left[-\frac{1}{T}\left(F_{A,Z,H} - \mu_{AZH}\right)\right],$$

$$\mu_{AZH} = A\mu + Z\nu + H\xi.$$

Statistical reaction models can be used not only for the production prediction:

Experimental yields of isotopes can be used for extracting properties of exotic cluster, e.g., the hyperon binding energies

Double ratio method :

ΔE_{bh} **vs** ΔA

difference of hyperon energies in hyper-nuclei:
Phys.Rev.C98(2018)064603

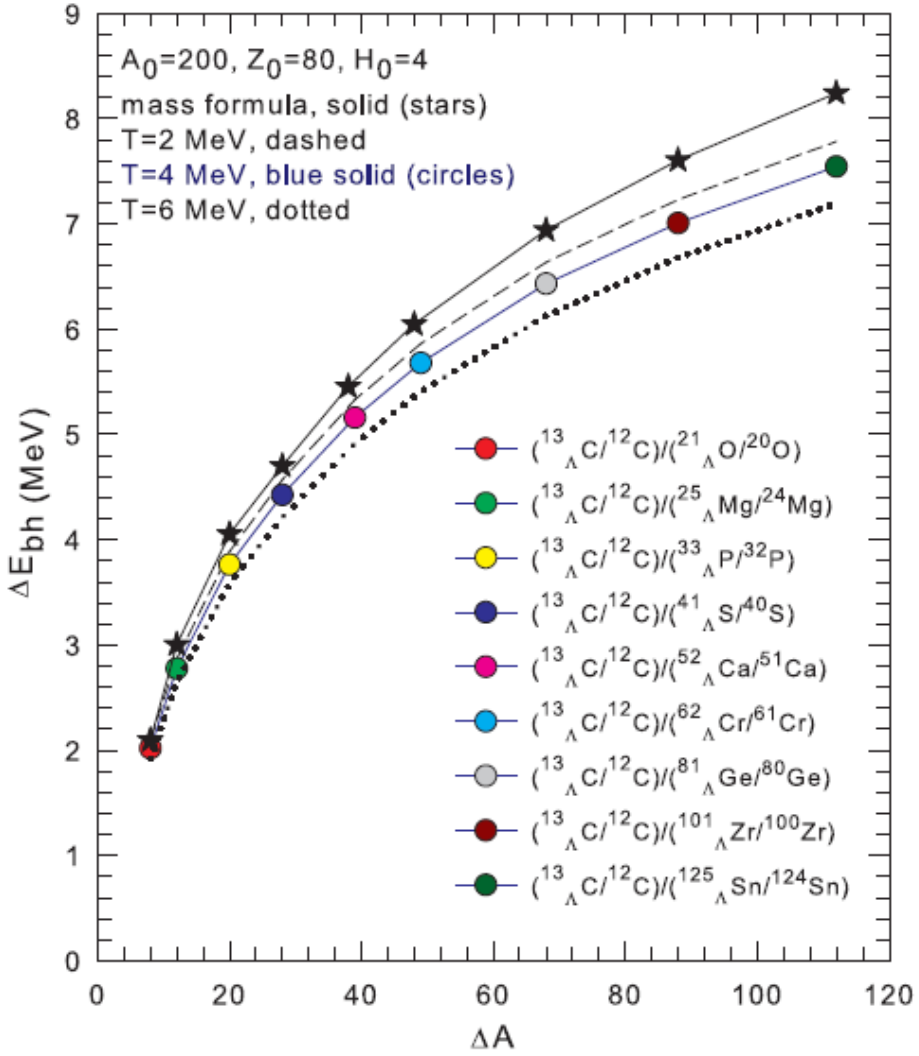

$$\Delta E_{bh} = T \cdot \left[ln\left(\frac{(g_{A_1,Z_1,H}/g_{A_1-1,Z_1,H-1}) \cdot (A_1^{3/2}/(A_1-1)^{3/2})}{(g_{A_2,Z_2,H}/g_{A_2-1,Z_2,H-1}) \cdot (A_2^{3/2}/(A_2-1)^{3/2})}\right) - ln\left(\frac{Y_{A_1,Z_1,H}/Y_{A_1-1,Z_1,H-1}}{Y_{A_2,Z_2,H}/Y_{A_2-1,Z_2,H-1}}\right)\right]$$

De-excitation of hot light hypernuclear systems

A.Sanchez-Lorente, A.S.Botvina, J.Pochodzalla, Phys. Lett. B697 (2011)222

For light primary fragments (with $A \leq 16$) even a relatively small excitation energy may be comparable with their total binding energy. In this case we assume that the principal mechanism of de-excitation is the explosive decay of the excited nucleus into several smaller clusters (the secondary break-up). To describe this process we use the famous Fermi model [105]. It is analogous to the above-described statistical model, but all final-state fragments are assumed to be in their ground or low excited states. In this case the statistical weight of the channel containing n particles with masses m_i $(i = 1, \ldots, n)$ in volume V_f may be calculated in microcanonical approximation:

$$\Delta\Gamma_f^{\mathrm{mic}} \propto \frac{S}{G}\left(\frac{V_f}{(2\pi\hbar)^3}\right)^{n-1}\left(\frac{\prod_{i=1}^{n} m_i}{m_0}\right)^{3/2}\frac{(2\pi)^{(3/2)(n-1)}}{\Gamma(\frac{3}{2}(n-1))}\left(E_{\mathrm{kin}} - U_f^C\right)^{(3/2)n-5/2}, \qquad (58)$$

where $m_0 = \sum_{i=1}^{n} m_i$ is the mass of the decaying nucleus, $S = \prod_{i=1}^{n}(2s_i + 1)$ is the spin degeneracy factor (s_i is the ith particle spin), $G = \prod_{j=1}^{k} n_j!$ is the particle identity factor (n_j is the number of particles of kind j). E_{kin} is the total kinetic energy of particles at infinity which is related to the prefragment excitation energy E^*_{AZ} as

$$E_{\mathrm{kin}} = E^*_{AZ} + m_0c^2 - \sum_{i=1}^{n} m_ic^2. \qquad (59)$$

U_f^C is the Coulomb interaction energy between cold secondary fragments given by Eq. (49), U_f^C and V_f are attributed now to the secondary break-up configuration.

Generalization of the Fermi-break-up model: new decay channels with hypernuclei were included ; masses and spins of hypernuclei and their excited states were taken from available experimental data and theoretical calculations

4.3.3. Evaporation from hot fragments

The successive particle emission from hot primary fragments with $A > 16$ is assumed to be their basic de-excitation mechanism. Due to the high excitation energy of these fragments, the standard Weisskopf evaporation scheme [2] was modified to take into account the heavier ejectiles up to ^{18}O, besides light particles (nucleons, d, t, α), in ground and particle-stable excited states [81]. This corresponds to the excitation energies $\epsilon^{(i)}$ of the ejectiles not higher than 7–8 MeV. By analogy with standard model the width for the emission of a particle j from the compound nucleus (A, Z) is given by:

$$\Gamma_j = \sum_{i=1}^{n} \int_0^{E^*_{AZ}-B_j-\epsilon_j^{(i)}} \frac{\mu_j g_j^{(i)}}{\pi^2 \hbar^3} \sigma_j(E) \frac{\rho_{A'Z'}(E^*_{AZ} - B_j - E)}{\rho_{AZ}(E^*_{AZ})} E\, dE \qquad (60)$$

Here the sum is taken over the ground and all particle-stable excited states $\epsilon_j^{(i)} (i = 0, 1, \ldots, n)$ of the fragment j, $g_j^{(i)} = (2s_j^{(i)} + 1)$ is the spin degeneracy factor of the ith excited state, μ_j and B_j are corresponding reduced mass and separation energy, E^*_{AZ} is the excitation energy of the initial nucleus (55), E is the kinetic energy of an emitted particle in the centre-of-mass frame. In Eq. (60) ρ_{AZ} and $\rho_{A'Z'}$ are the level densities of the initial (A, Z) and final (A', Z') compound nuclei. They are calculated using the Fermi-gas formula (41). The cross section $\sigma_j(E)$ of the inverse reaction $(A', Z') + j = (A, Z)$ was calculated using the optical model with nucleus–nucleus potential from Ref. [117]. The evaporational process was simulated by the Monte Carlo method using the algorithm described in Ref. [118]. The conservation of energy and momentum was strictly controlled in each emission step.

Evaporation from hypernuclei: nucleons, light particles, hyperons, light hypernuclei: New masses and assuming the level densities as in normal nuclei.

4.3.4. Nuclear fission

An important channel of de-excitation of heavy nuclei ($A > 200$) is fission. This process competes with particle emission. Following the Bohr–Wheeler statistical approach we assume that the partial width for the compound nucleus fission is proportional to the level density at the saddle point $\rho_{sp}(E)$ [1]:

$$\Gamma_f = \frac{1}{2\pi\rho_{AZ}(E^*_{AZ})} \int_0^{E^*_{AZ}-B_f} \rho_{sp}(E^*_{AZ} - B_f - E)\, dE, \tag{61}$$

where B_f is the height of the fission barrier which is determined by the Myers–Swiatecki prescription [120]. For approximation of ρ_{sp} we used the results of the extensive analysis of nuclear fissility and Γ_n/Γ_f branching ratios [121]. The influence of the shell structure on the level densities ρ_{sp} and ρ_{AZ} is disregarded since in the case of multifragmentation we are dealing with very high excitation energies $E^* > 30$–50 MeV when shell effects are expected to be washed out [122].

Fission of hypernuclei: New fission barriers including hyperon interaction (in the liquid-drop approach). It leads to increasing the barriers for ~ 1 MeV.
The level densities at the saddle point are taken as in normal nuclei (first approximation).

Evaporation & Fission of hypernuclei

(depending on mass and excitation energy)

A.S.Botvina et al., Phys. Rev. C94 (2016) 054615

These processes recall normal fission and evaporation. However, producing exotic hyper-fragments is possible (e.g. neutron rich ones) to investigate hyperon interactions in astro-physical conditions.

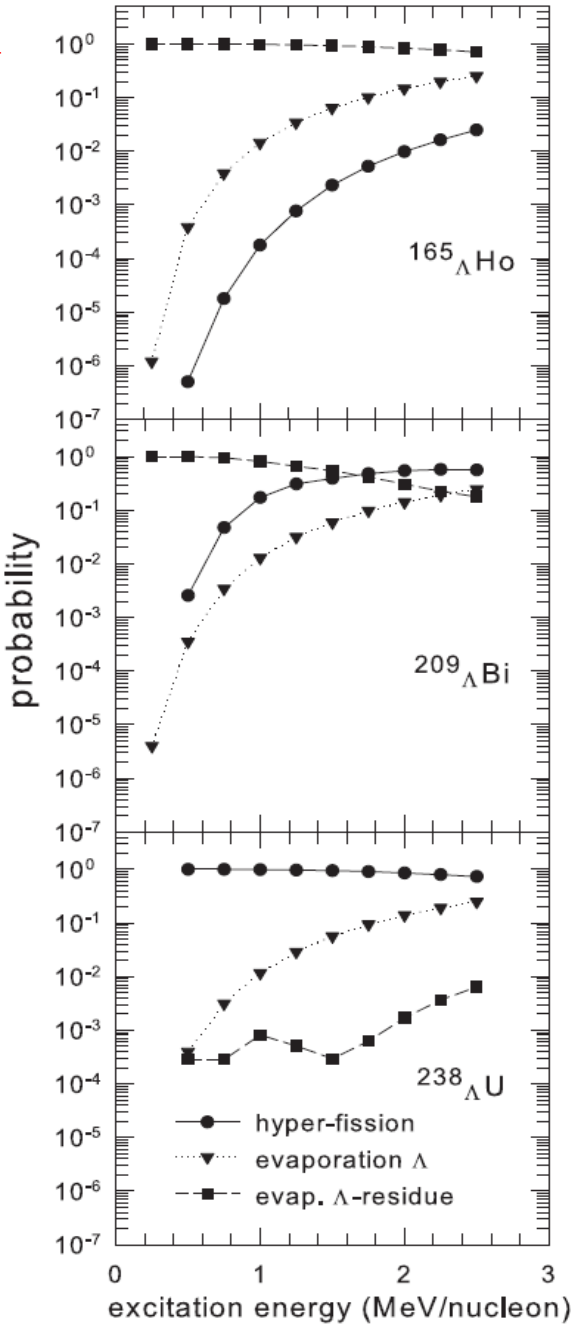

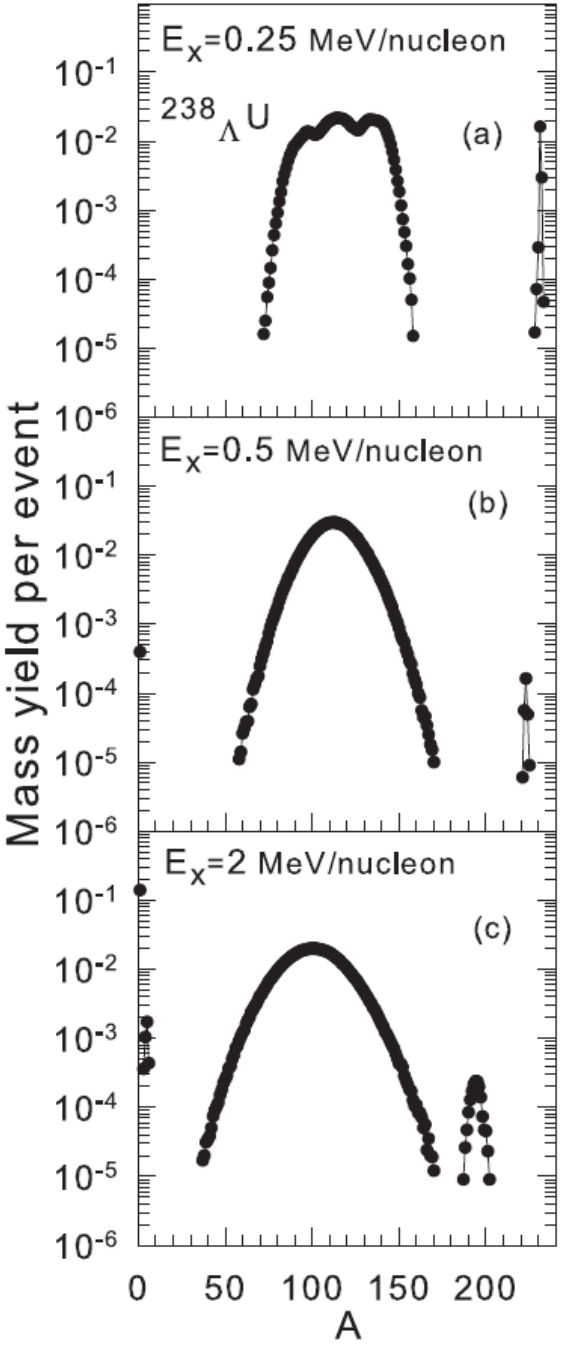

At sub-nuclear density: subdivision of matter into multiple clusters consisting of dynamically produced/spectator baryons, when baryons are close in the phase space (because of the remaining interaction). The clusters are excited, and are in chemical equilibrium leading to the nucleation inside clusters. This case can be realized in Heavy- Ion collisions of medium/high energies.

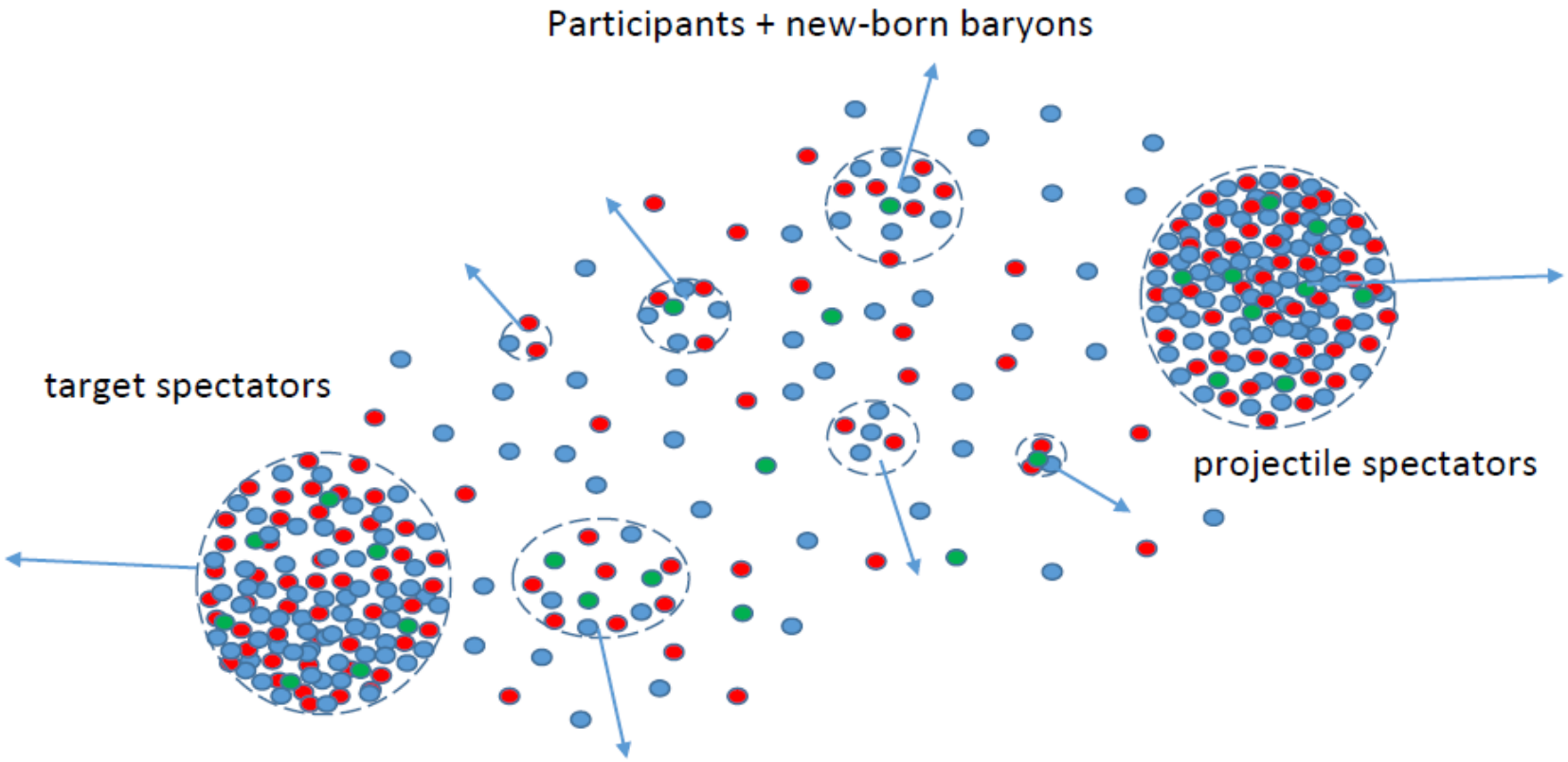

Excitation energies of the nuclear spectator residuals

DCM : PRC95, 014902 (2017)

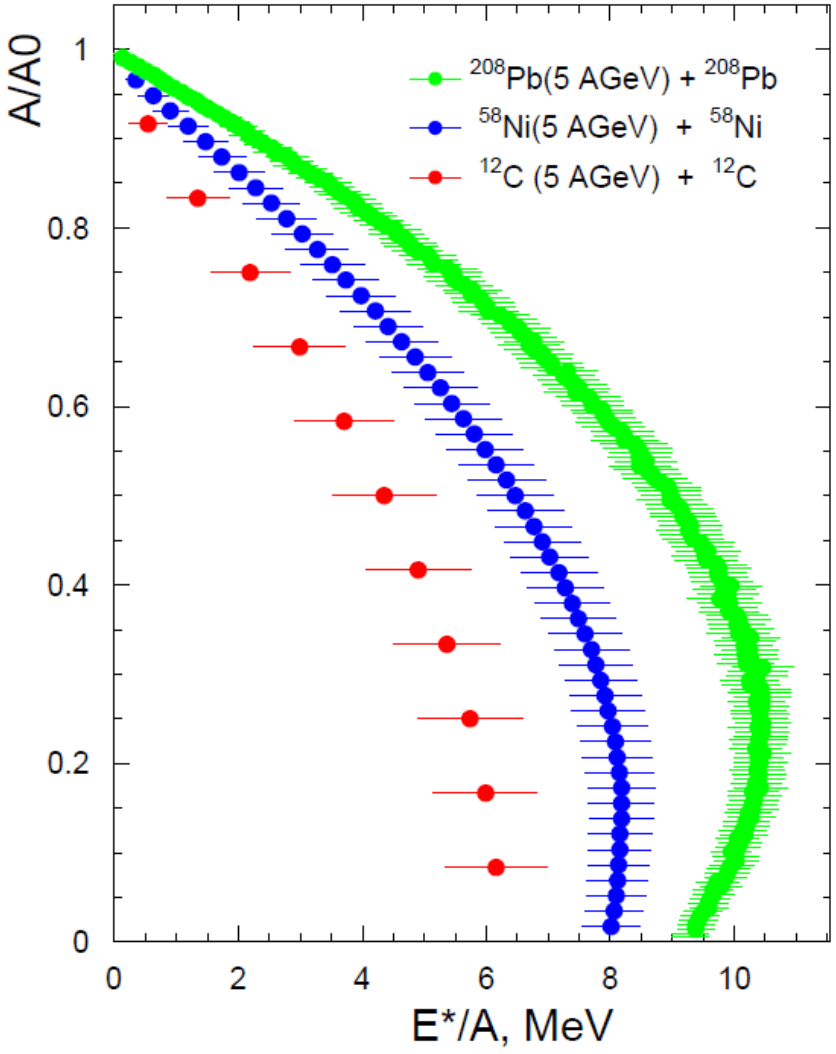

PRC84, 064904 (2011)

Masses of projectile residuals produced at dynamical stage (6b: H=0, 0.2b: H>0)

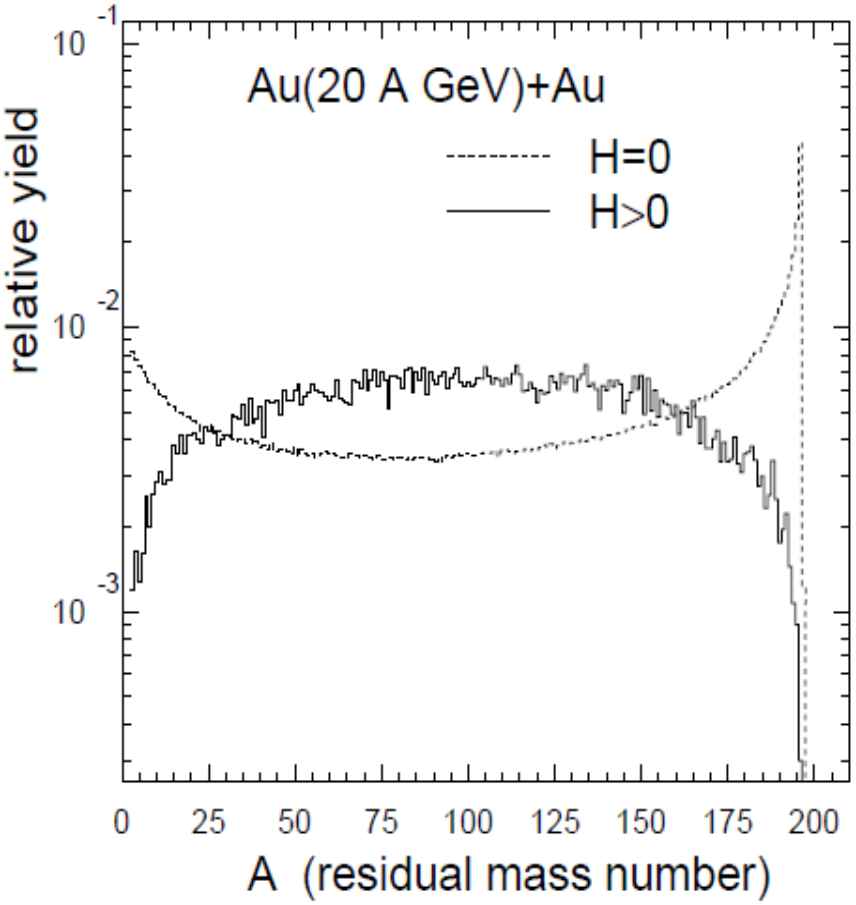

Dynamical+Statistical description of normal multifragmentation

ALADIN data

GSI

multifragmentation of relativistic projectiles

A.S.Botvina et al., Nucl.Phys. A584(1995)737

comparison with SMM (statistical multifragmentation model)

Statistical equilibrium has been reached in these reactions

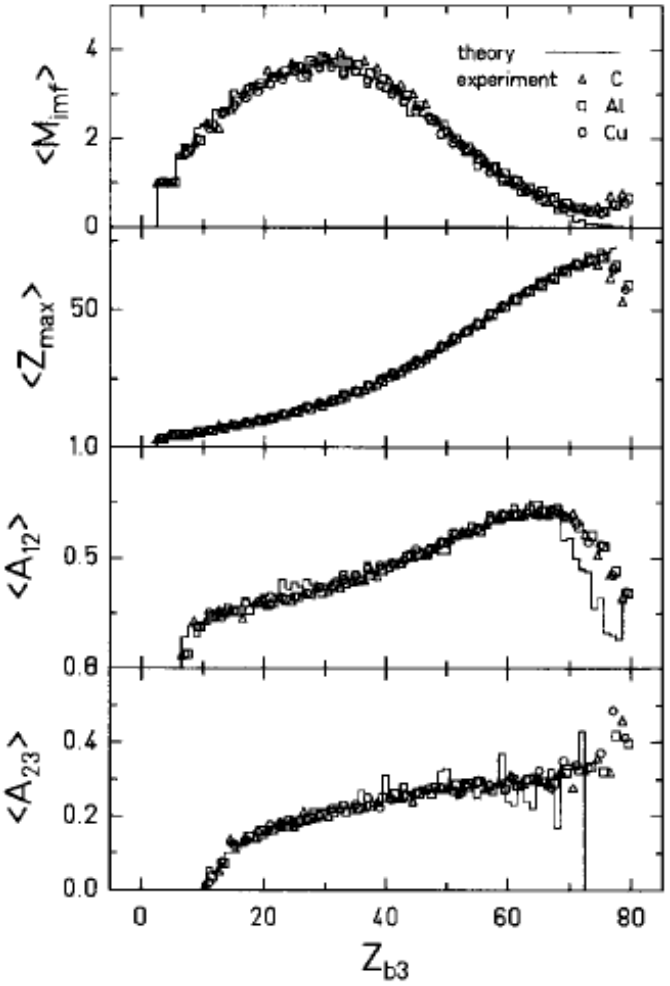

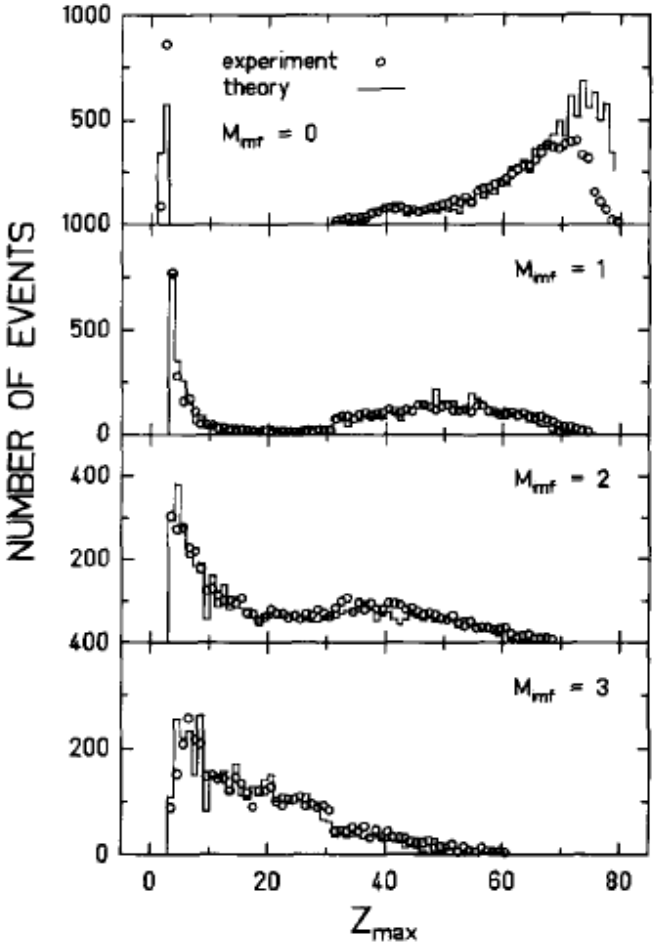

Correlation characteristics are very important for verification of models !

A mechanism for production of novel fragments: Capture of produced baryons by other nucleons and by spectator residues (nuclear matter)

Phenomenological models:

Coalescence (clusterization) of baryons into clusters: **CB**

momenta:

$$|Pi - P0| \le Pc$$

coordinates:

$$|Xi - X0| \le Xc$$

Capture in nuclear potential and coalescence are similar mechanisms

Hyperon capture in the spectator potential

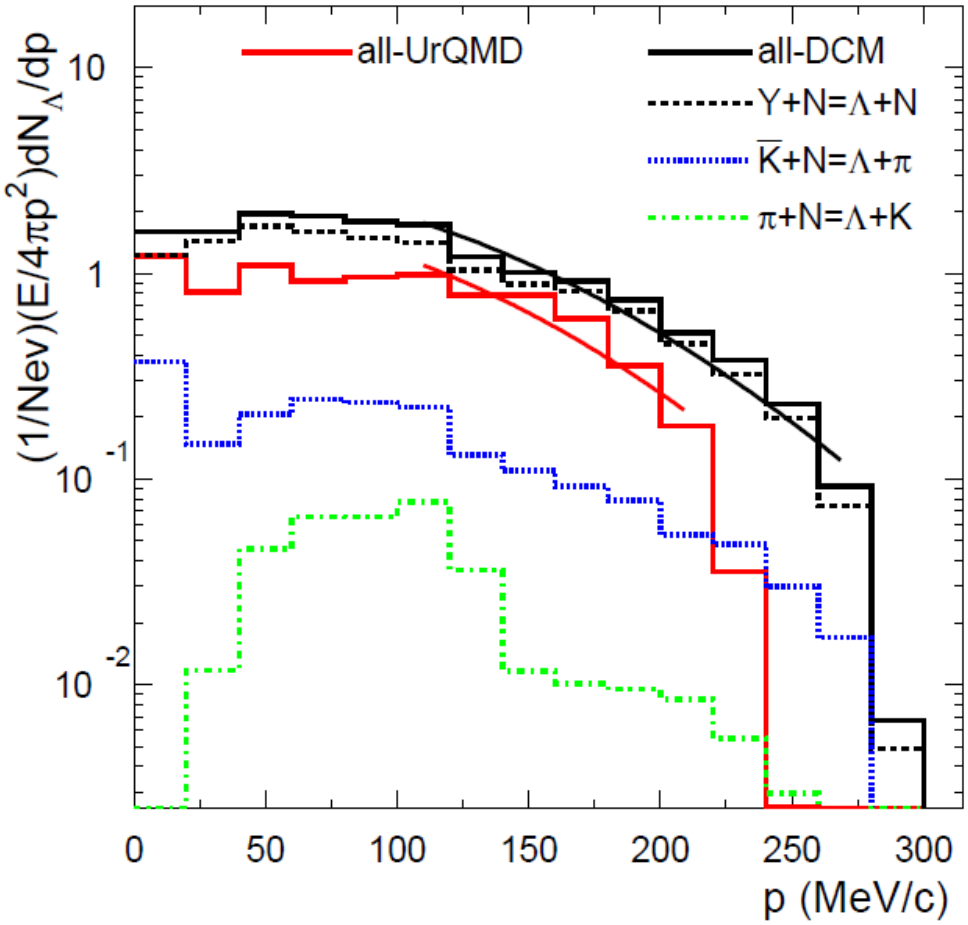

Au(20AGeV)+Au: UrQMD&DCM: PRC**84**, 064904 (2011)

Production of light nuclei in high energy central collisions

DCM, UrQMD, CB - Phys. Lett. B**714**, 85 (2012), Phys. Lett. B742, 7 (2015)

DCM versus experiment : coalescence mechanism

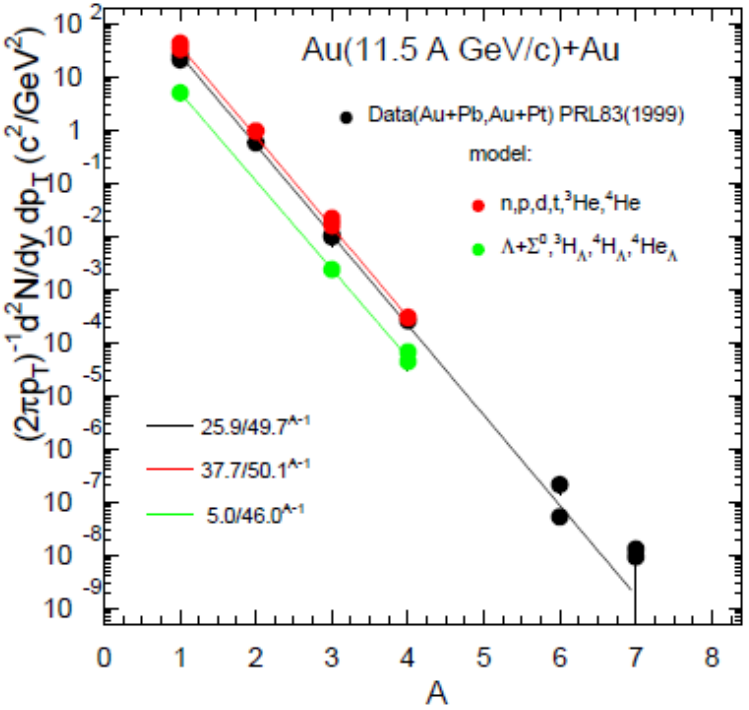

It is not possible to produce big nuclei !

Hybrid approach at LHC energies: UrQMD+hydrodynamics+coalescence

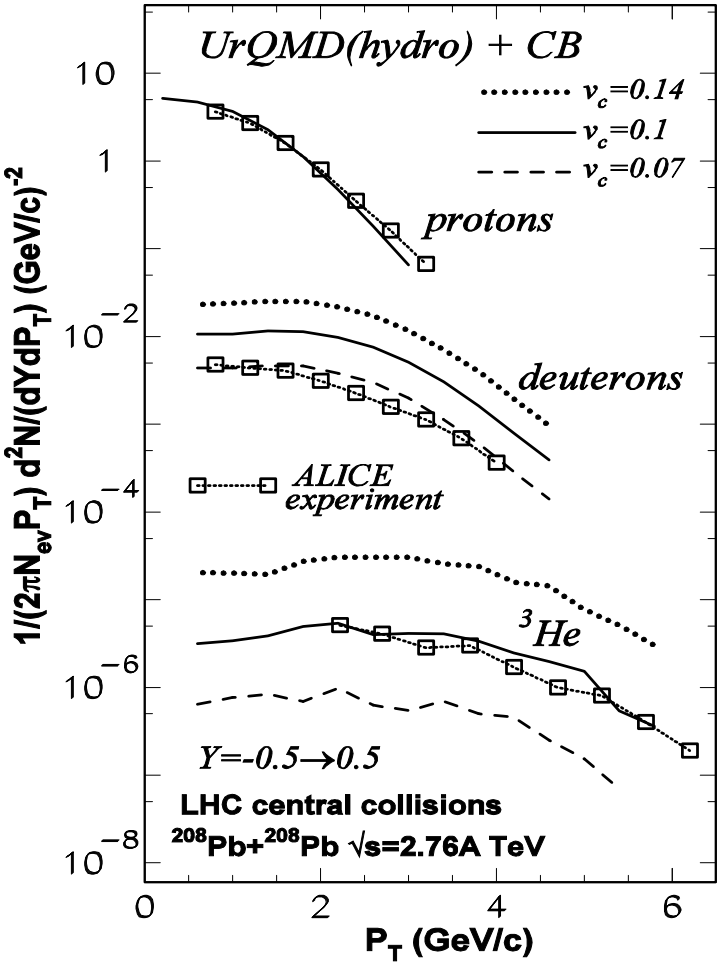

Phys. Rev. C96, 014913 (2017)

A.Botvina, J.Steinheimer, E.Bratkovskaya, M.Bleicher, J.Pochodzalla, PLB742(2015)7

normal- and hyper-fragments; hyper-residues @ target/projectile rapidities

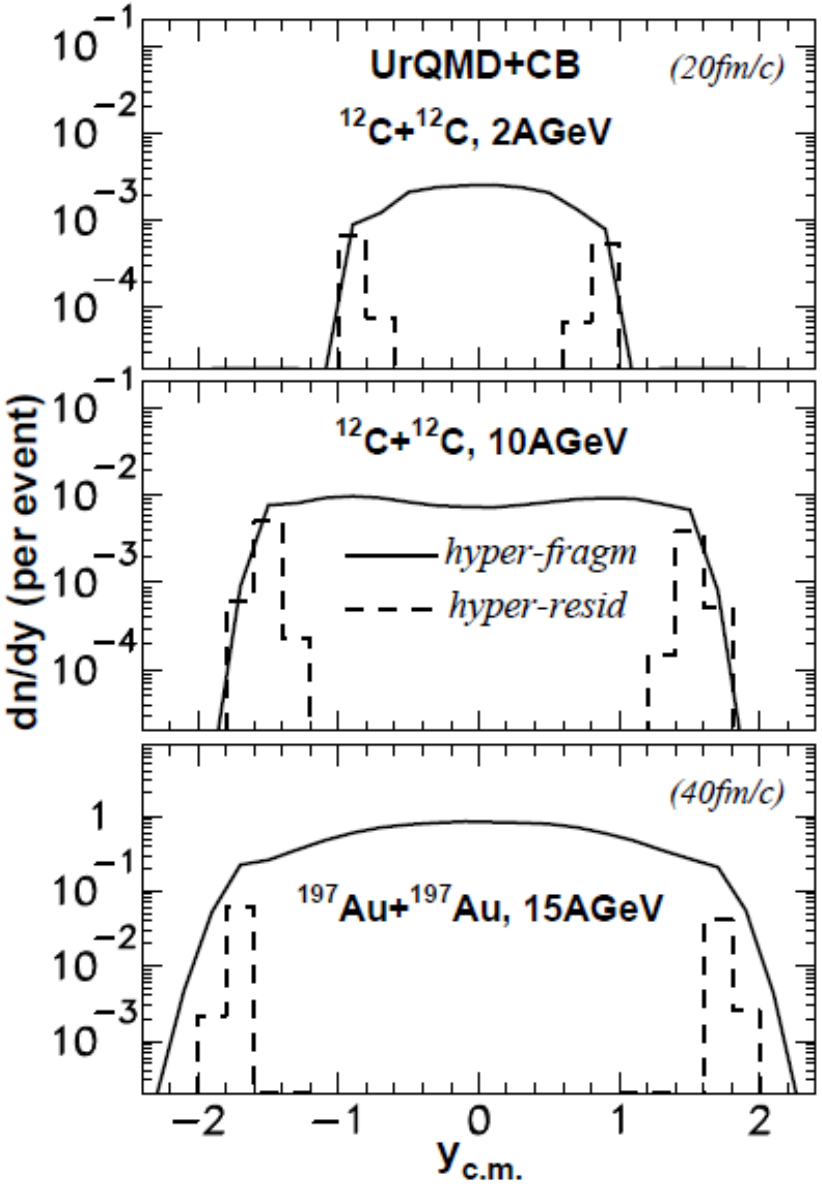

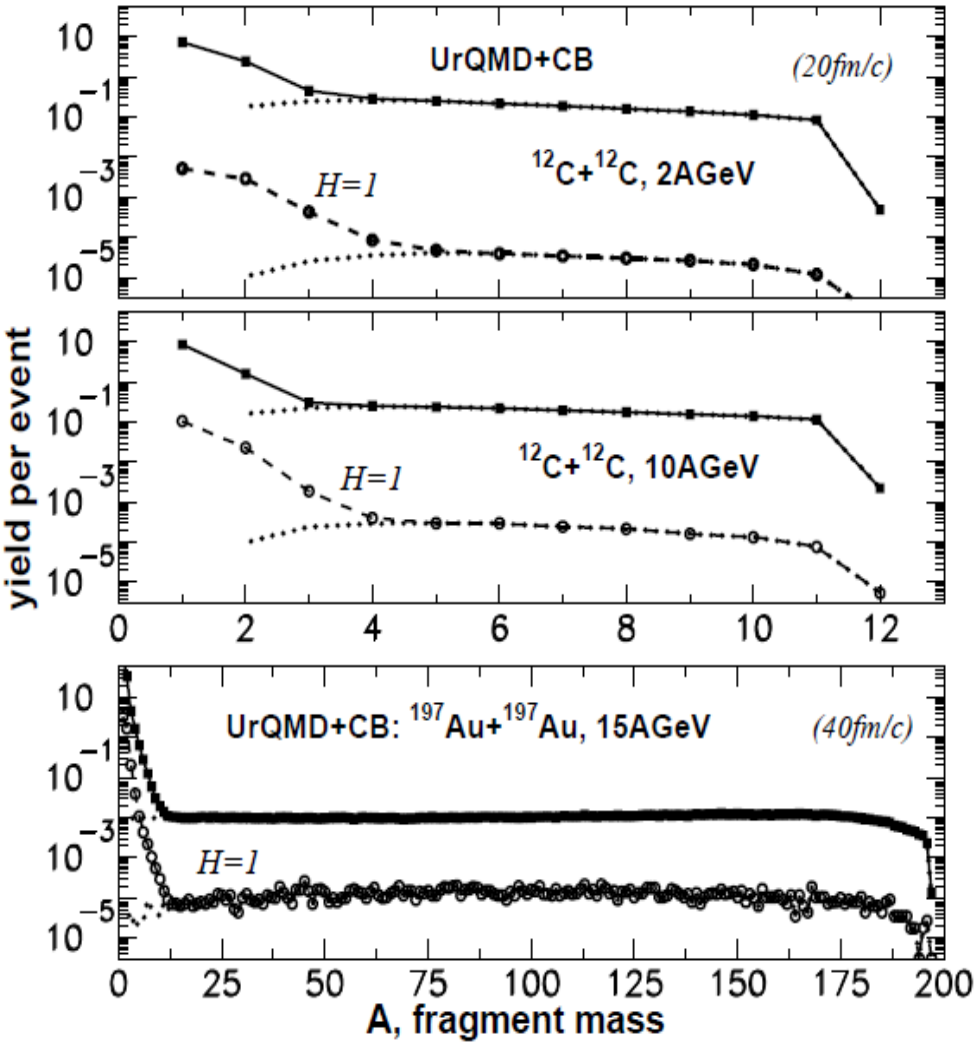

Because of secondary interactions the maximun of the fragments production is shifted from the midrapidity. Secondary products have relatively low kinetic energies, therefore, they can produce clusters and hypernuclei with higher probability.

for LHC @ 2.76 A TeV

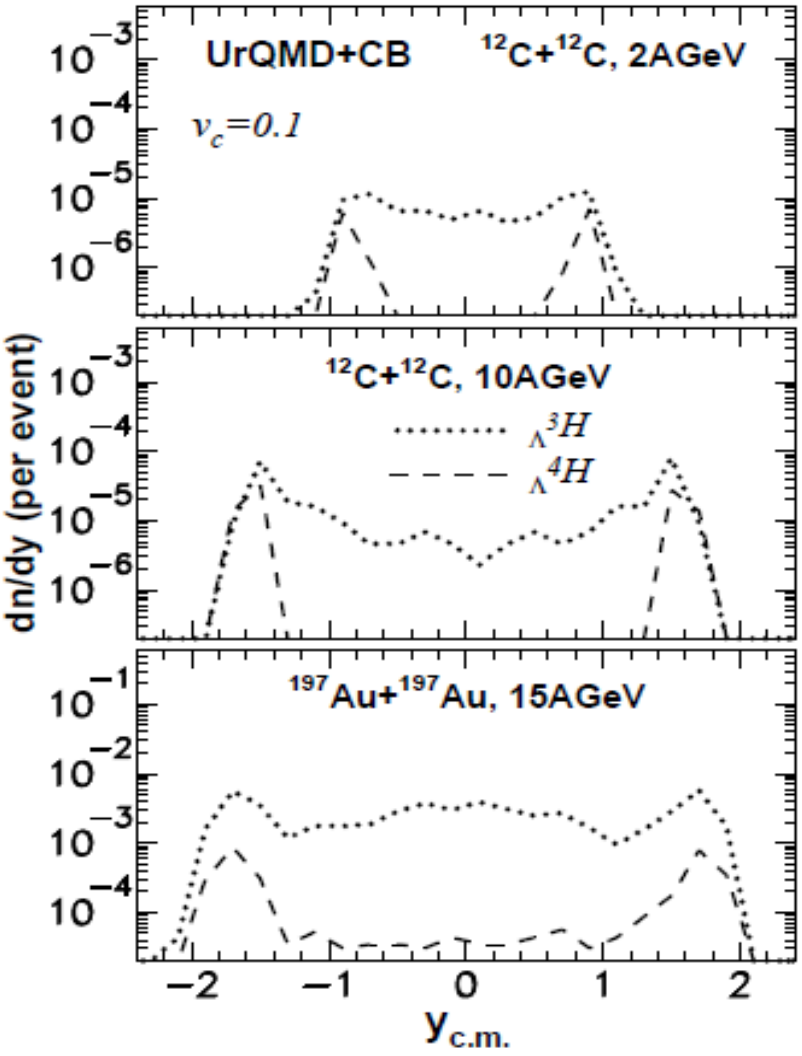

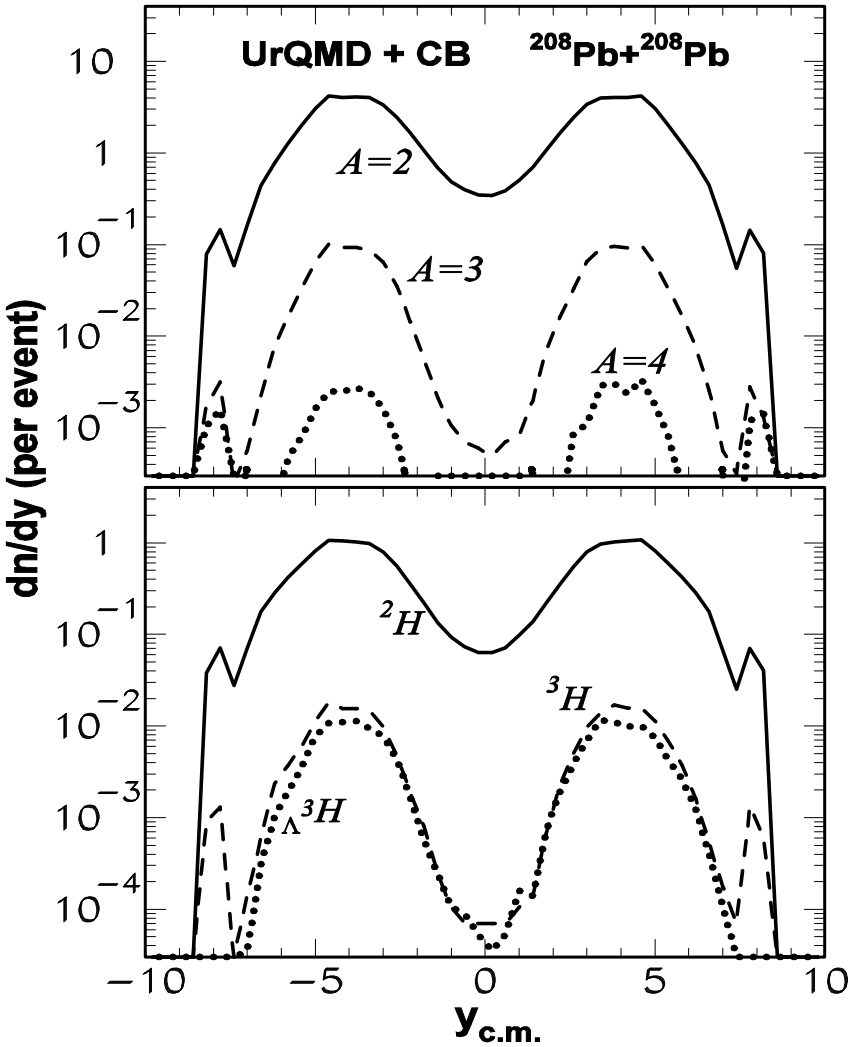

Coalescent-like fragments may be excited & undergo de-excitation

De-excitation influences mass distributions: Examples for transport (DCM) + clusterization of baryons (CB) + statistical de-excitation (De) calculation SMM is used.

Velocity clusterization parameter, **Vc=0.22 c** gives their excitation energies around ~10 MeV/nucl.

Final exponential-like decreasing of the mass yields with A.

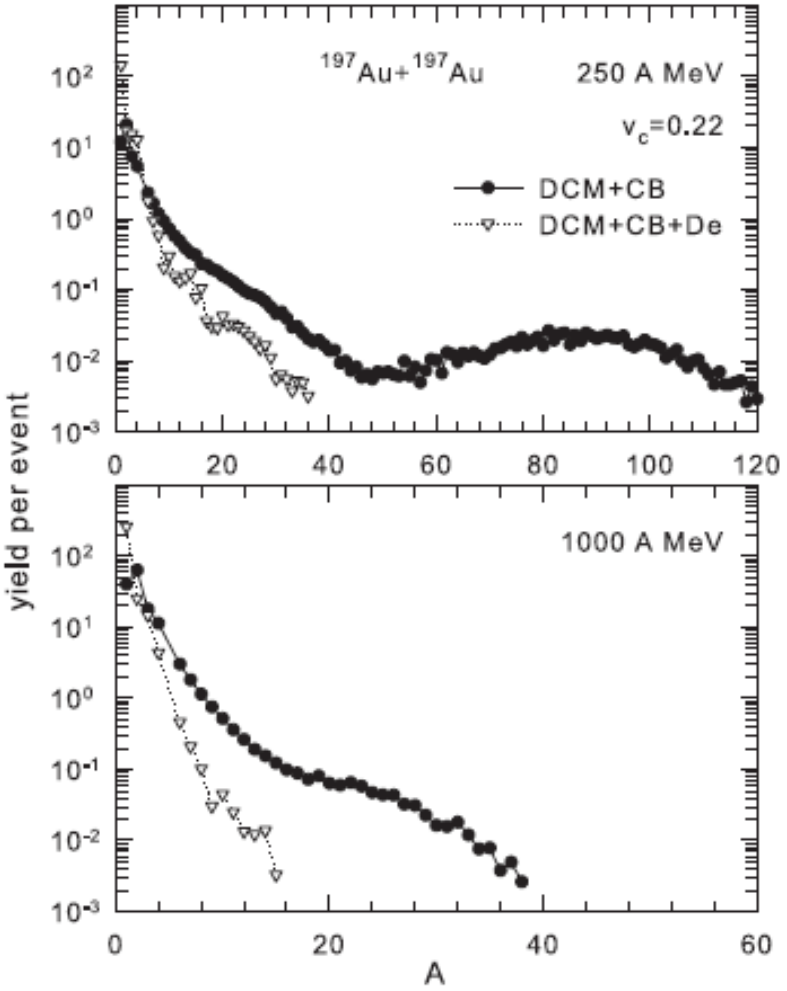

Novel: coalescent fragments can be excited & undergo de-excitation

De-excitation influences energy spectra of all produced particles.

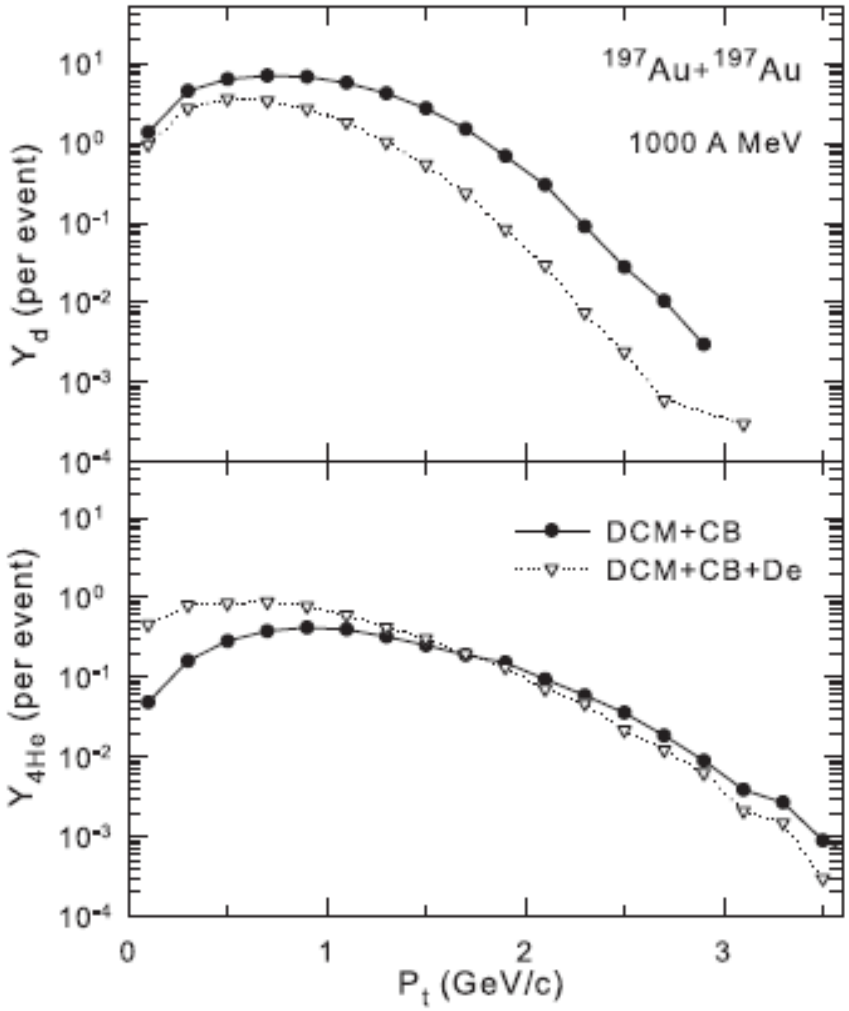

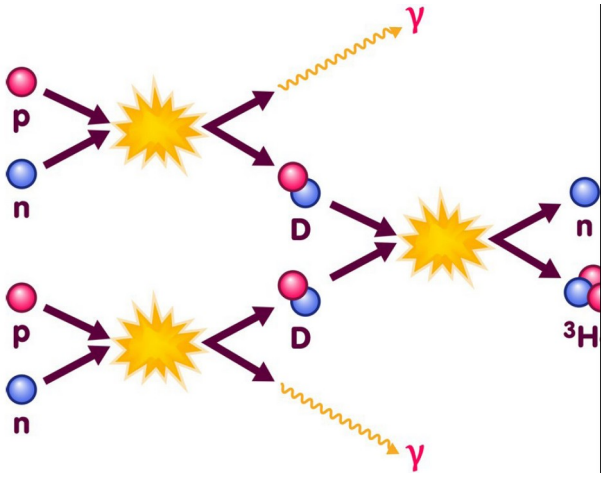
γ
p
n
D
n
p
D
^{3}H
n
γ

Chemical element abundances

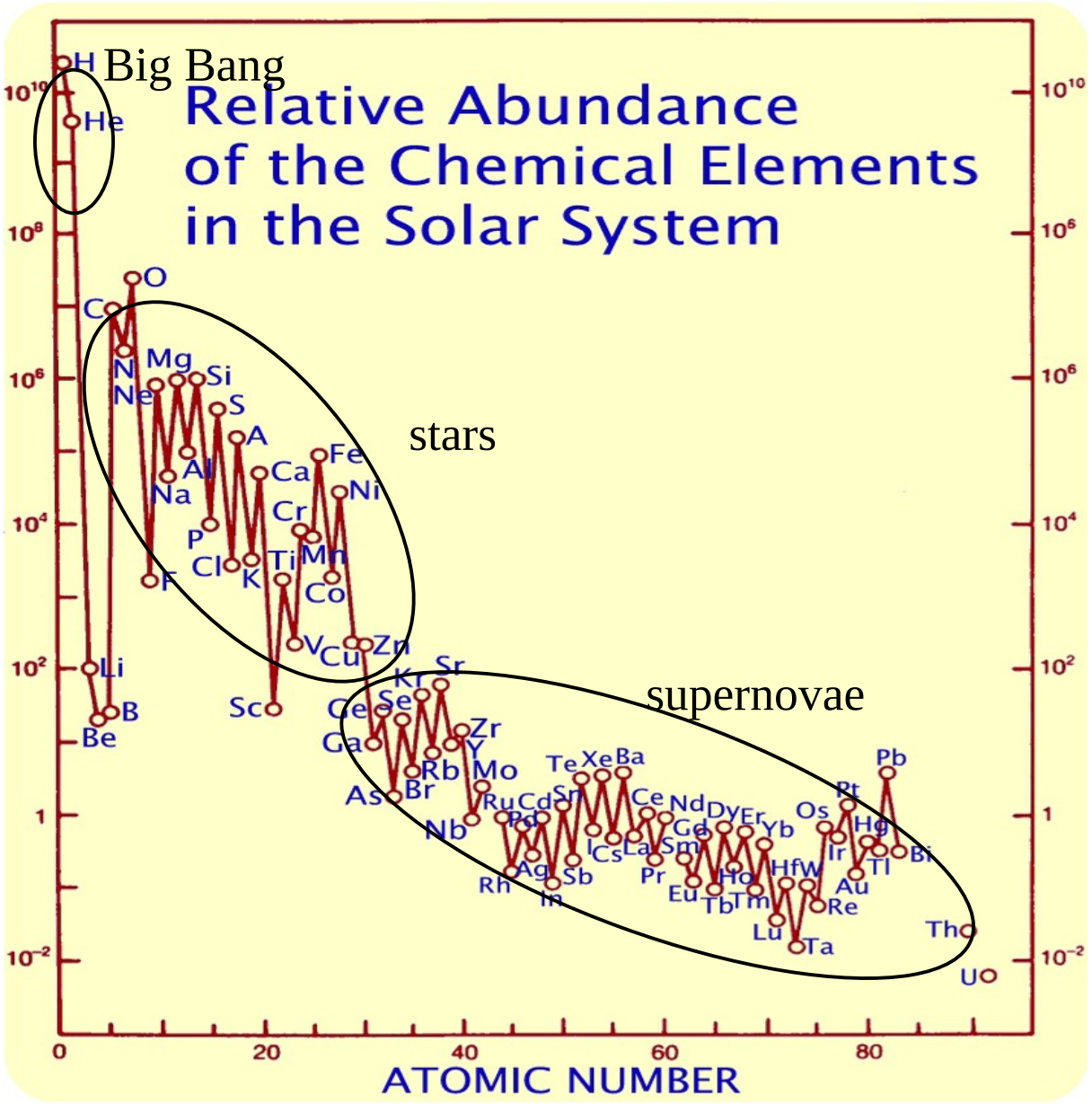

Energy evolution of mass distributions of fragments in multifragmentation reactions and in stellar mater

A.S. Botvina, I.N. Mishustin / Nuclear Physics A 843 (2010) 98–132